

JAERI-M

9 6 7 2

REACTOR ENGINEERING DIVISION ANNUAL REPORT

(April 1, 1980 - March 31, 1981)

September 1981

Division of Reactor Engineering

日 本 原 子 力 研 究 所
Japan Atomic Energy Research Institute

この報告書は、日本原子力研究所が JAERI-M レポートとして、不定期に刊行している研究報告書です。入手、複製などのお問い合わせは、日本原子力研究所技術情報部（茨城県那珂郡東海村）あて、お申しこしください。

JAERI-M reports, issued irregularly, describe the results of research works carried out in JAERI. Inquiries about the availability of reports and their reproduction should be addressed to Division of Technical Information, Japan Atomic Energy Research Institute, Tokai-mura, Naka-gun, Ibaraki-ken, Japan.

Reactor Engineering Division
Annual Report
(April 1, 1980 - March 31, 1981)

Division of Reactor Engineering,
Tokai Research Establishment, JAERI

(Received August 20, 1981)

Research activities in the Division of Reactor Engineering in fiscal 1980 are described.

The work of the Division is closely related to development of multi-purpose Very High Temperature Gas Cooled Reactor and fusion reactor, and development of Liquid Metal Fast Breeder Reactor carried out by Power Reactor and Nuclear Fuel Development Corporation. Contents of the report are achievements in fields such as nuclear data and group constants, theoretical method and code development, integral experiment and analysis, shielding, reactor and nuclear instrumentation, reactor control and diagnosis, and fusion reactor technology, and activities of the Committee on Reactor Physics.

Keywords: Reactor Engineering, Very High Temperature Gas Cooled Reactor, Thermonuclear Fusion Reactor, Liquid Metal Fast Breeder Reactor, Group Constant, Theoretical Method and Code, Integral Experiment and Analysis, Shielding, Reactor and Nuclear instrumentation, Reactor Control and diagnosis.

Board of Editors for Annual Report

J. Hirota (Chief Editor)

Y. Ishiguro (Associate Chief Editor)

H. Takano, M. Nakano, F. Akino, K. Ara

T. Fujisawa, N. Sasamoto, H. Maekawa, F. Yoshiwara

昭和 55 年度原子炉工学部年報

日本原子力研究所東海研究所原子炉工学部

(1981 年 8 月 20 日受理)

昭和55年度の原子炉工学部研究活動状況報告書である。原子炉工学部における研究は、多目的高温ガス炉の開発、核融合炉の開発、さらに動燃事業団による液体金属高速増殖炉の開発に密接に関連している。核データと群定数、炉理論とコード開発、積分実験と解析、遮蔽、炉計装と核計装、炉制御と診断、核融合炉技術、および炉物理に関する研究委員会活動の各分野にわたり、多くの成果を述べている。

年報編集委員会

弘田実弥 (編集委員長)

石黒幸雄 (副編集委員長)

高野秀機, 中野正文, 秋濃藤義, 荒 克之, 藤沢武夫, 笹本宣雄, 前川 洋, 吉原文夫

CONTENTS

Foreword	Vii
1. Nuclear Data and Group Constants	1
1.1 Benchmark Tests Using Group Constant Set JFS-3-J2	1
1.2 The Effect of REMO-Correction on Integral Quantities	6
1.3 Doppler Effect of Structural Materials in Fast Reactors ...	11
1.4 Effective Multiplication Factors and Reaction Rates Calculated by use of Fission Spectra of ^{235}U , ^{238}U and ^{239}Pu	16
2. Theoretical Methods and Code Development	20
2.1 Fuel Pin and Subassembly Heterogeneity Effect in Fast Power Reactor	20
2.2 Burn-up Calculations Applied to the NEACRP Fast Breeder Benchmark for International Comparison	25
2.3 Development of Interface Program JOINT for Fast Reactor Neutronics Calculation Code System	28
2.4 SRAC: A Standard Computer Code System for Lattice Cell and Core Calculations on Reactor Design and Analysis (II) ; Benchmark Test	31
2.5 A Fortran Program CLUPH of Collision Probabilities for Hexagonal Lattice and Its Application to VHTR	40
2.6 A Code Development for Calculating Double Differential Cross Section	42
2.7 A Program Package for the Solution of Linear, Integer, Quadratic and Nonlinear Programming Problems	44
2.8 Development of a Double Finite Element Method Program for Solving Three-Dimensional Multi-Group Neutron Transport Equation	46
2.9 ACCEL: A Computer Code System for Analyzing Nuclear Characteristics Proton Accelerator Target/Blanket Assembly	48
2.10 Computational Studies of High Energy Spallation and Fission Reactions	51
2.11 Neutronics Analyses of Accelerator Molten Salt Target/Blanket Assembly	55

2.12 High Resolution Electron Microscopy of Simple Defects in a (110) Silicon Crystal	59
3. Integral Experiment and Analysis	64
3.1 Measurement of Reactivity Worths of Control Rods in Enriched Uranium Graphite Moderated Core Related to VHTR ..	64
3.2 Reconstruction Program of SHE for Experimental VHTR	66
3.3 Heating Apparatus for Measurement of Reactivity Temperature Coefficient in SHE	67
3.4 Analysis of Fuel Slumping Experiment on FCA Assembly VIII-2	69
3.5 Integral Experiments for Actinides Cross Section Evaluation (I)	72
3.6 Integral Experiments for Actinides Cross Section Evaluation (II) FCA Standard Cores	77
4. Shielding	79
4.1 PALLAS-TS: A One-Dimensional Neutron Transport Code for Analyzing Fusion Blanket Neutronics	79
4.2 PALLAS-2DCY: A Code for Direct Integration of Transport Equation in Two-Dimensional (R,Z) Geometry	83
4.3 Transport Calculation of Gamma Rays Including Bremsstrahlung by Discrete Ordinates Code PALLAS	85
4.4 EEOSS: A Program for Calculation of Electron Energy Loss Data	87
5. Reactor and Nuclear Instrumentation	90
5.1 Development of High-temperature Neutron Detectors	90
5.2 Development of High-temperature Thermocouples for VHTR	95
5.3 Development of Cable Insulator and Cables for LMFBR Instrumentation	98
5.4 Development of Fuel Failure Detection System	102
5.5 Development and Test of Cover-gas On-line Gamma-ray Monitors	104
5.6 Performance of an Anticoincidence-shield High-purity Ge Gamma-ray Spectrometer System	106
5.7 Performance of a High-purity Ge Gamma-ray Spectrometer System Using a Closed-cycle Cryogenic Refrigerator	111
5.8 Fabrication of HgI ₂ Nuclear Radiation Detectors	116

5.9	Fabrication of Low Temperature Cryostats for Tandem Heavy-ion Accelerator	118
5.10	Program Development for Canberra Industries 8100/QUANTA System	120
5.11	Uncertainty Induced by Count Statistics in Enrichment Measurement with SAM-2 (II)	123
6.	Reactor Control and Diagnosis	125
6.1	Simulation Study of Sodium Boiling Detection Methods	125
6.2	Dynamic Model of the VHTR Plant for Analyzing Its Control Systems	126
6.3	Reactor Water Level Estimator of a BWR Plant	129
6.4	A New Method for Leak Detection in OWL-1 Loop Based on Time Series Analysis of Dewpoint Signals	132
7.	Fusion Reactor Technology	137
7.1	Construction of Accelerator System for Fusion Neutronics Source (FNS) --- Installation ---	137
7.2	Construction of Accelerator System for Fusion Neutronics Source (FNS) --- Performance Test ---	140
7.3	Parasitic D-D Neutron Production by Self-Target Reaction in FNS	145
7.4	Surface Temperature and Beam Profile Monitor for Metal Target of FNS	147
7.5	Modification of Tritium Monitoring System for Tritium Adsorption Plant (TAP)	149
7.6	Studies of Tritium Absorption and Desorption in Ionization Chamber for the Tritium Effluent Monitor	151
7.7	Neutron Dosimetry by the Spectrum Weighting Function Method with a NE 213 Liquid Scintillator	154
7.8	Depth Distribution of Defects by Ion Bombardment	157
7.9	Development of Thin Germanium Bolometer for Plasma Radiation Loss Measurement	161
8.	Activities of the Committees	163
8.1	Activities Related to the NEA Committee on Reactor Physics	163
8.2	Activities of the Subcommittees on Reactor Physics	165

8.3 Activities of the Japanese Organizing Committee for SMORN-III	167
Publication Lists	169

Foreword

In the present report is given the annual research activity of Division of Reactor Engineering, Japan Atomic Energy Research Institute, for the period of April 1980 - March 1981. The research activity of the Division extends to a broad area of reactor engineering. The major fields are thermal and fast reactor physics, fusion reactor physics, shielding, reactor instrumentation and control, and numerical analysis.

The total number of people working in the Division at the end of period was 89 in which regular members totalled to 73. Expenditures during the period amounted to about 0.47 billion yen, without including personnel expenses. In addition, a considerable amount of expenditures was covered under research contracts with outside organizations, among which Power Reactor and Fuel Development Corporation (PNC) offered the largest contribution.

The research activities were conducted in 8 Laboratories and the Committee on Reactor Physics. The Laboratories are

Reactor System Laboratory,
Fast Reactor Physics Laboratory,
Thermal Reactor Physics Laboratory,
Reactor Instrumentation Laboratory,
Reactor Control Laboratory,
Shielding Laboratory,
Fusion Reactor Physics Laboratory and
Reactor Physics Experiment Laboratory.

The major research and development projects related closely to research programs in the Division are

- (1) Development of very high temperature gas cooled reactor (VHTR) for multi-purpose use,
- (2) Engineering research of thermonuclear fusion reactor, and
- (3) Development of liquid metal fast breeder reactor (LMFBR).

As concerns research and development of VHTR, reactivity worths of control rods and burnable poison rods were measured on SHE and the results were analyzed with the LAMP code system based on the collision probability method. Long-term real-time operation tests for high-temperature neutron detectors have been continued in JRR-4 for more than 2 years to prove the high performance at 600°C. In addition, an irradiation test in JMTR has been carried out for a tungsten-rhenium thermocouple manufactured

experimentally and a trial production has been repeated for a platinum-molybdenum thermocouple to get the stable performance at around 1000°C. Furthermore, a dynamics simulator has been developed by using a hybrid computer to investigate the control characteristics of VHTR.

Concerning the fusion reactor physics, the construction of accelerator system for Fusion Neutronics Source (FNS) has been completed for getting a high intensity 14 MeV neutron source. In addition, a computer code has been developed to deal with one-dimensional neutron transport in the blanket.

As for the research and development of LMFBR, an analysis has been proceeded for the fuel slumping experiment performed on FCA. Several improvements were made on computer codes for neutronics calculations as well as multigroup constant productions. Furthermore, integral experiments have been carried out on FCA for the cross section evaluation of actinides for burning them in fast reactors. In addition, a simulation study has been conducted on the detection of sodium boiling.

As concerns researches other than those related closely to the projects, a shielding computer code has been developed for dealing with anisotropic transmission problems by using the direct-integration discrete ordinates method. The development of a standard computer code system SRAC has been proceeded for nuclear design calculations of thermal reactors. In addition, improvements have been made on semiconductor detectors and developments have been achieved on passive-gamma-ray type non-destructive assay techniques for nuclear materials. Furthermore, investigations have been proceeded on the reactor physics by the Committee on Reactor Physics.

Takumi ASAOKA, Acting Head
Division of Reactor Engineering

1. Nuclear Data and Group Constants

1.1 Benchmark Tests Using Group Constant Set JFS-3-J2

H. Takano

Benchmark calculations of critical experiments were performed to test the JFS-3-J2 group constant set¹⁾ which was produced with the processing codes PROF·GROUCH·GIIR²⁾ and TIMS-1³⁾ from the JENDL-2 compilation. Four large critical assemblies with clean core were studied in detail using one- and two-dimensional diffusion and transport theories. The four assemblies were the ZPPR assembly 2 and the ZPR-6 assemblies 7 (REF), 7 (H240) and 6A. The assemblies ZPPR-2 and ZPR-6-7 (REF) are similar in composition to a large LMFBR, and especially the ZPPR-2 has two-core zones of a more realistic LMFBR height and oxide blanket. The ZPR-6 assembly 7 (H240) has the high-240 plutonium zone at the center of assembly 7 (REF) to assess the effect of fuel burnup on the integral parameters. The assemblies 6A and 7 (REF) were designed to be identical each other as possible, the only significant difference being the fuel isotope, ^{235}U in the assembly 6A and plutonium in the assembly 7 (REF).

The integral quantities calculated in this study were k_{eff} , central reaction-rate ratios, central sample worth and ^{238}U Doppler coefficient. In these calculations, one- to two-dimensional, diffusion to transport and homogeneous to heterogeneous correction factors were studied by using some well-known calculational codes, EXPANDA-GS, SLAROM⁴⁾, CITATION, ANISN and TWOTRAN-II.

(1) Effective Multiplication Factors : Table 1.1.1

The effective multiplication factors calculated are underestimated by $\sim 0.9\%$ for three assemblies ZPPR-2, ZPR-6-7 (REF) and ZPR-6-7 (H240) with the plutonium fuel, though for ZPR-6-6A with the uranium fuel k_{eff} is about unit. In this table, the correction factors calculated by using three different group cross section sets are compared. Though the differences in the transport effects between the two different sets or one- and two-dimensional models are very small, the heterogeneity effects are considerably different between the results calculated with JFS-3 and ENDF/B-IV or B-III.

(2) ^{238}U Doppler Reactivity Coefficients : Table 1.1.2

The ^{238}U Doppler coefficient calculated for ZPR-6-6A with the uranium

fuel underestimates the experimental value by 18% while the calculational result are in very good agreement with the experiments in the plutonium fuel assemblies. The heterogeneity effects are 6~12%.

(3) Central Reaction Rate Ratios : Table 1.1.3

The calculated central reaction rate ratios, $^{235}\sigma_f/^{239}\sigma_f$, $^{238}\sigma_c/^{239}\sigma_f$ and $^{238}\sigma_f/^{239}\sigma_f$ overestimate the experimental values by 2~11%. The underestimate for k_{eff} and the overestimate for the reaction rate ratios may be attributed to the fact that the fission cross sections of ^{239}Pu are underestimated in the JFS-3-J2 set. The correction factors are very small, except for the heterogeneity effect for $^{236}\sigma_f/^{235}\sigma_f$ and $^{240}\sigma_f/^{235}\sigma_f$ in ZPPR-2.

(4) Central Sample Worths : Table 1.1.4

The calculational and experimental results are normalized to the Pu sample worth to avoid the scaling problem caused by the errors in the kinematic parameters. The calculated sample worths of Na and C are overestimated considerably in the plutonium fuel assemblies, and the ^{10}B worths are underestimated inversely.

The present work was performed under the contracts between Power Reactor and Nuclear Fuel Development Corporation and Japan Atomic Energy Research Institute.

References

- 1) Takano H., et al.: to be published in JAERI-M report
- 2) Takano H., Kaneko K.: to be published in JAERI-M report
- 3) Takano H., et al.: "TIMS-1 : A Processing Code for Production of Group Constants of Heavy Resonant Nuclei", JAERI-1267 (1980)
- 4) Nakagawa M., Tsuchihashi K.: "SLAROM : A Code for Calculation of Heterogeneous Core in Fast Reactor", JAERI-M 5916 (1974) (in Japanese)

Table 1.1.1.1 Comparison of effective multiplication factors calculated with one- and two-dimensional benchmark models

Assembly	Model	Homogeneous			Heterogeneity effect			Transport effect			Corrected Keff		
		ENDF/B-III	ENDF/B-IV	JFS3	B-III	B-IV	JFS3	B-III	B-IV	JFS3	B-III	B-IV	JFS3
ZPPR-2	1-D	0.9795	0.9777	0.97872	0.0175		0.0104	0.0024		-0.0026	0.9994	0.9976	0.99292
	2-D	0.9792		0.97786			0.0114			0.0026			0.99186
	1D-2D	0.0003		0.00086			-0.0010			0.0000			0.00106
ZPR-6-7 (Ref.)	1-D	0.9744	0.9735 (0.9682)	0.97667	0.0166	0.0159	0.01221	0.0016		0.00145	0.9926	0.9917 (0.9864)	0.99033
	2-D	0.9746	(0.9686)	0.97704		0.0162	0.01214			0.00150			0.99068
	1D-2D	-0.002	-0.0004	-0.00037		-0.0003	0.00007			-0.00005			-0.00035
ZPR-6-7 (H240)	1-D			0.97757			0.01276			0.00155			0.99188
	2-D			0.97732			0.01256			0.00116			0.99104
	1D-2D			0.00025			0.0002			0.00039			0.00084
ZPR-6-6A	1-D		0.9881 (0.9774)	0.99373	0.0073	0.0081	0.00473	0.0013		0.00112	0.9988	0.9967	0.99958
	2-D		(0.9770)	0.99414		0.0080	0.00470			0.00093			0.99977
	1D-2D	-0.0013	0.0004	-0.00041		0.0001	0.00003			0.00019			-0.00019

Table 1.1.2 The C/E -values and correction factors for Doppler reactivity coefficients of ^{238}U

Assembly	T (K)	correction factor			C/E - value	
		$\frac{70\text{G}}{20\text{G}}$	$\frac{2\text{-D}}{1\text{-D}}$	$\frac{\text{Hetero}}{\text{Homo}}$	1-D(70G)	Corrected
ZPPR-2	300-500	1.04	0.79	1.06	1.16	0.97
ZPR-6-7 (Ref.)	300-500	1.02	1.02	1.06	0.89	0.96
ZPR-6-7 (H240)	300-500	1.02	1.01	1.07	0.87	0.94
ZPR-6-6A	300-514	1.03	1.03	1.12	0.71	0.82

Table 1.1.3 The C/E - values and correction factors for central reaction rate ratios

	Correction factor			C/E-value			Correction factor			C/E-value	
	$\frac{2\text{-D}}{1\text{-D}}$	$\frac{\text{Hetero}}{\text{Homo}}$	$\frac{\text{Tra.}}{\text{Dif.}}$	1-D	Corrected		$\frac{2\text{-D}}{1\text{-D}}$	$\frac{\text{Hetero}}{\text{Homo}}$	$\frac{\text{Tra.}}{\text{Dif.}}$	1-D	Corrected
ZPPR-2						ZPR-6-7(Ref.)					
$^{233}\sigma_f / ^{235}\sigma_f$	1.000	1.001	0.999	0.978	0.978	$^{238}\sigma_c / ^{239}\sigma_f$	1.00	0.974	1.00	1.09	1.06
$^{234}\sigma_f / ^{235}\sigma_f$	0.999	1.064	0.991	0.993	1.046	$^{238}\sigma_f / ^{239}\sigma_f$	1.006	1.009	1.00	1.05	1.07
$^{236}\sigma_f / ^{235}\sigma_f$	0.999	1.088	0.990	1.049	1.129	$^{235}\sigma_f / ^{239}\sigma_f$	0.999	1.008	1.00	1.04	1.05
$^{238}\sigma_f / ^{235}\sigma_f$	0.998	1.008	0.990	1.11	1.097						
$^{239}\sigma_f / ^{235}\sigma_f$	1.000	1.007	0.998	0.971	0.976						
$^{240}\sigma_f / ^{235}\sigma_f$	0.999	0.952	0.992	1.087	1.026						
ZPR-6-7 (H240)						ZPR-6-6A					
$^{238}\sigma_c / ^{239}\sigma_f$	1.00	0.974	1.00	—	—	$^{238}\sigma_c / ^{235}\sigma_f$	1.009	0.985	1.00	0.961	0.955
$^{238}\sigma_f / ^{239}\sigma_f$	1.00	1.006	1.00	1.10	1.11	$^{238}\sigma_f / ^{235}\sigma_f$	1.00	0.979	1.00	1.01	0.989
$^{235}\sigma_f / ^{239}\sigma_f$	1.00	1.006	1.00	1.05	1.06						

Table 1.1.4 The C/E - values and correction factors for central sample worth

Sample	ZPR - 2			ZPR-6-7 (Ref.)			ZPR-6-7 (H240)			ZPR-6-6A		
	2-D T-D	Hetero Homo	Tra Dif C/E	2-D T-D	Hetero Homo	Tra Dif C/E	2-D T-D	Hetero Homo	Tra Dif C/E	2-D T-D	Hetero Homo	Tra Dif C/E
Pu-239	1.00	1.02	0.99 1.00	1.00	1.02	0.98 1.00	1.00	1.02	0.98 1.00	1.00	1.05	0.98 1.00
Pu-241	1.00	1.01	0.99 1.11									
U-235	1.00	1.02	0.99 1.13	1.00	1.02	0.98 0.99	1.00	1.02	0.98 1.04	1.00	1.06	0.98 1.08
U-238	1.00			1.00	0.97	1.01 0.79	1.00	1.01	1.02 0.93	1.00	1.02	1.01 1.09
Na	1.00	1.05	1.01 1.42	1.00	1.08	1.02 1.45	1.00	1.05	1.03 1.67	1.01	2.08	1.33 -7.22
Fe	1.00	1.06	1.00 1.13	1.00	1.00	1.00 1.04						
Cr	1.00	1.04	1.00 1.10	1.00	0.95	1.00 0.97						
Ni	1.00	1.01	1.00 1.23	1.00	0.96	1.01 1.15						
Mn	1.00	1.10	1.00 1.76									
Mo	1.00	1.03	1.00 0.95	1.00	1.01	1.00 1.04						
C	1.00	1.04	1.02 1.30	1.00	0.98	1.05 1.50	1.00	1.03	1.05 1.60	1.00	0.66	0.74 0.22
Al	1.00	1.06	1.00 1.27	1.00	0.67	1.01 0.94						
B-10	1.00	1.05	1.00 0.90	1.00	1.04	1.00 0.90	1.00	1.05	1.00 0.91	1.00	0.90	1.00 0.79

1.2 The Effect of REMO-Correction on Integral Quantities

H. Takano

Assumption of "1/E - spectrum" overestimates the elastic removal cross sections. The overestimate brings an inaccuracy in the calculation of neutron flux. In order to correct the overestimate, the method called "REMO-correction"¹⁾ is used here, that is, the group cross sections are weighted by the collision density spectrum calculated for the core composition in a typical fast reactor. The two sets of group constants are generated by weighting two different spectra of "collision density" and "1/E" using the basic nuclear data of the JENDL-2 compilation, and they are called the CDS- and SDS-sets respectively. The effects of the REMO-correction on integral quantities (effective multiplication factors, central reaction rate ratios, central sample worths, Doppler reactivity coefficients, sodium void reactivity coefficients and control rod reactivity worth) are studied by performing the benchmark calculations for the critical assemblies²⁾ used often for cross section test.

Effective Multiplication Factors : Figure 1.2.1

The percent deviations of k_{eff} calculated with the CDS-set from those calculated with the SDS-set are shown in Figure 1.2.1. The deviations are not more than 0.35 percent.

Central Reaction Rate Ratios

The difference between the results calculated with the two sets are small and $\sim 1\%$.

Central Sample Worth of ^{10}B : Figure 1.2.2

The sample worth of ^{10}B is sensitive to the variation of neutron spectrum, because of a typical " $\frac{1}{v}$ cross section". The results calculated with the CDS-set increase the tendency of underestimate for the SDS-results, and also for the dependence of the C/E-values on the core volume.

Doppler Reactivity Coefficients : Table 1.2.1

The Doppler reactivity coefficient is very sensitive to the neutron spectrum at core. The neutron spectra calculated with the SDS-set are softened, because of the overestimate for the elastic removal cross sections. Hence, the Doppler coefficients calculated with the CDS-set are reduced by $8 \sim 14\%$ than the SDS-results as shown in Table 1.2.1.

Radial Reaction Rates : Figure 1.2.3

In the ZPPR assembly 2, the reaction rates were calculated by using the two sets. The deviations of the SDS-results from the CDS-results are shown in Fig. 1.2.3. The differences between the two results are seen in the blanket and reflector regions.

Control Rod Reactivity Worth

The control rod worth was calculated with two-dimensional diffusion theory for the NEACRP LMFBR model. The result calculated with the CSD-set becomes larger than the SDS-result, though the difference between the two results is ~2%.

Sodium-Void Reactivity

The difference between the sodium-void reactivities calculated with the two sets was very small, because of cancellation for the reactivity differences between Δk by $\Sigma_{i \rightarrow j}$ and Σ_a .

As the result in the present study, the REMO-correction should be considered in the calculations for Doppler reactivity, sample worth of ^{10}B and reaction rates in the blanket, which are very sensitive to the neutron flux shape in the low energy region below 1 KeV.

References

- 1) Huschke H.: KFK770 (1968)
- 2) Takano H., et al.: "JAERI Fast Reactor Group Constants Set, Version II", JAERI-1255 (1978)

Table 1.2.1 Doppler reactivity coefficients (C/E-values) calculated with the CDS and SDS-sets using one-dimensional diffusion code

Assembly	Temperature (°K)	C/E-value		SDS/CDS
		SDS	CDS	
SEFOR*	677 ~ 1365	1.05	0.97	1.08
FCA-V-1**	300 ~ 573	0.97 (1.06)	0.86 (0.94)	1.13
	300 ~ 823	0.99 (1.06)	0.87 (0.93)	1.14
	300 ~ 1073	0.96 (1.03)	0.85 (0.91)	1.13
FCA-V-2**	300 ~ 1073	0.82	0.72	1.14
FCA-VI-1**	300 ~ 623	0.99 (1.03)	0.88 (0.92)	1.13
	300 ~ 823	0.95 (0.99)	0.84 (0.87)	1.13
	300 ~ 1073	0.97 (1.01)	0.86 (0.89)	1.13
FCA-VI-2**	300 ~ 823	0.91 (0.96)	0.81 (0.86)	1.12
	300 ~ 1073	0.90 (0.95)	0.81 (0.86)	1.11
ZPR-3-47**	300 ~ 500	0.98	0.90	1.09
	300 ~ 800	0.95	0.86	1.10
	300 ~ 1100	0.94	0.86	1.09
ZPPR-2** (normal)	300 ~ 500	1.00 (1.11)	0.90 (1.00)	1.11
	300 ~ 800	0.97 (1.08)	0.87 (0.97)	1.11
	300 ~ 1100	0.95 (1.05)	0.85 (0.94)	1.12
ZPPR-2** (Na-voided)	300 ~ 500	0.84 (0.94)	0.76 (0.85)	1.11
	300 ~ 800	0.81 (0.92)	0.73 (0.82)	1.11
	300 ~ 1100	0.79 (0.89)	0.71 (0.80)	1.11

* Whole core Doppler experiment

** Small sample Doppler experiments for natural UO₂

The results corrected by the heterogeneity effect taken from Ref.(2) are presented in the parentheses.

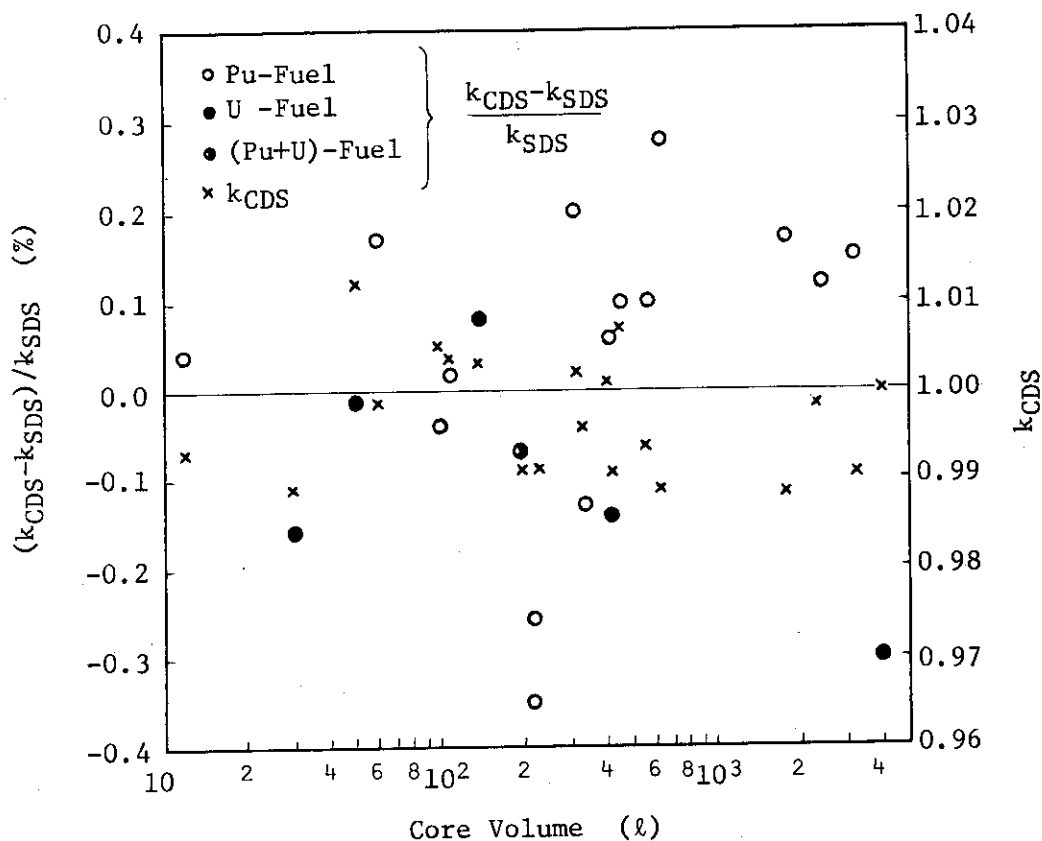


Fig. 1.2.1 The effective multiplication factors (k_{CDS}) calculated with the CDS-sets and the deviations of k_{CDS} from those calculated with the SDS-set.

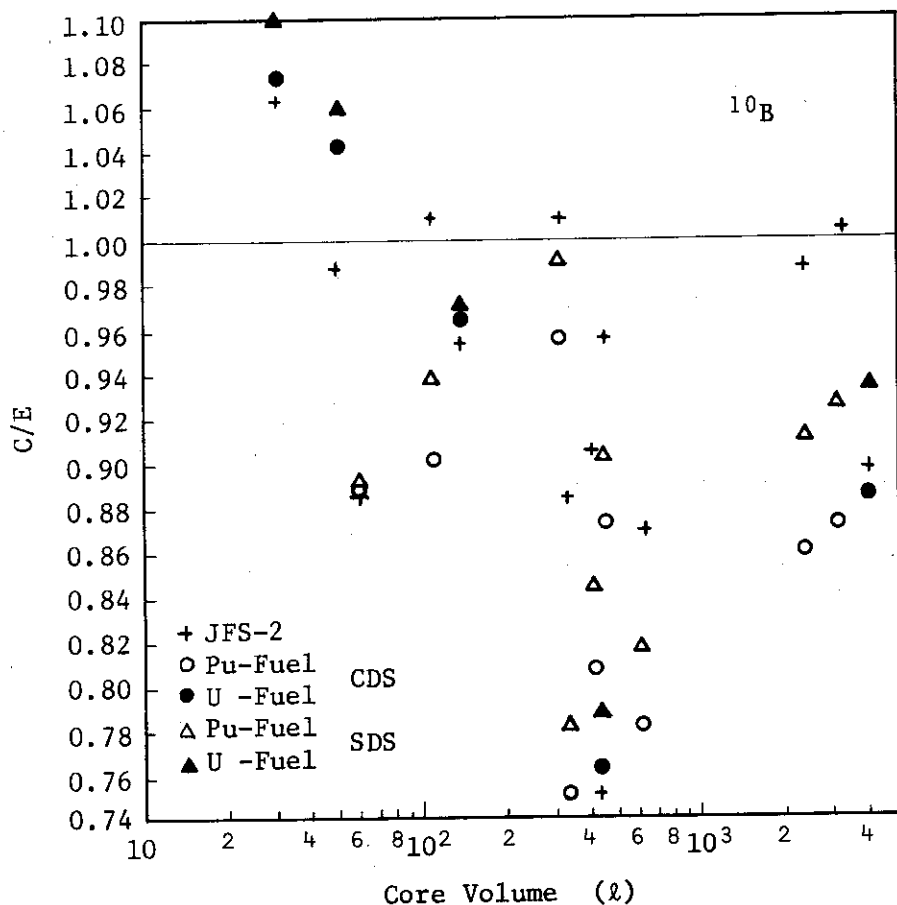


Fig. 1.2.2 Comparison of the C/E-values for the central sample worth of ^{10}B calculated with the SDS- and CDS-sets.

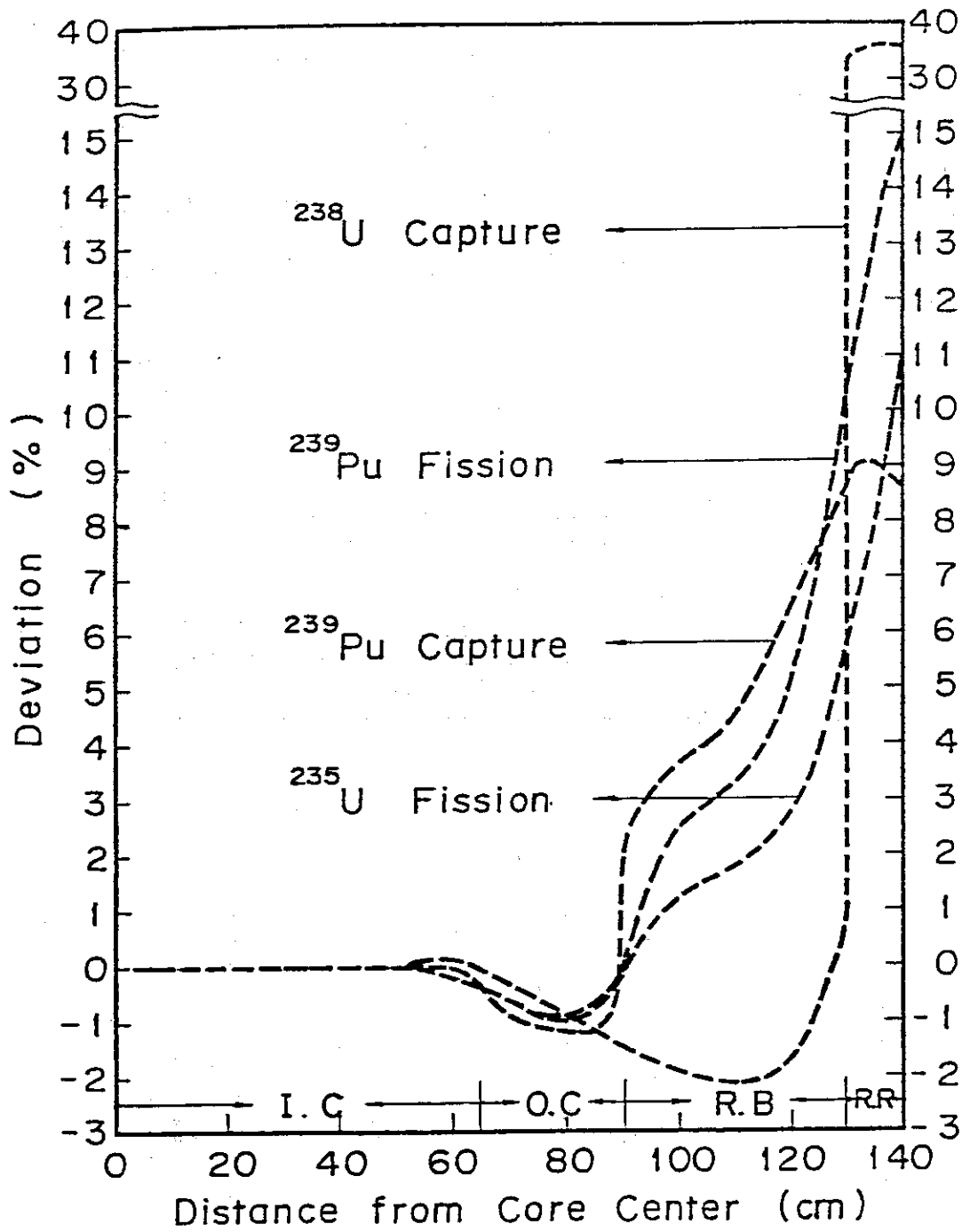


Fig.1.2.3 Deviation of the reaction rates calculated with the SDS-set from those calculated with the CDS-set in ZPPR-2

1.3 Doppler Effect of Structural Materials in Fast Reactors

H. Takano and H. Inoue*

Temperature dependence of capture cross sections for the structural materials is mainly due to p-wave neutron resonances and seen in the energy range from 1 to 300 keV, where lies the important range of neutron spectrum in fast reactor. However, the temperature dependence of the cross sections has not been considered in the group constants library such as JFS-II⁽¹⁾ and/or JENDL-2B⁽²⁾, that is, the cross sections at the zero temperature ($T = 0^\circ\text{K}$) are used in fast reactor calculations. Benchmark tests of the group constants libraries have been performed^{(1), (2)} by using the cross sections of the structural materials for $T = 0^\circ\text{K}$.

In the present study, the structural material Doppler effects for the temperature rise from 0 to 300°K are calculated for 23 fast critical assemblies. The correction factors for the k_{eff} -values in the benchmark calculations are evaluated from the calculated Doppler effects. In order to test the temperature dependence of the capture cross sections, furthermore, the sample Doppler experiments in FCA assemblies are analysed by using the nuclear data of JENDL-2 and ENDF/B-IV. For this purpose, the temperature dependent self-shielding factors of iron, chromium and nickel are calculated with the assumption of collision density constant by using the PROF GROUCH G-IIR/code⁽³⁾. The group constants are produced with the seventy group structure of JFS-III⁽⁴⁾, in which the energy range below 10 MeV is divided with an equal lethargy width 0.25.

The benchmark calculations for the 23 fast critical assemblies used in the benchmark tests of JFS-II⁽¹⁾ were performed with one-dimensional diffusion theory by using the group constants library generated from the JENDL-2 compilation. The calculated effective multiplication factors (k_{eff}) are shown in Table 1.3.1. The k_{eff} -values are corrected by the necessary factors such as heterogeneity and transport effects taken from Ref.(5). Table 1.3.1 shows also the structural material Doppler effect for the temperature rise from 0 to 300°K . The magnitude of the Doppler effects varies depending on the assemblies, i.e., the core size, compositions and neutron spectra. Especially, the effects become larger for the assemblies with large core volume such as MZB, ZPPR-2, ZPR-6-7 and

* Japan Information Service Co. Ltd., Tokyo.

ZPR-6-6A in which the concentration of the structural materials is comparatively high. The Doppler effects on k_{eff} are more than 0.2% for these assemblies, and the effects are comparable to the transport correction factors⁽⁵⁾.

In order to test the temperature dependence of cross sections of Fe, Cr and Ni in JENDL-2 and ENDF/B-IV, we performed the analyses of the sample Doppler experiments. The calculated results are shown in Figs. 1.3.1~3 including the experimental results. As seen from these figures, the results calculated with the nuclear data of JENDL-2 considerably overestimate the Doppler coefficients in FCA-V-1 and 2, while they give a good estimate for FCA-VI-1 and 2. On the other hand, the results of ENDF/B-IV are in good agreement with the experimental values in FCA-V-1 and 2, while they underestimate for FCA-VI-1 and 2. Very large discrepancies are seen between the results for JENDL-2 and ENDF/B-IV and especially for the Doppler coefficient of natural iron. The main cause for these discrepancies can be considered as follows: The neutron spectra in cores of small assemblies FCA-V-1 and 2 are harder than those of FCA-VI-1 and 2. As seen from Fig. 1.3.4, furthermore, the capture cross sections for iron of JENDL-2 are larger than those of ENDF/B-IV in the high energy range, and smaller in lower energy side, especially for resonance cross section at 1.15 keV.

From these results, we can remark that the cross sections of the structural materials should be calculated by considering the Doppler effect, especially when we consider the goal accuracies ($\pm 0.3\%$ ⁽⁷⁾ for k_{eff} and $\pm 7\%$ ⁽⁶⁾ ~ 15% ⁽⁷⁾ for Doppler effect) required from LMFBR design study. Hence, the temperature dependent self-shielding factors for the structural materials were taken into account in the JFS-III⁽⁴⁾ group constants library produced recently at JAERI.

References

- 1) Takano H., Hasegawa, A., Nakagawa M., et al.: "JAERI Fast Reactor Group Constants Set, Version II", JAERI 1255 (1978).
- 2) Kikuchi Y., et al.: J. Nucl. Sci. Technol., 17[7], 567 (1980).
- 3) Takano H., Kaneko K.: to be published.
- 4) Takano H., et al.: "JAERI Fast Reactor Group Constants Library Based on New Concepts", to be published in JAERI-M report.
- 5) Hardie R.W., Schenter R.E., Wilson R.E.: Nucl. Sci. Eng., 57, 222 (1975).

- 6) Vieider G., et al.: Fast Breeder Reactors Status 1977, STUDSVIK/RA-78/1 (1978).
- 7) Hammer P.: "Nuclear Data Needs for Plutonium Breeders", Proc. Inter. Conf. on Nuclear Cross Sections for Technology, Knoxville, Oct. 22-26, 1979.

Table 1.3.1 Doppler effect of structural materials on effective multiplication factor for temperature change from 0 to 300°K. The calculations were performed with one-dimensional diffusion theory using the group constant library generated from JENDL-2

Assembly	Ratio*	k_{eff}		Doppler effect (% $\Delta k/k$)
		T = 0 °K	T = 300 °K	
VERA-11A	1.1	0.99452	0.99445	0.01
ZEBRA-3	0.2	0.99989	0.99988	0.0
SNEAK-7A	1.1	1.00688	1.00654	0.03
ZPR-3-54	2.3	0.95886	0.95742	0.15
ZPR-3-53	2.3	0.99651	0.99562	0.09
SNEAK-7B	0.8	1.00448	1.00410	0.04
ZPR-3-50	1.1	1.00342	1.00270	0.07
ZPR-3-48	1.5	1.00534	1.00449	0.08
ZPR-3-49	1.5	1.01011	1.00946	0.06
ZPR-3-56B	2.2	0.99174	0.98969	0.21
ZPR-6-7	2.5	0.99741	0.99506	0.24
ZPPR-2	2.5	1.00417	1.00213	0.20
SEFOR	2.3	1.00180	0.99971	0.21
MZA	2.5	0.99930	0.99774	0.16
MZB(1)	2.5	0.99630	0.99400	0.23
FCA-6-2	2.2	0.99872	0.99756	0.12
FCA-5-2	2.3	0.99178	0.99125	0.05
VERA-1B	1.1	1.00162	1.00151	0.01
ZPR-3-6F	0.7	1.01384	1.01379	0.0
ZPR-3-12	0.4	1.00767	1.00759	0.01
ZPR-3-11	0.2	1.00401	1.00402	0.0
ZEBRA-2	0.3	0.99567	0.99559	0.0
ZPR-6-6A	2.5	1.01120	1.00879	0.24

* Atomic number density ratio of structural (Fe+Cr+Ni) to fuel (U+Pu) materials in the core region

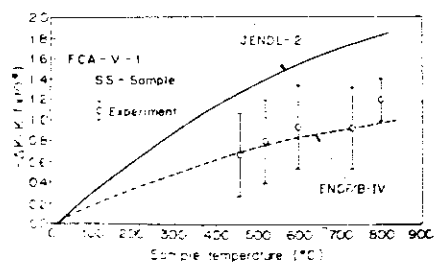


Fig.1.3.1 Comparison of Doppler reactivity effects of stainless steel calculated and measured in FCA-V-1

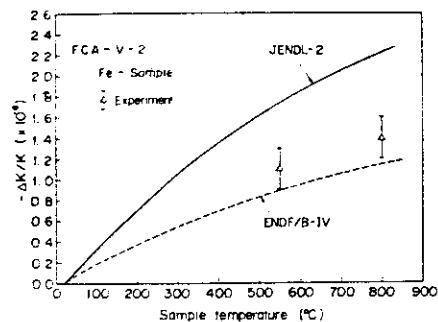
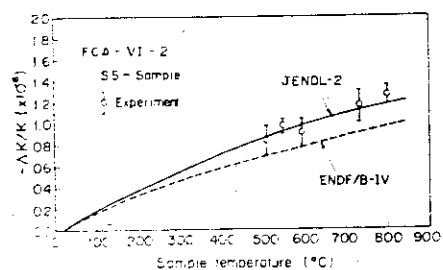
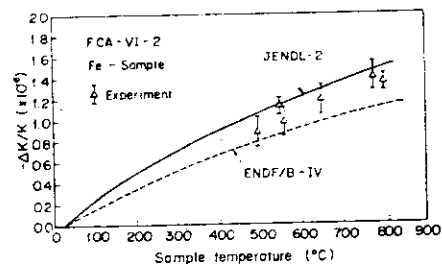


Fig.1.3.2 Comparison of Doppler reactivity effects of natural iron calculated and measured in FCA-V-2



(a) Stainless steel



(b) Natural iron

Fig.1.3.3 (a), (b) Comparison of Doppler reactivity effects of stainless steel and natural iron calculated and measured in FCA-VI-2

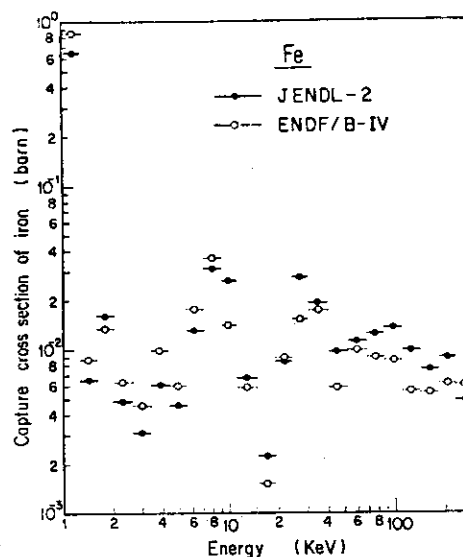


Fig.1.3.4 Comparison of capture cross sections of Fe of JENDL-2 and ENDF/B-IV

1.4 Effective Multiplication Factors and Reaction Rates Calculated by Use of Fission Spectra of ^{235}U , ^{238}U and ^{239}Pu

H. Takano and K. Kaneko*

The effects of the difference among the fission spectra of $^{235}\chi$, $^{239}\chi$ and $^{238}\chi$ on effective multiplication factor and radial reaction rate are calculated by using a one-dimensional diffusion code with the group constants library JFS-III-B4⁽¹⁾ which was generated by the processing codes PROF.GROUCH.G-II R⁽²⁾ and TMS-1⁽³⁾ from ENDF/B-IV nuclear data. In the calculations, an average fission spectrum for an energy group (g) in the fuel region is defined by

$$\tilde{\chi}_g = \frac{\sum_{i=1}^3 W_i \chi_{i,g}}{\sum_{i=1}^3 W_i}, \quad W_i = \sum_g N_i \sigma_{f,i,g} \phi_g, \quad (1)$$

where ϕ_g is the neutron spectrum at core center in the prototype fast reactor mockup assembly MZB, the subscript i means the nuclide of ^{235}U , ^{238}U and ^{239}Pu , and N_i the atomic number density in the core region. In the blanket region, only $^{238}\chi$ is used as it is.

The effective multiplication factors were calculated for the fifteen benchmark critical assemblies with the Pu-fueled cores^{(4),(5)}. The results calculated are shown in Table 1.4.1. The effective multiplication factors calculated with $^{235}\chi$ become smaller by 1.09% for ZEBRA-3 with the high concentration of ^{238}U and about 0.6% for MZB, ZPR-3-48 and ZPR-6-7 assemblies, that is the use of $^{235}\chi$ for the Pu-fueled cores produces considerably less reactivities as compared with the results calculated with $^{239}\chi$. In the other hand, the use of only one fission spectrum of $^{239}\chi$ produces larger effective multiplication factors than those calculated with the average fission spectrum of Eq.(1).

The difference between the results calculated with the spectra $^{235}\chi$ and $^{239}\chi$ is about 0.5% in FCA-5-2 which contains both the fuels of ^{239}Pu and ^{235}U . Using the neutron spectrum at the core center in FCA-5-2, the average fission spectrum of Eq.(1) was calculated. A middle value between the results calculated with $^{235}\chi$ and $^{239}\chi$ is obtained by using the average

* Japan Information service Co. Ltd., Tokyo.

fission spectrum.

In FCA-6-2 assembly, the inner core is Pu-fueled zone and the outer core is the driver zone with U-fuel. Hence, the average fission spectrum method results in the use of the region dependent spectra, i.e., $^{239}\chi$ for the inner core, $^{235}\chi$ for the outer core and $^{238}\chi$ for the blanket region. The use of this region dependent fission spectra affects the effective multiplication factors by about 0.4%.

Figure 1.4.1 shows the deviations of the reaction rates calculated with $^{235}\chi$ and $^{239}\chi$ from those calculated with $\tilde{\chi}$ in the FCA-5-2 assembly. In the blanket region, the fission reaction rates calculated with $^{239}\chi$ are larger by about 4% for ^{238}U and about 2% for ^{235}U than those calculated with $\tilde{\chi}$, while the differences between the results calculated with $^{235}\chi$ and $\tilde{\chi}$ are very small.

Figure 1.4.2 shows the deviations of the reaction rates calculated with $^{239}\chi$ from those calculated with the region dependent fission spectra in FCA-6-2 assembly. The radial fission reaction rates of ^{238}U calculated with $^{239}\chi$ are overestimated by about 8% in the blanket region.

For the cores with the high concentration of ^{238}U such as ZEBRA-3, with the mixed fuels of U and Pu such as FCA-5-2 and with the driver zone such as FCA-6-2, the use of one fission spectrum, for example, only $^{239}\chi$, provides non-negligible errors for the effective multiplication factors and radial fission reaction rates of ^{238}U .

References

- 1) Takano H., et al.: to be published as JAERI-M report.
- 2) Takano H., Kaneko K.: to be published.
- 3) Takano H., Ishiguro Y., Matsui Y.: "TIMS-1: A Processing Code for Production of Group Constants of Heavy Resonant Nuclei", JAERI-1267 (1980).
- 4) Takano H., Hasegawa A., Nakagawa M., et al.: "JAERI Fast Reactor Group Constants Set, Version II", JAERI-1255 (1978).
- 5) Hardie R.W., et al.: Nucl. Sci. Eng., 57, 222 (1975).

Table 1.4.1 Effect of different fission spectra on effective

multiplication factor (K_{eff}), $\Delta K = \frac{K_{\text{eff}} - K_{\text{eff}}(^{239}\chi)}{K_{\text{eff}}(^{239}\chi)} \times 100$

Assembly	Fertile to Fissile	$K_{\text{eff}}(^{239}\chi)$	$\Delta K(^{235}\chi)$	$\Delta K(\tilde{\chi})$
VERA-11A	0.05	0.9852	-0.40	-0.13
ZPR-3-53	1.6	0.9837	-0.31	-0.07
ZPR-3-54	1.6	0.9401	-0.10	-0.01
FCA-5-2	2.3	0.9845	-0.48	-0.31
SNEAK-7A	3.0	0.9940	-0.59	-0.12
MZA	3.9	0.9864	-0.48	-0.08
ZPR-3-48	4.5	0.9922	-0.66	-0.12
ZPR-3-49	4.5	0.9947	-0.71	-0.13
ZPR-3-50	4.5	0.9864	-0.64	-0.11
ZPR-3-56B	4.6	0.9807	-0.44	-0.06
MZB	5.8	0.9836	-0.56	-0.11
ZPR-6-7	6.5	0.9854	-0.59	-0.11
ZPPR-2	6.5	0.9918	-0.52	-0.08
FCA-6-2	6.5	0.9837	-0.53	-0.37
SNEAK-7B	7.0	0.9914	-0.84	-0.25
ZEBRA-3	8.6	0.9922	-1.09	-0.31

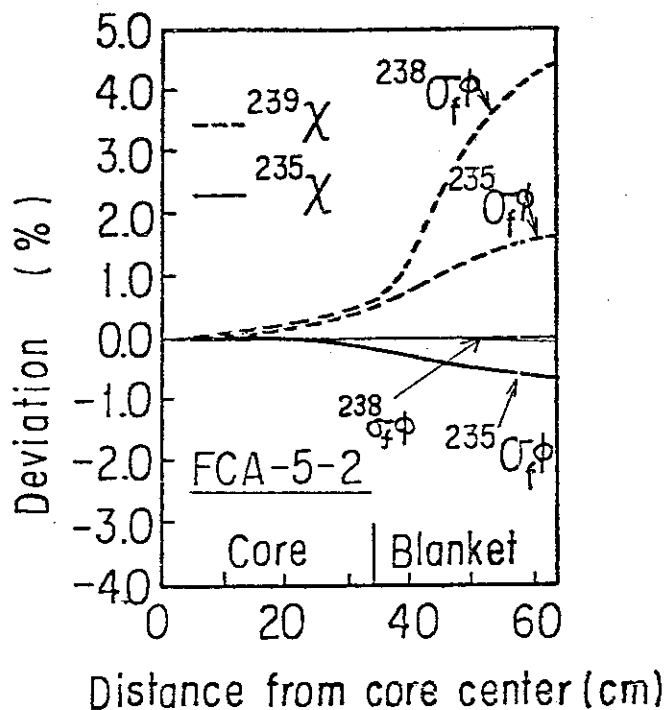


Fig.1.4.1 Deviations of the radial reaction rates calculated with the ^{235}U or ^{239}Pu fission spectrum from those calculated with the average fission spectrum in FCA-5-2 assembly

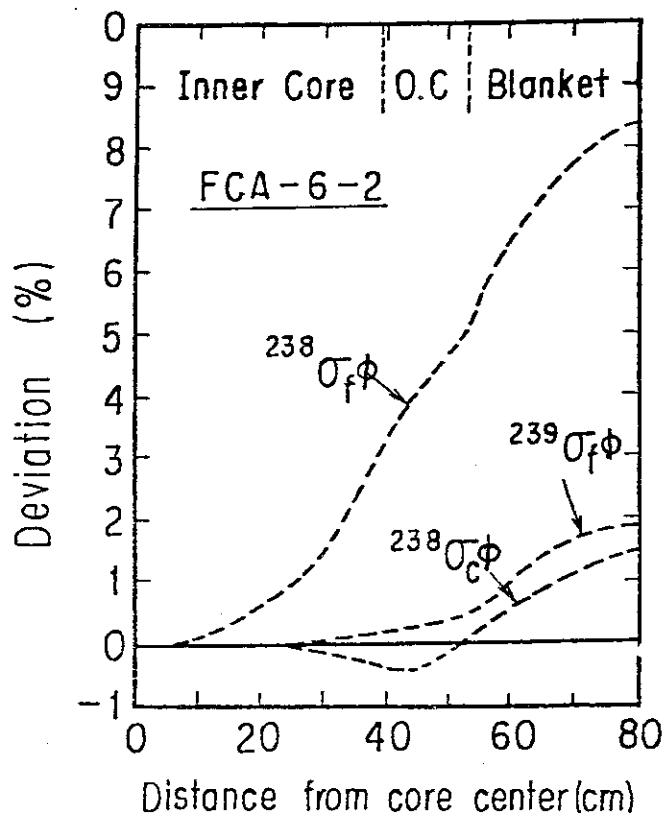


Fig.1.4.2 Deviations of the radial reaction rates calculated with the ^{239}Pu fission spectrum from those calculated with the region dependent fission spectra in FCA-6-2 assembly

2. Theoretical Methods and Code Development

2.1 Fuel Pin and Subassembly Heterogeneity Effect in Fast Power Reactor

M. Nakagawa and H. Inoue*

The heterogeneity effect of fuel pin and subassembly is estimated for criticality factor, Doppler effect, sodium void reactivity and reaction rate distributions in the proto-type fast reactor. The core of the power reactor under study consists of the hexagonal subassemblies with 169 and 61 pins for the core and the radial blanket, respectively. The unit subassembly and fuel pin are illustrated in Fig. 2.1.1. The analysis has been performed basing on the JAERI Fast set V2¹⁾ with the seventy group structure. The cell calculations were performed by SLAROM²⁾ which was modified for the application to the concentric hexagonal cell and the clustered pin rods with annular tube³⁾. The cell averaged effective cross sections were collapsed into the twenty five groups by weighting with neutron flux obtained in one dimensional diffusion calculations. The criticality factors have been calculated by the r-z diffusion calculations and the reactivities by the perturbation method.

At the present work, the investigation is made by using several geometrical and calculational models. In the cell calculations, it is important how to determine the appropriate admixture cross section σ_0 of the fuel element since the heterogeneity significantly affects on the resonance shielding effects.

The model description is given below.

1. Model 1 (homogeneous model)

The admixture cross section is defined by

$$\sigma_0^m = \frac{\sum_{n \neq m} N^n \sigma_t^n}{N^m} .$$

2. Model 2

The unit pin cell consists of the fuel, cladding, sodium and wrapper tube which has a equivalent volume per a single pin. The σ_0 value is defined by

* Japan Information Service Co. Ltd., Tokyo.

$$\sigma_0^m = \frac{\sum_{n \neq m} N^n \sigma_t^n}{N^m} + \frac{S_p}{4N^m V_p} \frac{(1-C)a}{1+(a-1)C}$$

where C is Dancoff factor for an infinite regular array of pin and given by the modified Bell approximation, and a, Bell factor. In this model, the contribution from the wrapper tube to the σ_0 value is taken into account equally for all the fuel pin in the subassembly.

3. Model 3

The unit pin cell consists of the fuel, cladding and sodium regions. The definition of σ_0 is the same as that the model 2, but the contribution from the wrapper tube is not taken into account.

4. Model 4

The unit pin cell is the same as the model 3, however, the contribution to σ_0 from the wrapper tube is considered as follows,

$$\sigma_0^m = \frac{\sum_{n \neq m} N^n \sigma_t^n}{N^m} + \frac{S_p}{4N^m V_p} \frac{(1-\Gamma)a}{1+(a-1)\Gamma} + \frac{\sum^W V^W P_{wk}}{N^m \sum_{n \neq m} V^l P_{lk}}$$

where Γ is Dancoff factor of the cluster geometry and P_{lk} the collision probability from the layer l to k, \sum^W , V^W the total cross section and volume of the wrapper tube. The collision probability is calculated for the concentric hexagonal geometry where each pin layer is represented as one region. The final cell averaged cross sections are obtained through the two steps of cell calculations. The first one is the unit pin cell calculations by using the σ_0 values mentioned above. The second one is the concentric hexagonal cell calculation by using the cross sections obtained in the first step.

The criticality factors and the heterogeneity effects are summarized in Table 2.1.1. The comparison of the criticality factors for the model 4 and 1 indicates the positive heterogeneity effect, $\Delta k = 0.488\%$. The Doppler reactivities are compared in Table 2.1.2 for the temperature change, $1340^\circ\text{K} \rightarrow 1740^\circ\text{K}$. The heterogeneity effect increases the negative Doppler reactivity by seven percents. The comparison of the sodium void reactivities is shown in Table 2.1.3 which indicates a decrement of the positive effect by 26 percents. The heterogeneity effect on the radial reaction rate distribution is about 2~3% for the capture of ^{238}U , and less than 1% in the core and 0~6% in the blanket for the fission of ^{239}Pu .

The present work was performed under the contracts between Power Reactor and Nuclear Fuel Development Corporation and Japan Atomic Energy Research Institute.

References

- 1) Takano H., et al.: "JAERI Fast Reactor Group Constants set, version II", JAERI 1255 (1978).
- 2) Nakagawa M. and Tsuchihashi K., "SLAROM", JAERI-M 5916 (1974).
- 3) Tsuchihashi K., "LAMP-B", JAERI 1259 (1979).

Table 2.1.1 Heterogeneity effect on criticality factor

Model	k_{eff}	Heterogeneity effect Δk (%)
Model 1 (Homo)	1.03287	
Model 2	1.03678	0.371
Model 3	1.04005	0.718
Model 4	1.03775	0.488

Table 2.1.2 Heterogeneity effect on Doppler reactivity

Model	$\Delta k/k'$ (1340°k- 1740°k)	($\times 10^{-3} \Delta k/k'$)
		Hetero / Homo
Model 1 (Homo)	-1.69	
Model 2	-1.79	1.06
Model 3	-1.86	1.10
Model 4	-1.81	1.07

Table 2.1.3 Heterogeneity effect on sodium void reactivity

Model	$\Delta k/k'$	($\times 10^{-3} \Delta k/k'$)
		Hetero / Homo
Model1 (Homo)	8.56	
Model 2	6.81	0.796
Model3	5.78	0.675
Model 4	6.33	0.739

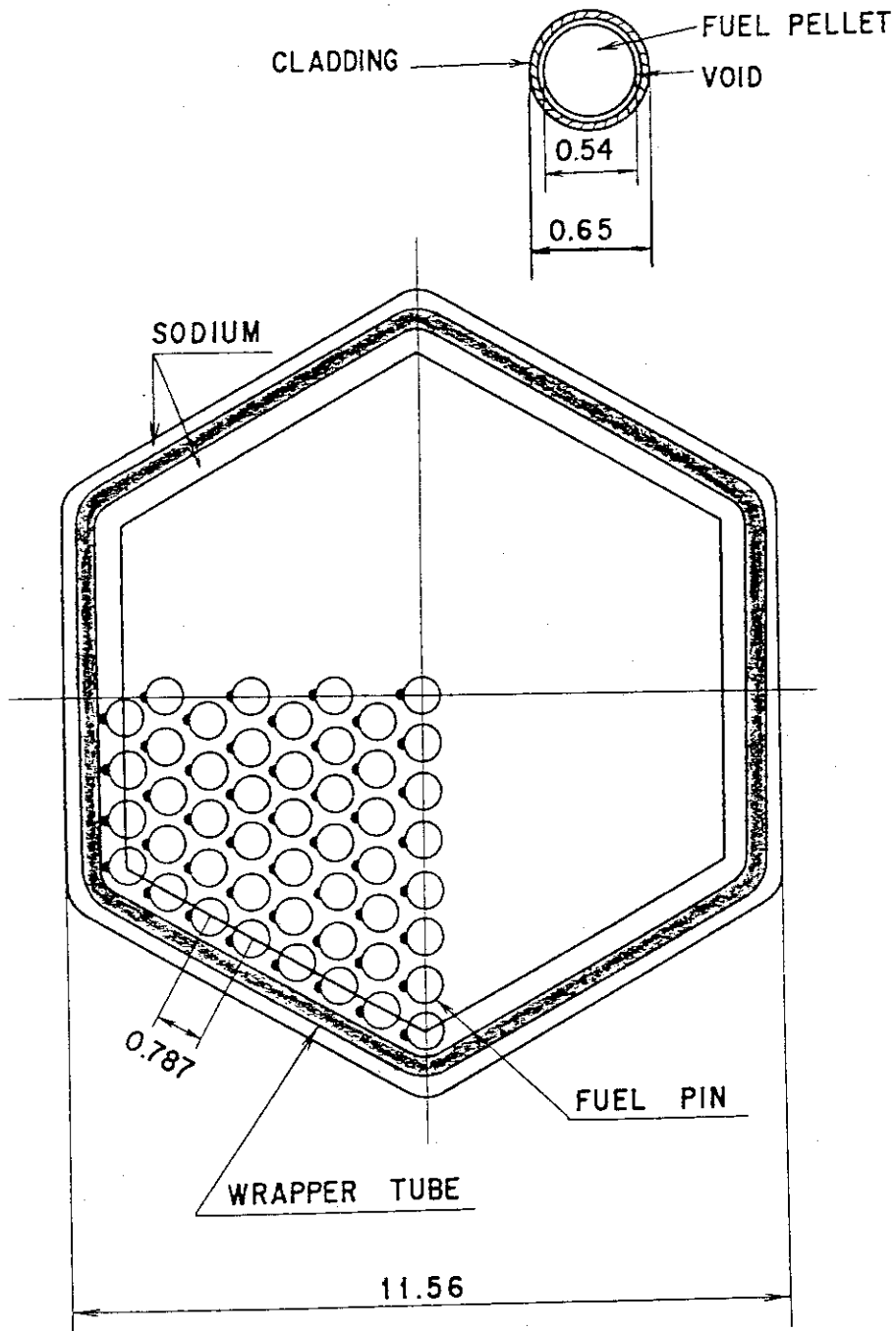


Fig.2.1.1.1 Cross sectional view of subassembly and fuel pin.
All dimensions are given in centimeters

2.2 Burn-up Calculations Applied to the NEACRP Fast Breeder Benchmark for International Comparison

M. Nakagawa, H. Yoshida and F. Ohta*

An international comparison calculation of a large (1250 MWe) LMFBR benchmark model was proposed at the annual NEACRP meeting in 1975. Ten countries participated in the comparison and sixteen solutions were contributed. The specialist's meeting was held in 1978 at ANL to discuss the results, and the final report on the solutions and the discussions published in ANL-80-78, NEACRP-L-243¹⁾. According to what was decided at the 22nd NEACRP meeting in 1979, a proposal was made for burn-up calculations applied to the identical LMFBR benchmark model. The aim of such an exercise is to provide a comparison of the multigroup data used by various laboratories for what concerns isotopes specifically involved in fuel burn-up problems; fission products (F.P.) and actinides. The following core characteristic parameters are investigated by comparing the end-of-cycle values to the fresh core ones:

- Reactivity loss per cycle
- The internal and external breeding gains,
- Radial and axial fission rate distributions,
- Pu balance for the inner and outer cores and for the axial and radial blanket, and
- Sodium void effect corresponding to the inner core voiding

For the previous intercomparison, three solutions were contributed from Japan. Three were calculated basing on the JENDL-1²⁾, the JAERI Fast 2 data³⁾ and the JAERI Fast V2 set with 25 group structure⁴⁾. Since the present proposal aims to compare the nuclear data of F.P. and actinides, these data are insufficient for such a purpose. The present calculations have been performed basing on the JENDL-2. The parameter of the fresh core have been recalculated in order to enable direct comparisons with those of the end-of-cycle core.

The effective microscopic cross sections for fresh core elements have been obtained with use of the ESELEMS⁵⁾ code in 25 groups by weighting with a fundamental mode fine spectrum. Those of F.P. and actinides

* Japan Information Service Co. Ltd., Tokyo.

have been generated by using the PROF-GROUCH G2 code⁶⁾ by weighting with the 1/E and fission spectrum. The burn up calculations have been performed in R-Z geometry by the diffusion theory code PHENIX⁷⁾ and the irradiated fuel composition have been obtained at the end-of-cycle of the inner core zone 1 by using the zero dimensional burn up code FPGS-3⁸⁾.

The calculational model is almostly identical to the previous comparison, but the core and the blanket regions are divided into six inner zones, four outer core zones, four radial blanket zons and ten axial blanket zones. The calculational methods are also identical to those used for the fresh core.

In the following, we show the parts of the solution. Table 2.2.1 compares the core parameters between the fresh-core and the end-of-cycle core. In the previous calculations, the JENDL-1 gave 1.0066 of K_{eff} and 0.0220 $\Delta k/k$ for the inner core sodium void reactivity. Table 2.2.2 shows the reactivity loss due to the one cycle burn up (The cycle length 360 full equivalent power days with a constant level of 3000 MWth.). Table 2.2.3 shows the Pu balance for the inner core and the axial blanket. The final results of all countries will be compiled and published by Hammer (France) in near future.

References

- 1) Lesage L.G., et al.: "International Comparison Calculation of a Large Sodium-Cooled Fast Breeder Reactor", ANL-80-78, NEA-CRP-L-243 (1980).
- 2) Yoshida H., et al.: *ibid.*
- 3) Nakagawa M. and Zukeiran A.: *ibid.*
- 4) Zukeiran A. and Nakagawa M.: *ibid.*
- 5) Nakagawa M., et al.: "ESELEM4", JAERI-1245 (1976).
- 6) Hasegawa A., Kaneko K. and Takano H., to be published.
- 7) O' dell R.D. and Hirons T.J.: "PHENIX, a Two-dimensional Diffusion-Burnup-Refueling Code", LA-4231 (1970).
- 8) Ihara H., et al.: "FPGS-3", Unpublished report.

Table 2.2.1 Comparison of core parameters between fresh core and end-of-cycle core

Parameter	Fresh core	End-of-cycle core
k_{eff}	1.0071	0.9923
Total B.R.	1.3605	1.3191
Total B.G.	0.3386	0.3216
1/C sodium void reactivity	0.02710	0.03254
Central reaction rate		
$^{28}_{C} / ^{49}_{f}$	0.1619	0.1612
$^{28}_{f} / ^{49}_{f}$	0.0238	0.0240
$^{49}_{c} / ^{49}_{f}$	0.3228	0.3172

Table 2.2.2 Reactivity loss per cycle *

	Δk
Global reactivity loss	-0.0147
Reactivity gain due to Pu build up in blanket	0.0056
Reactivity loss due to F.P. build-up	-0.0187
Reactivity loss due to core heavy isotope burn-up	-0.0007

* It is assumed that all $^{239}_{Np}$ decays to $^{239}_{Pu}$.

Table 2.2.3 Pu balance for inner core and axial blanket
(unit : 10^{24} atom/cm³)

	Inner core		Axial blanket	
	N (Fresh)	N (End)	N (Fresh)	N (End)
$^{238}_{Pu}$	0.0	3.811 -9	0.0	3.033 -10
$^{239}_{Np}$	0.0	1.915 -6	0.0	6.623 -7
$^{239}_{Pu}$	7.704 -4*	8.081 -4	0.0	9.591 -5
$^{240}_{Pu}$	2.208 -4	2.530 -4	0.0	1.938 -6
$^{241}_{Pu}$	1.165 -4	8.809 -5	0.0	2.860 -8
$^{242}_{Pu}$	2.79 -5	3.240 -5	0.0	2.461 -10

* Read as 7.704×10^{-4} .

2.3 Development of Interface Program JOINT for Fast Reactor Neutronics Calculation Code System

M. Nakagawa and J. Abe*

In the course of analysis of neutronics parameters in fast reactors or fast critical assemblies, we must use many codes handling various type of data. Since the data formats of input and output are usually not unified, we must convert them many times. Such works are laborious and cause many troubles and errors for users. It is very effective to unify the data format and to reduce the data handling of users in the course of analysis. We are developing a code system for fast reactor analysis since 1979. We intended at first to unify the format of cross sections and to develop the interface program which links many codes. This code system consists of the following codes at present stage.

1. Generation code of multi-group data library
 PROF-GROUCH-G2, TIMS1, JFSMAKE, PRESM, PRETIM
2. Lattice cell calculation codes (These produce geometry-, composition- and temperature- dependent effective cross sections.)
 SLAROM, ESELEM5, TIMS-2
3. Diffusion theory codes
 EXPANDA-G (1D), CITATION-FBR (2, 3D)
4. Transport theory codes
 ANISN-JR, TWOTRAN2, MORSE
5. Perturbation codes
 CIPER, PERKEY, SNPRT
6. Burn-up code
 PHENIX (2D)
7. Interface and utility codes
 JOINT, PDS utility, plotter utility codes

In the code system, cross sections, fission spectrum and buckling produced are saved in the PDS file (partitioned data set file) with the unified format together with the identification data. The data set of macroscopic cross sections consist of the following quantities: Σ_a , $\nu\Sigma_f$, D_{av} , $D_{v'}$, D_{\perp} , Σ_{tr} , Σ_t , Σ_f , Σ_s , $\Sigma_{sg \rightarrow i}$, $\Sigma_{sl, g \rightarrow i}$ (elastic scattering matrix

* Japan Information Service Co. Ltd. (Tokyo)

of P_{ℓ} component) and that of microscopic cross sections have σ_a , $\nu\sigma_f$, σ_{tr} , σ_f , σ_s , σ_{in} , $\sigma_{n,2n,\bar{u}}$, σ_D , $\sigma_{sg \rightarrow i}$, $\sigma_{sl, g \rightarrow i}$ for each energy group. The undefined data are set to be 0. The interface program JOINT reads cross sections from the PDS file and convert format to prepare the input file of the neutronics calculation codes. The input data file for these code are also prepared by the JOINT code. The flow of data and the interrelations of the codes are shown in Fig. 2.3.1 The utility programs have been developed to write, read, dump and delete the data in the PDS file. The JOINT code is designed to be able to extent the function by adding new subroutines when new codes are introduced into the system. In essential, this code does not perform algebraic computations, so the CPU time is very short.

The present work was performed under the contracts between Power Reactor and Nuclear Fuel Development Corporation and Japan Atomic Energy Research Institute.

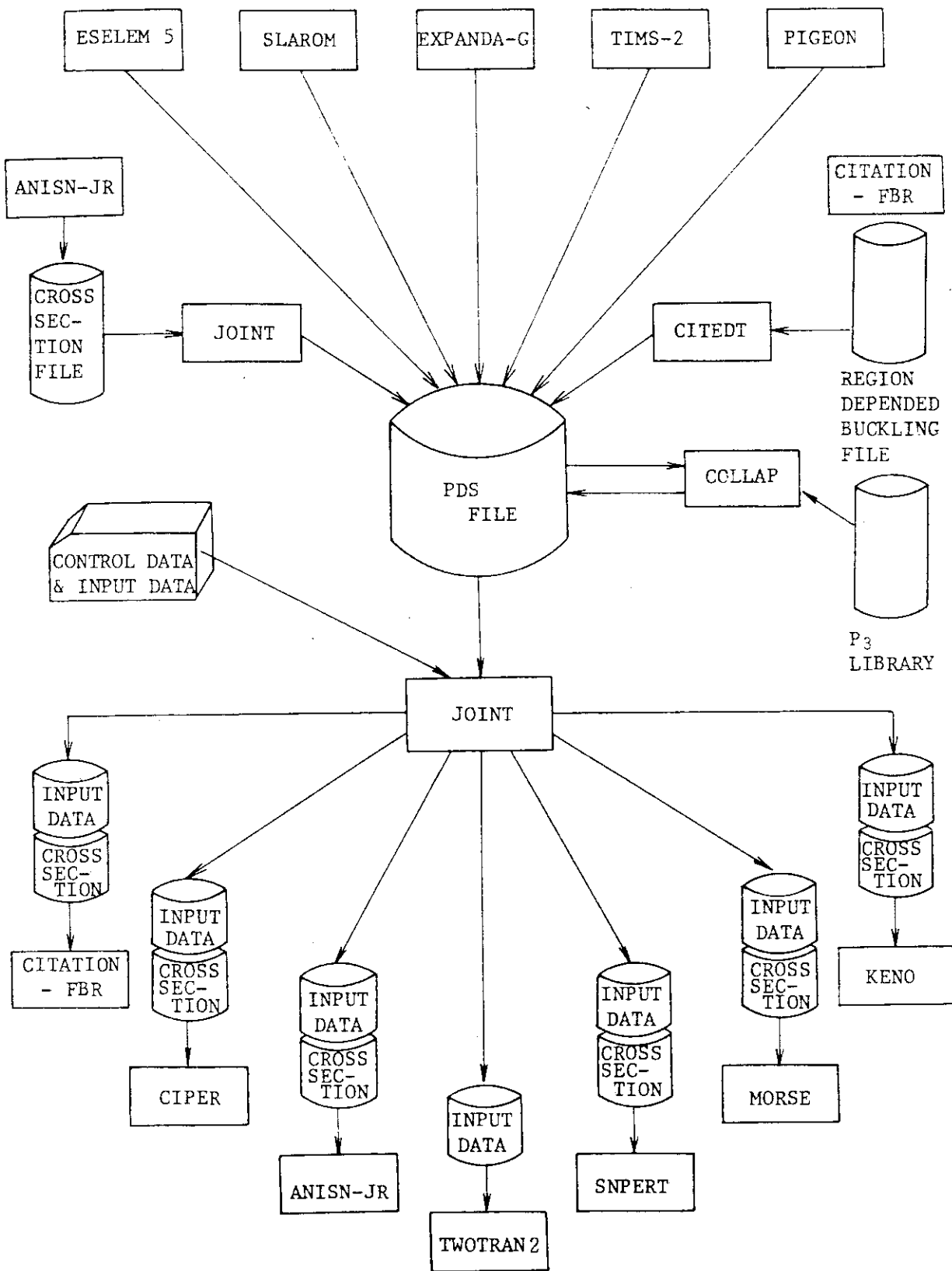


Fig.2.3.1 Flow of input data and cross section

2.4 SRAC : A Standard Computer Code System for Lattice Cell and Core Calculations on Reactor Design and Analysis (II); Benchmark Test

K. Tsuchihashi, F. Akino, H. Nagaoka*, K. Horikami, H. Takano and Y. Ishiguro

The SRAC system was completed excepting the part of fuel depletion calculation in fiscal year 1980. A series of Benchmark Tests had been done for the K_{eff} values of the various types of thermal reactor critical assemblies. The assemblies adopted for these Benchmark Test are summarized in Table 2.4.1. Here, the Benchmark problem for fast reactor was settled to assess to accuracy of the library adopted in the fast energy region.

For thermal reactor problems, the effective macroscopic cross sections in the resonance energy region were calculated by using both the IRA method and the ultrafine group code PEACO to check the applicability of the former simple and time saving method. In the thermal energy region, the cell calculations were made with the collision probability method, and the effective cross sections were calculated by a cell-homogenization procedure without collapsing the User Lib. energy group⁸⁾. The resulting macroscopic section sections were collapsed into few groups constants by using the 1-d. diffusion code TUD to take account of their space dependence. The overall K_{eff} calculations were carried out through the diffusion code path with the 2- or 3-d. option depending on the geometry under study.

The results obtained are shown in Tables 2.4.2 ~ 2.4.7. It will be seen that the K_{eff} values obtained from the SRAC system are generally in an excellent agreement with experimental results. The values for the fast-reactor Benchmark problems are however fairly underestimated. This underestimate can be attributed to the well-known fact that a group constant set based on the ENDF/B-4 nuclear data file gives lower K_{eff} value.

A detailed description of these rescriptions, together with the additional calculated results, will be published in near future.

* Division of JMTR, Oarai Research Establishment.

References

- 1) Tsuruta H., et al.: "Critical Sizes of Light-Water Moderated UO₂ and PuO₂-UO₂ Lattices", JAERI 1254 (1977).
- 2) Nagaoka H., et al.: to be published.
- 3) Hachiya Y., et al.: J. Nucl. Sci. Technol., 13(11), 618 (1976).
- 4) Kaneko Y., et al.: JAERI 1257 (1978).
- 5) IAEA-TECDOC-233 (1980).
- 6) NNCSC (Ed.): "CSEWG benchmark specifications", ENDF-202 (1974).
- 7) Iijima T., et al.: "FCA Assembly VI-2 Critical Experiment", JAERI-M 7888 (1978) (in Japanese).
- 8) Tsuchihashi K.: "LAMP-B: A Fortran Program Set for the Lattice Cell Analysis Collision Probability Method", JAERI 1259 (1979).
- 9) Hasegawa A., et al.: "A One-Dimensional Diffusion Code for Multigroups Criticality and Perturbation Calculations with JAERI-Fast Set of 70-group Structure: EXPANDA-70D", JAERI-M 4953 (1972) (in Japanese).

Table 2.4.1 Critical assemblies used for benchmark tests

No.	Assembly	Case	Remarks	Ref.
1	TCA	9	light-water moderated UO_2 lattices	1)
2	JMTRC	4	critical assembly for Japan MTR	2)
3	DCA	1	D_2O moderated assembly for ATR (initial loading core)	3)
4	SHE	7	Graphite moderated critical assembly with 20% enriched ^{235}U fuel.	4)
5	(IAEA Benchmark Problem)	1	Safety related benchmark problems on RERTR (reduction of enrichment of research reactor)	5)
6	(Benchmark Problem for Fast Reactors)	21	CSEWG Benchmark problems + four ZPR-3 assemblies + FCA assembly ⁷⁾	6)

Table 2.4.2 Calculated K_{eff} values for TCA

Core pattern ($V_{\text{H}_2\text{O}} / V_U$)	Critical water level (cm)	K_{eff}^*
20 (20 x 20) (1.50)	73.49	0.9960 (0.9926)**
24 (22 x 22) (1.50)	53.12	0.9976 (0.9915)
28 (24 x 24) (1.50)	43.89	0.9985 (0.9883)
1 (12 x 29) (1.83)	131.94	0.9975
2 (14 x 27) (1.83)	69.01	0.9998
15 (18 x 18) (1.83)	75.32	0.9983
20 (20 x 20) (1.83)	51.65	0.9992
5 (15 x 15) (3.00)	90.75	1.0044
18 (19 x 19) (3.00)	41.54	1.0078

*) The exposed part of fuel pin above the water level was corrected by a simple model based on the diffusion calculation.

**) The parentheses show the uncorrected value.

Table 2.4.3 Calculated K_{eff} values for JMTRC

Core Case	Experiment	S R A C						THERMOS-JMTR, GGC-4	
		1	2	3	4	5	6		
1	1.01654	1.01974	1.01921	1.01656	1.01598	1.00896	1.00839		
2	1.01059	1.01400	1.01347	1.01047	1.00986	1.00286	1.00223		
3	1.00343	1.00772	1.00717	1.00383	1.00315	0.99620	0.99551		
4	1.00127	1.00484	1.00428	1.00086	1.00011	0.99309	0.99229		
Cell and	Fuel Flower	No Extra Region							
Collapsing Model	32S 4F ALFR	→	→	Extra Region (Cylindrical)	Extra Region (Plane)	→	Extra Fuel Region(2cm) (thermal only)		
		→	TUD	TUD	TUD	→	No Extra		
Reflector									

Table 2.4.4 Calculated K_{eff} values for DCA Initial Core

Conditions	K_{eff}	$\Delta K_{eff}(\%)$
SRAC Standard*	1.0007	—
σ_t by summation	1.0008	0.01
Σ_{tr} by consistent transport correction	0.9997	-0.10
D by Isotropic Behrens Benoist	0.9896	-1.11
Resonance Integral by I.R.A	1.0020	0.13
Resonance Integral by Table-Look-Up	0.9980	-0.27
LAMP-A (Ref. 8)	1.0113	1.04

*) Standard Specifications

Lattice Pitch	22.5 cm square
Critical Radius	139.2 cm
Critical Height	96.2 cm (heavy water)
Theoretical Critical Height	105.0 cm ($B_z^2 = .000895 \text{ cm}^{-2}$)
Core Radius	150.0 cm
σ_{tr} by Harmonic Average	
Σ_{tr} by B_1 Approximation	
D by $1 / (3 \Sigma_{tr})$	

Table 2.4.5 Calculated effective multiplication factor K_{eff} for SHE

Core configuration	C/235 _U	core radius (cm)	calculated values of K_{eff}
SHE-5	5483	35.10	1.0015
SHE-6	4395	33.17	1.0050
SHE-7	3359	31.04	1.0071
SHE-8	2316	28.71	1.0075
SHE-12	6785	37.28	1.0140 (1.0053)*
SHE-13	15724	55.76	1.0184 (1.0097)*
SHE-14	7158	39.54	1.0127 (1.0040)*

*) Corrected values for neutron streaming and end cap effect.

Table 2.4.6-1 Comparison of SRAC-CELL k_{∞} with ANL results (T=300°K)

Burnup (%)	Enrichment			
	93%		20%	
	ANL	JAERI*	ANL	JAERI*
0	1.73698	1.7451	1.65475	1.6473
5	1.63697	1.6531	1.56410	1.5725
10	1.61653	1.6415	1.54447	1.5621
25	1.54853	1.6009	1.47972	1.5255
30	1.52227	1.5846	1.45544	1.5109
45	1.42692	1.5217	1.37191	1.4574
50	1.38761	1.5024	1.33935	1.4362

*) The lumped fission products were not included.

Table 2.4.6-2 Control rod worths

Core	Fuel	Control Rod	Control Rods Withdrawn	Control Rods Fully inserted $\Delta\rho$, %
HEU	BOL	Ag/In/Cd		0.9360(0.8787) 10.83(17.03)
		B ₄ C	1.0496 (1.0333)*	0.9582(0.8438) 8.70(21.74)
HEU	Fresh	Ag/In/Cd		1.0727(1.0337) 9.51(12.97)
		B ₄ C	1.1855 (1.1937)	1.0825(0.9924) 8.68(17.00)
HEU	BOL	Ag/In/Cd		0.9410(0.8915) 9.55(14.47)
		B ₄ C	1.0403 (1.02353)	0.9502(0.8575) 8.67(18.91)
HEU	Fresh	Ag/In/Cd		1.0557(1.0305) 8.44(11.53)
		B ₄ C	1.1531 (1.1695)	1.0568(0.9911) 8.35(15.39)

*) The parentheses show ANL results.

Table 2.4.7 Calculated K_{eff} values for Benchmark test problems of fast reactors

No.	Assembly	Fuel	JFS data	JENDL-II B	ENDF/B-4 data	
			EXPANDA code for fast reactor(Ref.9)			SRAC
1	VERA-11A	P _U	0.99240	0.99236	0.9855	0.9861
2	VERA-1B	U	1.00360	0.99537	0.9954	0.9953
3	ZPR-3-6F	U	1.01660	1.01225	1.0095	1.0095
4	ZEBRA-3	P _U	0.99797	0.99825	0.9917	0.9850
5	ZPR-3-12	U	1.00697	1.00114	0.9987	0.9985
6	SNEAK-7A	P _U	1.00508	1.00135	0.9915	0.9892
7	ZPR-3-11	U	1.00800	1.00211	1.0050	1.0041
8	ZPR-3-54	P _U	0.95435	0.95443	0.9338	0.9347
9	ZPR-3-53	P _U	0.99650	0.99116	0.9777	0.9747
10	SNEAK-7B	P _U	1.00436	0.99852	0.9896	0.9842
11	ZPR-3-50	P _U	0.99848	0.99709	0.9817	0.9747
12	ZPR-3-48	P _U	1.00306	1.00049	0.9891	0.9852
13	ZEBRA-2	U	0.98523	0.98314	0.9781	0.9751
14	ZPR-3-49	P _U	1.00416	1.00546	0.9924	0.9882
15	ZPR-3-56B	P _U	0.99668	0.98885	0.9775	0.9750
16	ZPR-6-7	P _U	1.00332	0.99368	0.9816	0.9736
17	ZPR-6-6A	U	1.00191	0.99884	0.9895	0.9857
18	ZPPR-2	P _U	1.00874	1.00037	0.9887	0.9789
19	MZA	P _U	1.00119	0.99446	0.9842	0.9904
20	MZB	P _U	1.00129	0.99114	0.9809	0.9784
21	FCA-V-2	P _U	1.00910	1.00567	0.9787	0.9797

2.5 A Fortran Program CLUPH of Collision Probabilities for Hexagonal Lattice and Its Application to VHTR

K. Tsuchihashi and Y. Gotoh

The design study of the multi-purpose very high temperature gas cooled reactor has been advanced in JAERI. In the course of the study it has been realized that the severe accuracy is required in the prediction of the reactivity worth of the control rods in the safety aspect and also of reactivity worth of the burnable poison rods in the fuel management aspect.

To solve the obscurity arising from asymmetric insertion of the control rods or the burnable poison rods into the graphite block (Fig. 2.5.1), a geometric sub-program CLUPH is developed and added to the program set LAMP-B⁽¹⁾ to complete the cell calculation by the collision probability method.

CLUPH⁽²⁾ has the following function to analyze the fuel and control rod block. Each rod may have the different diameter and composition. The moderator region can be divided into the sectors by the lines radiated from the center of the cell. The hexagonal block can be treated exactly. In addition to the reflective condition on the boundary of cell, the periodic and the rotational arrays of hexagonal blocks can be considered. The block which is surrounded by the fuel and graphite blocks, can be analyzed.

The program developed is applied to the analysis of Mk-III core of VHTR. The difference are estimated between the hexagonal and the cylindrical cell analysis of fuel block. The average cross section of control rod block are derived from the calculation of the super cell shown in Fig. 2.5.2.

References

- 1) Tsuchihashi K.: "LAMP-B; A Fortran Program Set for the Lattice Cell Analysis by Collision Probability Method", JAERI 1259 (1979).
- 2) Tsuchihashi K. and Gotoh Y.: "CLUPH; A Fortran Program of Collision Probabilities for Hexagonal Lattice and its Application to VHTR." JAERI-M 9301 (1981).

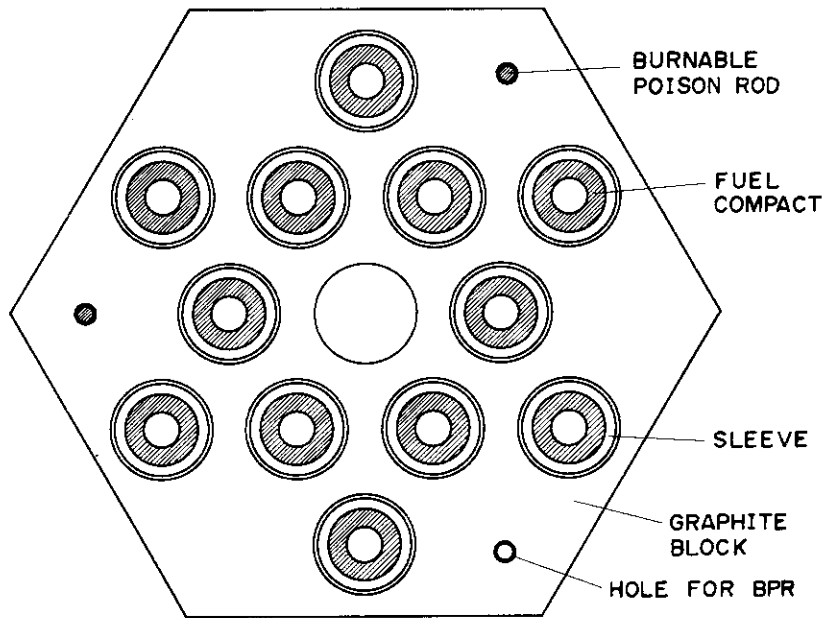


Fig.2.5.1 Standard fuel block of VHTR

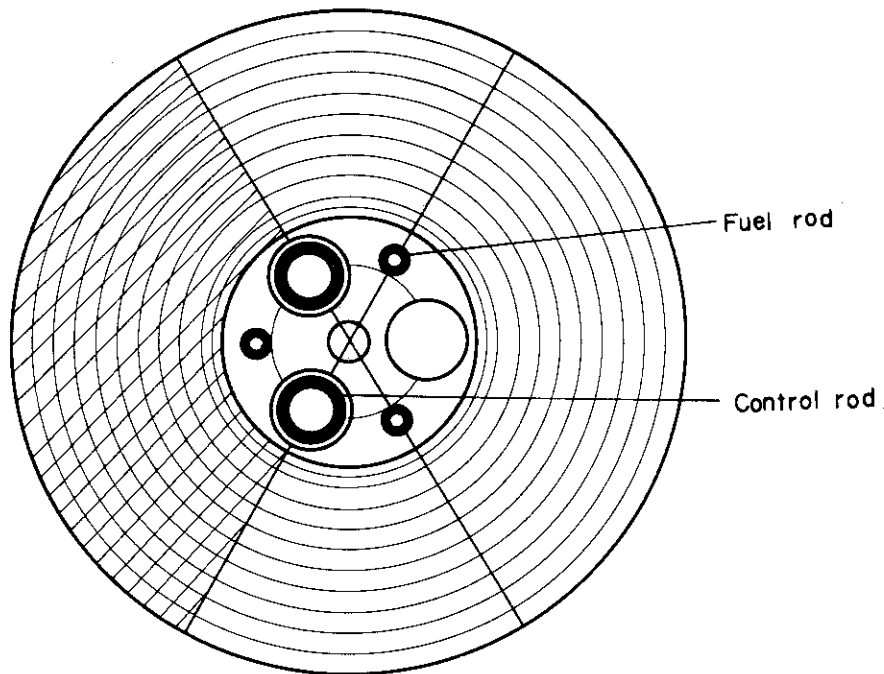


Fig.2.5.2 Super cell of control rod block

2.6 A Code Development for Calculation of Double Differential Cross Section

Y. Ishiguro

A revised version of SUPERTOG code, PROF-GROUCH-GII, has been modified to generate a group constants library of the neutron production double differential cross section $\sigma(\mu_0; E' \rightarrow E)$, where μ_0 is the neutron scattering angle in the laboratory system. This library aims to be used in a neutronics code for shielding and/or fusion reactor blanket physics problems. By the use of the library, the neutron slowing down source in a neutron transport code can be directly calculated by the relation

$$\mu_0 = \mu\mu' + \sqrt{(1-\mu^2)(1-\mu'^2)} \cos(\phi-\phi'),$$

where the μ_0 -values can be tabulated for the discrete values of μ , μ' and $(\phi-\phi')$. The library can be also applicable to a transport code based on the li-method¹⁾.

This modified code can treat a nuclear data file in the ENDF/B Format²⁾. For the present, the exact treatment for angular-energy correlation is available only for elastic scattering and discrete $(n, n')\gamma$ reaction, but the neutrons produced by the other reactions are assumed to be isotropically distributed in the laboratory system. The other approximations assumed to reduce the core and/or disk memories are as follows:

- The ratio $R_{xg} \equiv m_x \langle \sigma_x \rangle_g / \langle \sigma_{pr} \rangle_g$ is let be zero when $R_{xg} \leq \epsilon$, where m_x is the neutron multiplicity, $\langle \sigma_x \rangle_g$ and $\langle \sigma_{pr} \rangle_g$ is, respectively, the group cross section for the reaction x and for the total neutron production.
- The group cross section, $\langle \sigma_{in,i} \rangle_g$, is set to zero for the energy group where the threshold energy, $E_{th} = Q_i A / (A+1)$, exists.
- The maximum number of energy groups is restricted to be 100.

The expressions used in the present code are as follows:

$$\langle \sigma_{pr} \rangle_g = \sum_x m_x \langle \sigma_x \rangle_g, \quad R_{xg} = \frac{m_x \langle \sigma_x \rangle_g}{\langle \sigma_{pr} \rangle_g}$$

$$\sigma(\mu_{0k}; E_{g'} \rightarrow E_g) = \langle \sigma_{pr} \rangle_g \sum_x R_{xg} I_x(\mu_{0k}; E_{g'} \rightarrow E_g)$$

$$\equiv \langle \sigma_{pr} \rangle_g I(\mu_{ok}; E_{g'} \rightarrow E_g)$$

$$I_x(\mu_{ok}; E_{g'} \rightarrow E_g) = \begin{cases} \frac{f_x(E_{g'}, \mu_c(g', g)) \Delta \mu_{ok}}{\pi (1-\gamma) \beta_{xg'} E_{g'}} & \text{if } \mu_0(g', g) E \Delta \mu_{ok}, \\ 0 & \text{otherwise} \end{cases}$$

$$\beta_{xg'} = 1 - \frac{Q_x}{E_{g'}}$$

$$I_x(\mu_{ok}; E_{g'} \rightarrow E_g) = \frac{1}{4\pi} \frac{\langle \sigma_x(E_{g'} \rightarrow E_g) \rangle}{\langle \sigma_x \rangle_g}$$

References

- 1) Takahashi A. and Dusch D.: KFK 2832/1 (1979).
- 2) Data Formats and Procedures for the ENDF Neutron Cross Section Library
: ed. by Drake M.K., BNL 50274 (T-601) ENDF 102 Vol.1

2.7 A Program Package for the Solution of Linear, Integer, Quadratic and Nonlinear Programming Problems

K. Horikami, T. Fujimura and Y. Nakahara

In many fields, it is often faced that one wishes to maximize or minimize some function in order to optimize complex arrangement of equipments, operations, or processes.

For the solution of several kinds of mathematical programming problems twentyfour computer programs have been prepared and these programs are at present on FACOM M200 computer as a member of JSSL (JAERI Scientific Subroutine Library). A set of auxiliary programs has also equipped to facilitate the use of this program package, with the main stress on the reduction of users' effort for the preparation of their main program.

For Linear programming problems, five programs have been made, one of which is specially designed to solve large scale problems by using decomposition algorithm. Two programs for quadratic programming problems, one for integer programming problems, twelve for nonlinear programming problems without constraint and four programs for nonlinear programming problems with constraints have been created. The formulation together with associated constraint type, the explanation on the calculational procedure, the meaning of the arguments in the calling sequence of each program and the instructions about input data requirements of each auxiliary program have been given in the references^{1),2),3)}.

In the following, all programs with brief comment on the method are listed. The programs in the parenthesis show the auxiliary programs concerned.

Programs for linear programming problems

SIMPLX (SIMPLM) : simplex method
 DUSEX (DUSEXM) : dual simplex method
 RESEX (RESEXM) : revised simplex method
 DUOPLX (DUOPLM) : duoplex method
 DEPRI (DEPRIM) : decomposition principle

Programs for quadratic programming problems

BEALE (BEALEM) : Beale's algorithm
 WOLFE (WOLFEM) : Wolfe's algorithm

Program for Integer programming problems

GOMORY (GOMORM) : Gomory's algorithm

Programs for nonlinear programming problems without constraint

ALCODR (ALCODM) : direct search method by Powell

ALPS (ALPSM) : direct search method by Hooke and Jeeves

ALSIM (ALSIMM) : direct search method by Nelder and Mead

DSC (DSCM) : direct search method by Davies, Swann and Compey

ROTAX (ROTAXM) : direct search method by Rosenbrock

ALPART (ALPARM) : pararell trangent method

BROYDN (BROYDNM) : variable metric method by Broyden

CGD (CGDM) : conjugate gradient method by Flecher and Reeves

FPD (FPDM) : variable metric method by Davidon, Fletcher and Powell

PRJNEW (PRJNEM) : projected Newton method

MINIM (MINIMM) : Neuton method mixed with steep descent method

NEWTON (NEWTOM) : Newton method

Programs for nonlinear programming problems with constraints

COMPLX (COMPLM) : random method by Box

CORASE (CORASM) : random method by Price

FLXPLX (FLXPLM) : flexible telerance method

KEELE (KEELEM) : Murtagh and Sargent method

References

- 1) Horikami K., Fujimura T. and Nakahara Y.: "A Program Package for Solving Linear Optimization Problems: User's Manual", JAERI-M 9048 (1980).
- 2) Horikami K., et al.: "A Program Package for Solving Nonlinear Optimization Problems: User's Manual", JAERI-M 9154 (1980).
- 3) Fujimura T., Horikami K. and Nakahara Y.: "DEPRI, DEPRIM: Programs for Solving Large Linear Optimization Problems by Decomposition Principle", JAERI-M 9315 (1981).

2.8 Development of a Double Finite Element Method Program for Solving Three-Dimensional Multi-Group Neutron Transport Equation

Y. Nakahara, T. Fujimura and M. Matsumura*

Following the successes in structural analysis, the finite element method (FEM) has been recently applied to radiation transport problems. But in the three-dimensional multi-group neutron transport problem, computer codes based on the Monte Carlo and S_n methods have been mainly used as yet. The Monte Carlo computation is expensive and it does not give the deterministic solutions. The diamond difference S_n method lacks in the geometric flexibility and has inherent difficulty in giving a reasonable angular distribution due to the ray effects.

With the intention of overcoming these difficulties, we have been developing a double FEM code, in which the space and angle finite elements are applied. At first, we tried to use the Vlasimirov-Ritz-Galerkin method in formulating the solution algorithm, but the method was found later not to be appropriate to the anisotropic scattering problem. Now the simple Galerkin method is employed in our algorithm, main features of which are as follows:

- (1) The whole, a quarter or a one-eighth of multilateral prism-shaped (parallel with z-axis) reactor system is considered¹⁾.
- (2) The boundary conditions are assumed to be vacuum or reflective.
- (3) The system is divided into a number of (x, y) planar layers.
- (4) Each layer is divided into a number of prism or box-shaped elements.
- (5) Six directions that are perpendicular each other are defined in the angular domain.
- (6) Angular flux of each group is approximated by the bilinear function of the space and angle bases²⁾.
- (7) Order of anisotropy of scattering cross sections are assumed at most P_3 . Thus, the scattering source can be anisotropic.
- (8) The system equation is obtained by adopting Galerkin procedure for the residual.
- (9) The equation is solved by applying point SOR successively to (x, y) planes. In the inner iterations, coarse mesh rebalance technique is

* I.S.L. Co. Ltd., Tokyo

used and the outer iterations are accelerated by source extrapolation.

These algorithms have been incorporated in a new computer code FEMTRAN-3D and the test calculations for model problems are in progress.

References

- 1) Ise T., Yamazaki T. and Nakahara Y.: "FEM-BABEL A Computer Program for Solving Three-Dimensional Neutron Diffusion Equation by the Finite Element Method", JAERI 1256 (1978).
- 2) Kaper H.G., Leaf G.K. AND Lindeman A.J.: "Applications of Finite Element Methods in Reactor Mathematics. Numerical Solution of the Neutron Transport Equation", ANL-8126 (1974).

2.9 ACCEL : A Computer Code System for Analyzing Nuclear Characteristics of Proton Accelerator Target/Blanket Assembly

Y. Nakahara, T. Tsutsui and Y. Taji

A Computer code system ACCEL has been prepared for analyzing nuclear characteristics of target/blanket assemblies of a proton accelerator. ACCEL is used to perform feasibility studies of accelerator breeding and transmutation concepts. Interrelations of computer codes and flow of calculations are shown in Fig. 2.9.1. The design concept of the code system is based on the BNL code system¹⁾ prepared for the analysis of Light Water Reactor Fuel Enricher/Regenerator²⁾.

Main outputs from ACCEL are the followings:

- (a) neutron yield, neutron flux distribution and spectrum,
- (b) distributions of primary and secondary protons, spectrum of secondary protons,
- (c) mass and charge distributions of spallation and fission products,
- (d) reaction rates distributions, etc.

The first stage of nuclear reactions (cascade, evaporation and fission) and nucleon transport processes, initiated by incident protons from a linear accelerator, is simulated by the Monte Carlo code NMTC/JAERI³⁾, which is a new version of NMTC⁴⁾ modified at JAERI to include the high energy fission in competition with the evaporation. The outline of our fission model and the scheme of how to perform the Monte Carlo simulation of the fission process is described in Section 2.10 of this report.

The cascade cut-off energies for neutrons and protons are taken to be 15 MeV. The neutron cross sections used in the neutron transport calculations in the energy range below 15 MeV are based on the ENDF/B-4 nuclear data file. The fine energy group cross sections with the GAM-II 100 group structure are obtained for each nuclide by processing the ENDF/B-4 data with SUPERTOG-JR3⁵⁾. The 100 group cross section set with up to the P_3 component are combined by TAPEMAKER⁵⁾ into a single file. TOTAL COUPLE and GROUP INDEPENDENT⁵⁾ are used to convert the format to that of one dimensional neutron transport S_n code ANISN⁶⁾. The 100 group data are collapsed to the 10 group data with ANISN for use as input data to the two dimensional neutron transport S_n code TWOTRAN-II⁷⁾.

A collision event file prepared during a NMTC/JAERI calculation is analyzed with the HIST3D/A and HIST3D/B⁸⁾ codes to make neutron source distribution files to be used as inputs to ANISN and TWOTRAN-II, respectively.

The final neutron transport calculations in the energy range below 15 MeV are performed with TWOTRAN-II. The total neutron yield in the whole energy range (1000 ~ 0 MeV) is obtained from the results of NMTC/JAERI and TWOTRAN-II calculations.

Mass and charge distributions of spallation and high energy fission products are obtained by analyzing a reaction event file prepared during the NMTC/JAERI calculation with use of NMTA⁹⁾.

Acknowledgements are much due to Dr. H. Takahashi (BNL) for his aides to the present work.

References

- 1) Takahashi H. and Nakahara Y.: Bull. Amer. Phys. Soc., 24, 874 (1979).
- 2) Kouts H.J., et al.: "Conceptual Design and Economic Analysis of a Light Water Reactor Fuel Enricher/Regenerator", BNL-50838 (1978).
- 3) Nakahara Y. and Tsutsui T.: unpublished.
- 4) Coleman W.A. and Armstrong T.W.: "NMTC Monte Carlo Nucleon Meson Transport Code System", RSIC ORNL CCC-161.
- 5) Koyama K., et al.: "RADHEAT-V3, A Code System for Generating Coupled Neutron and Gamma-ray Group Constants and Analyzing Radiation Transport", JAERI-M 7155 (1977).
- 6) Engle W.W. Jr.: "ANISN, A One Dimensional Discrete Ordinate Transport Code", RSIC ORNL CCC-82.
- 7) Lathrop K.D. and Brinkley F.W.: "TWOTRAN-II, An Interfaced, Exportable Version of the TWOTRAN code for Two-Dimensional Transport", LA-4848-MS (1973).
- 8) Takahashi H., et al.: unpublished.
- 9) Armstrong T.W. and Chandler K.C.: "Analysis Subroutines for the Nucleon-Meson Transport Code NMTC", ORNL-4736 (1971).

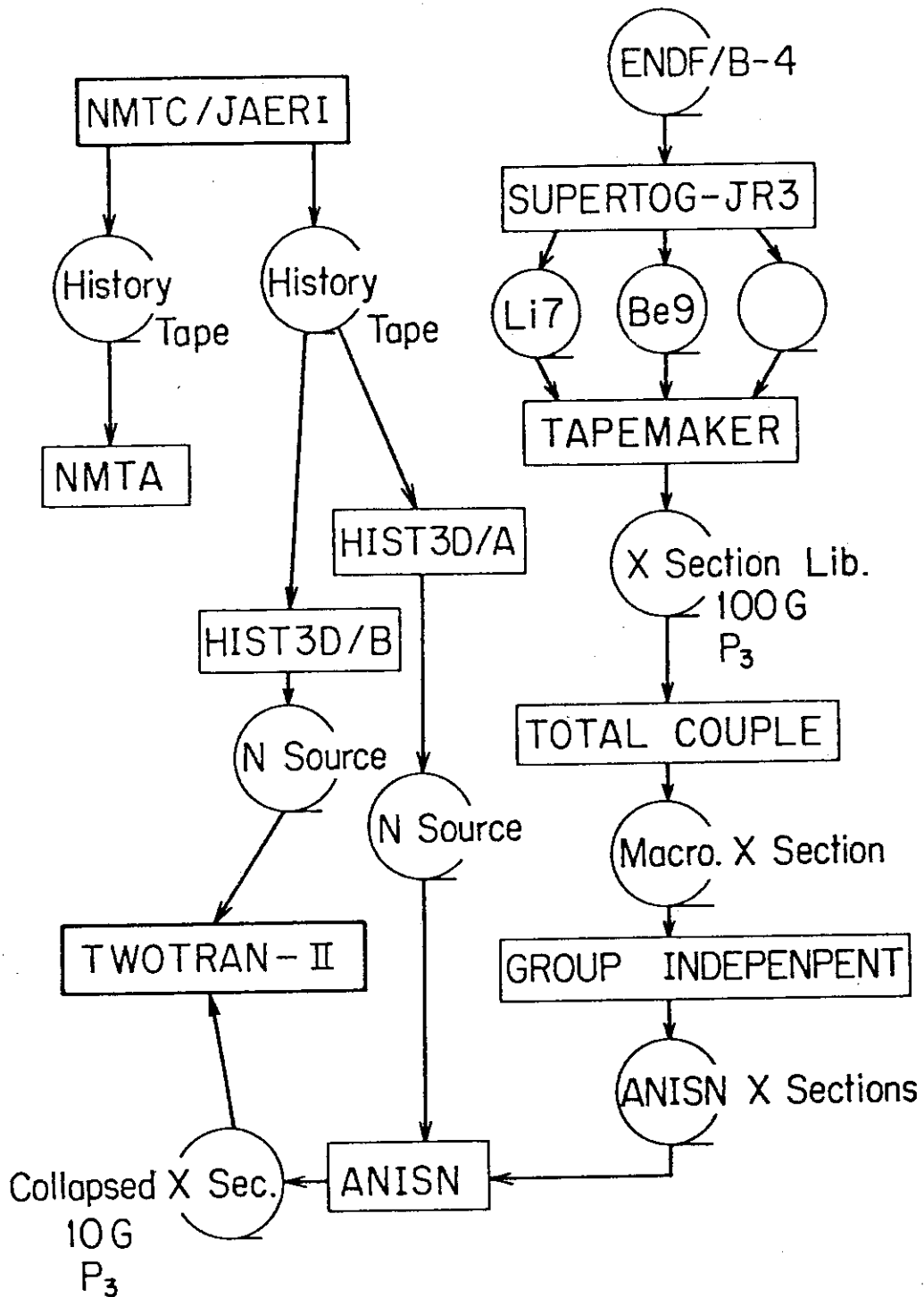


Fig.2.9.1 Flow of neutronics calculations

The base of NMTC / JAERI is the NMTC version revised at LASL and BNL.

2.10 Computational Studies of High Energy Spallation and Fission Reactions

Y. Nakahara and T. Tsutsui

In the feasibility studies of accelerator driven nuclear fuel breeders and the designs of intense spallation neutron sources, the first stage of nuclear reactions and nucleon transport processes has been simulated by the Monte Carlo codes NMTC¹⁾ and HETC²⁾. It was reported, however, that these codes underestimate the average number of neutrons produced in a target/blanket system per incident proton by several tens % in comparison with experiments^{3),4)}. In this regard, the importance to include the fission reactions was pointed out by several persons. Atchison⁵⁾ and Takahashi⁶⁾ tried to improve HETC and NMTC to include the fission process, respectively. It also has been included in the calculations by Barashenkow et al⁷⁾.

Our method to treat the fission process is close to the Atchison's, but more consistent with the Cameron's mass formula used in NMTC, into which our scheme has been incorporated. The computational flow in our NMTC/JAERI is illustrated in Fig. 2.10.1. The possibility of fission is considered only for nuclides with $Z^2/A \geq 29$ and nuclear excitation energy ≥ 6 MeV, where Z and A are the charge and mass number, respectively. The fission occurs in competition with the evaporation after the high energy nucleon cascade through a nucleus. At the fission the nucleus splits into two fragments, from which particles would or would not evaporate further. The fission probability has been calculated by the use of the statistical theory of fission.

The most difficult problem is how to select masses of fission fragments. For actinides it is well known that when the excitation energy of the fissioning nucleus is high, the fission is symmetric, but changes gradually to asymmetric as the excitation energy decreases. To simulate this situation, a normal and folded normal distributions are employed selectively depending on the excitation energy.

Charges of fission fragments have been sampled from the normal distribution with the Pik-Pichak and Strutinskii's expressions for the most probable charge and the fluctuation.

In Table 2.10.1 comparisons are made between our calculations and Vasil'kov et al.'s experiments⁸⁾ on a natural uranium target of relatively

great bulk. About 36% increase is seen in the value of N obtained by NMTC/JAERI in comparison with those by NMTC in the case of $E_p = 660$ MeV. A good agreement is seen between computed and measured values of N_p for $E_p = 660$ MeV⁹⁾.

In Figs. 2.10.2 and 2.10.3 are shown the mass distributions of spallation and spallation-fission products in an effectively infinite target of a molten salt LiF-UF_4 . The characteristic features of spallation and fission reactions are clearly seen in these figures. In this case the value of N increases by 18% from 28.1 ± 2.8 to 33.2 ± 2.6 due to the high energy fission.

Valuable discussions with Dr. H. Takahashi (BNL) and Prof. K. Tsukaka (Nihon Univ.) are greatly acknowledged.

References

- 1) Coleman W.A. and Armstrong T.W.: "NMTC Monte Carlo Nucleon Meson Transport Code System", RSIC ORNL CCC-161.
- 2) Chandler K.C. and Armstrong T.W.: "Monte Carlo High Energy Nucleon Meson Transport Code", RSIC ORNL CCC-178.
- 3) Takahashi H. and Nakahara Y.: Bull. Amer. Phys. Soc., 24, 878 (1979).
- 4) Garvey P.: "Neutron Production by Spallation in Heavy Metal Targets", Jül-Conf-34 (1980).
- 5) Atchison F.: "Spallation and Fission in Heavy Metal Nuclei under Medium Energy Proton Bombardment", *ibid.*
- 6) Takahashi H.: "Fission Reaction in High Energy Proton Cascade", BNL-NCS-51245 (1980).
- 7) Barashenkov V.C. et al.: "On the Calculations of the Electro-Nuclear Method of Neutron Production", JINR-R2-7694 (1974).
- 8) Vasil'kov et al.: *Atomnaya Energiya*, 44, 329 (1978).
- 9) Nakahara Y.: "Studies on the High Energy Spallation and Fission Reactions", Proc. ICANS-IV, KENS-II (1981).

Table 2.10.1 Analysis of number of neutrons captured by ^{238}U per primary proton

Target	E_p	N	N_c	Exper. N_c
Nat. U	660 MeV	(a) 31.1 ± 3.5	44.9 ± 5.1	$46. \pm 4.$
		(b) 22.9 ± 2.1	33.1 ± 3.0	
	400 MeV	(a) 11.81 ± 3.44	15.96 ± 4.65	22.1 ± 2.4
		(b) 9.95 ± 0.60	13.44 ± 0.81	

E_p = energy of proton beam,

N = average number of neutrons per one primary proton, produced by reactions in the nucleon energy range above 15 MeV.

(a) cascade·evaporation·fission (NMTC/JAERI),
 (b) cascade·evaporation^{a)} (NMTC),

N_c = number of neutrons captured by ^{238}U per one primary proton (NMTC + TWOTRAN-II results),

Exper. N_c = experimental N_c due to Vasil'kov et al.

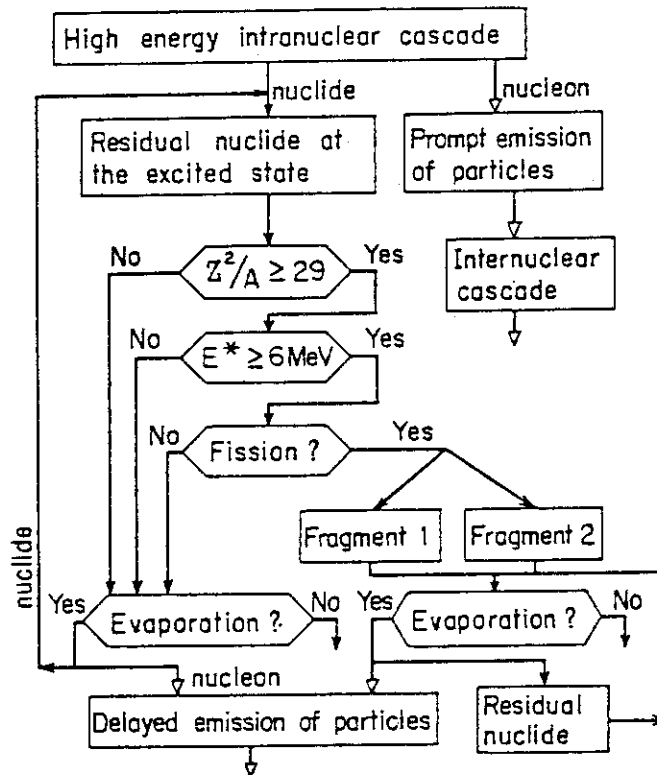


Fig.2.10.1 Computational scheme of the competition of evaporation and fission processes

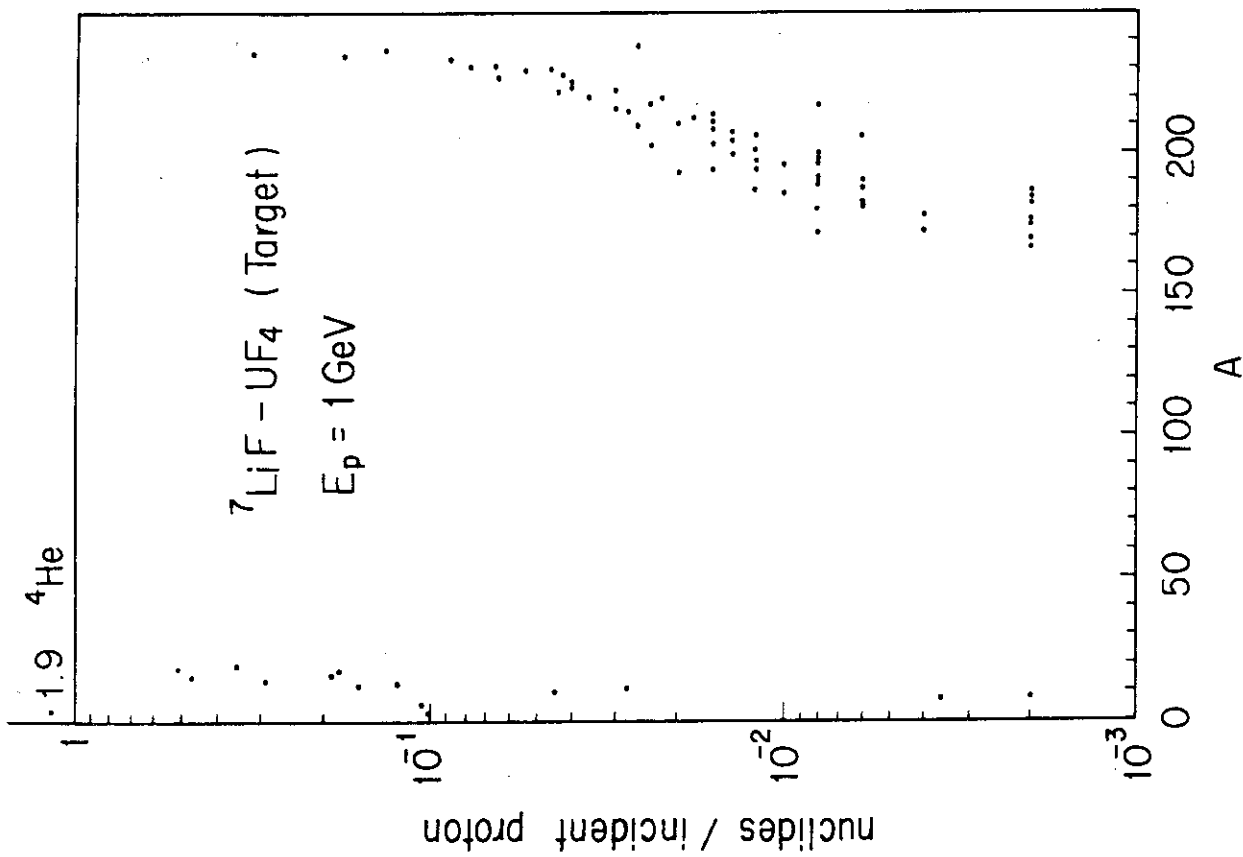


Fig.2.10.2 Mass distribution of cascade-evaporation products

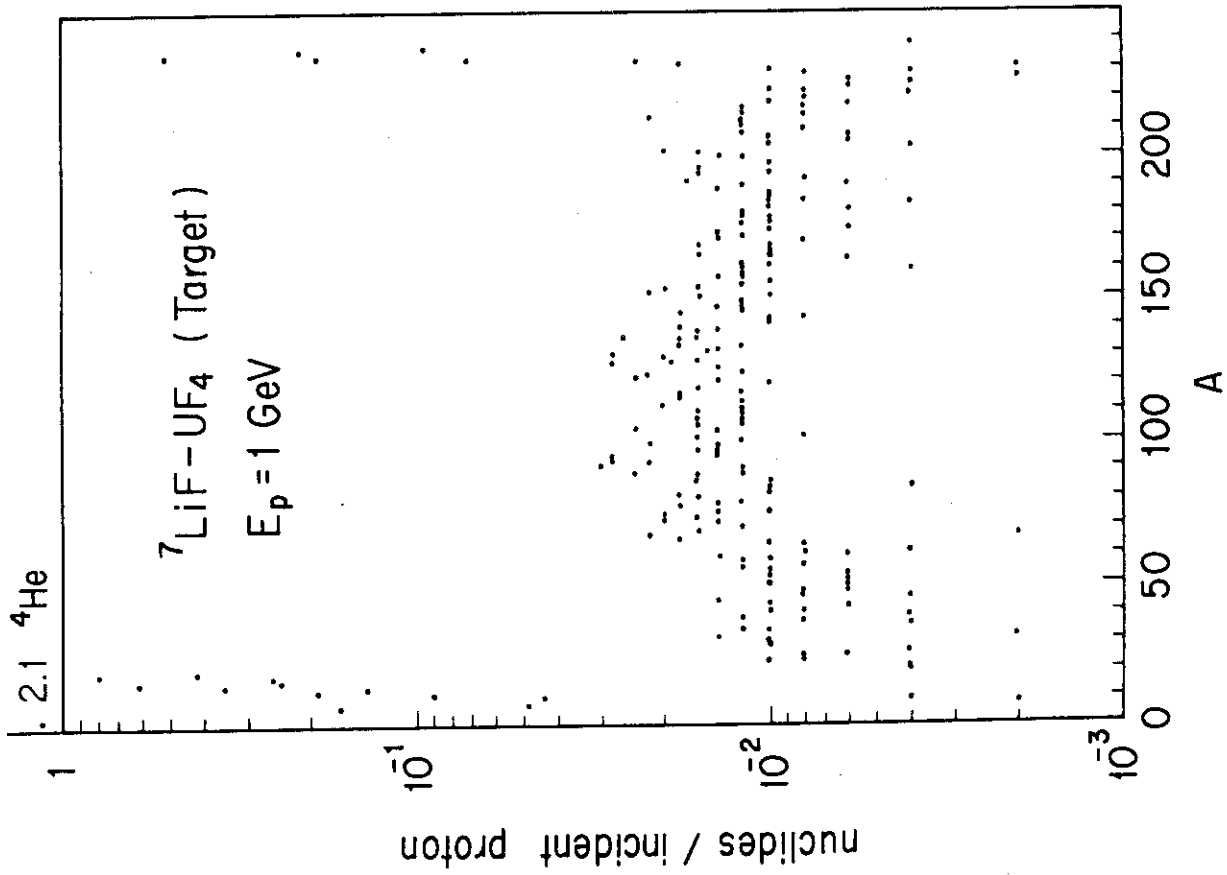


Fig.2.10.3 Mass distribution of cascade evaporation-high energy fission products

2.11 Neutronics Analyses of Accelerator Molten Salt Target/Blanket Assembly

Y. Nakahara and T. Tsutsui

The knowledge about the neutronic characteristics of Pb, U, Th and other heavy metals as the targets of proton accelerators has been accumulated owing to the enduring research efforts at several Laboratories. But little has been known about the neutronic characteristics of molten salt targets. We find only the unfavourable description that the calculated production of ^{233}U for the molten salt target/blanket concept is relatively low¹⁾. To reexamine this statement and to get more definite view of target/blanket concepts, calculations have been performed about the molten salt target/blanket assemblies by the use of a computer code system ACCEL, the description of which is given in Section 2.9 in this report.

A computational model of the molten salt target/blanket assembly is an effectively almost infinite homogeneous cylinder with the diameter and the depth of 6 m each. The defocussed proton beam of 1 GeV enters the assembly from the top, where the beam radius is assumed to be 0.75 m²⁾.

The spatial distributions in the beam direction of primary and total protons are shown in Fig. 2.11.1 for the case of $^7\text{LiF-UF}_4$. From the figure the mean free path of the primary proton is estimated to be 39 cm. In the figure also are shown the distributions of total neutrons in the energy range above the cascade cut-off (15 MeV). It is seen that the maximum of the neutron distribution appears at 60 cm from the surface of salt. Some irregularities seen in the figure are probably due to the insufficient number of samplings in the Monte Carlo calculations.

The group flux spectrum defined as

$$\phi_g = \int_{\Delta E_g} \phi dE$$

for the neutrons in the energy range below 15 MeV is shown in Fig. 2.11.2 for a region in $^7\text{LiF-BeF}_2\text{-UF}_4$, where spatial neutron distribution is maximum.

Some computational results of the neutron yield (the average number of neutrons produced per one incident proton) are summarized in Table

2.11.1, blank spaces in which mean that our calculations have not been done. Little difference is seen between the neutron yields from the cascade-evaporation processes in ${}^7\text{LiF-ThF}_4$ (Case c) and ${}^7\text{LiF-UF}_4$ (Case e). From the example for ${}^7\text{LiF-UF}_4$ it is seen that the inclusion of high energy fission makes a gain of 18% in the neutron yield. Comparison of Cases b and d gives an estimate of the effects of the low energy fission. The increase in the neutron yield due to fissions of Th in the energy range below 15 MeV is only 3%, while for U it is 23%.

It should be noticed that the contribution of the Be (n, 2n) reaction is not taken into consideration correctly. The values of the neutron yield for the salts including Be can be expected to get a gain further, if the Be (n, 2n) contribution is estimated properly.

The effect of ${}^{233}\text{U}$ enrichment on the neutron yield was estimated for Case a and the results are shown in Fig. 2.11.3.

Our computational results are not so poor as were imagined, but give a promising prospect of the molten salt target/blanket concept.

Acknowledgements are due to Prof. K. Tsukada (Nihon Univ.) and Dr. K. Furukawa for stimulating discussions.

References

- 1) Mynatt F.R.: "Analysis of Accelerator Breeder Concepts with LMFBR, GCFR and Molten Salt-type Blankets", CONF-770107 (1977).
- 2) Furukawa K., Tsukada K. and Nakahara Y.: "Molten Salt Target and Blanket Concepts", Proc. ICANS-IV, KENS-II (1981).

Table 2.11.1 Comparison of neutron yields per incident 1 GeV proton for some salt trangets including Th and U

	molten salt	cascade + evaporation (≥ 15 MeV)	cascade + evaporation + fission (≥ 15 MeV)	whole energy range (1000 ~ 0 MeV)**
a)	${}^7\text{LiF}-\text{BeF}_2-\text{ThF}_4$ (71-9-20)*	26.1 ± 2.1	29.6 ± 2.1	30.7 ± 2.2
b)	${}^7\text{LiF}-\text{BeF}_2-\text{ThF}_4$ (64-18-18)		27.0 ± 2.0	27.8 ± 2.1
c)	${}^7\text{LiF}-\text{ThF}_4$ (71-29)	27.3 ± 2.2	33.04 ± 1.9	
d)	${}^7\text{LiF}-\text{BeF}_2-\text{UF}_4$ (61-21-18)		31.2 ± 2.4	38.4 ± 3.0
e)	${}^7\text{LiF}-\text{UF}_4$ (71-29)	28.1 ± 2.8	33.2 ± 2.6	

*) Numbers in parentheses indicate mole % of each fluoride.

**) Including fission in the energy range both above and below 15 MeV.

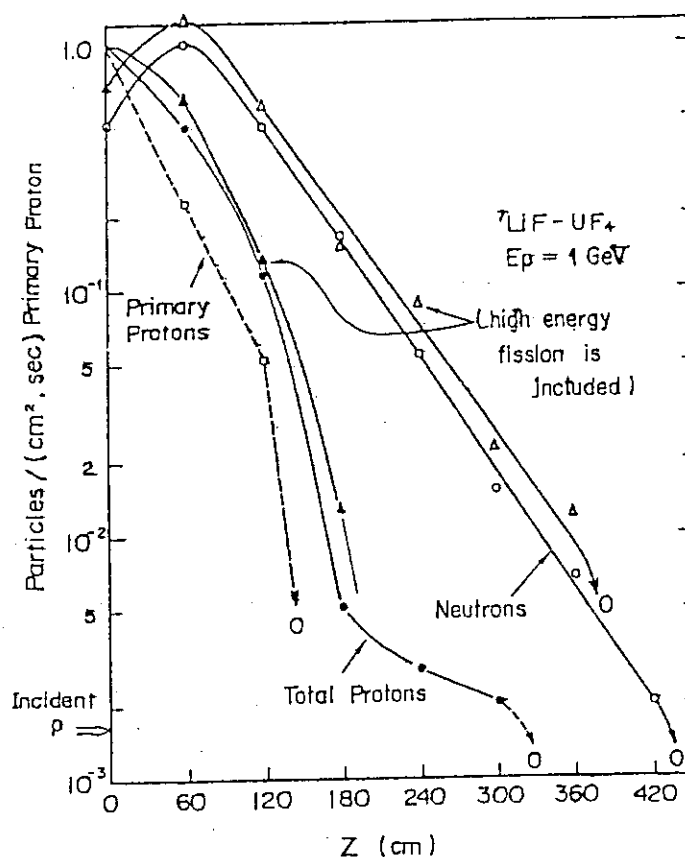


Fig.2.11.1 Spatial distributions of primary and total protons, neutrons in the beam direction and in the energy range above 15 MeV.

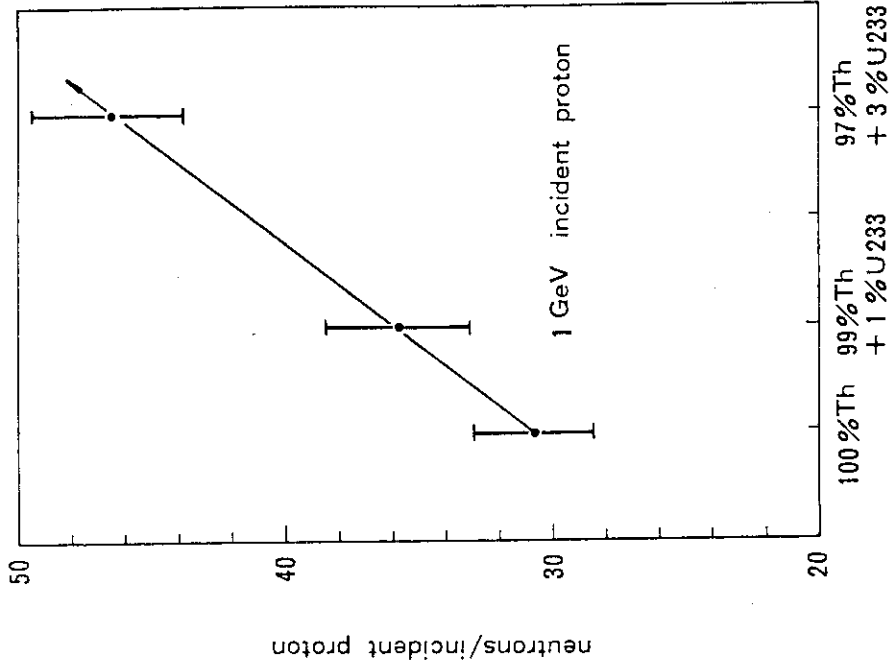


Fig.2.11.3 Linear dependence of the neutron yield on the concentration of ^{233}U in $^7\text{LiF}\cdot\text{BeF}_2\cdot\text{Th}(\text{U})\text{F}_4$ (71-9-20). (Calculations with the ACCEL code system)

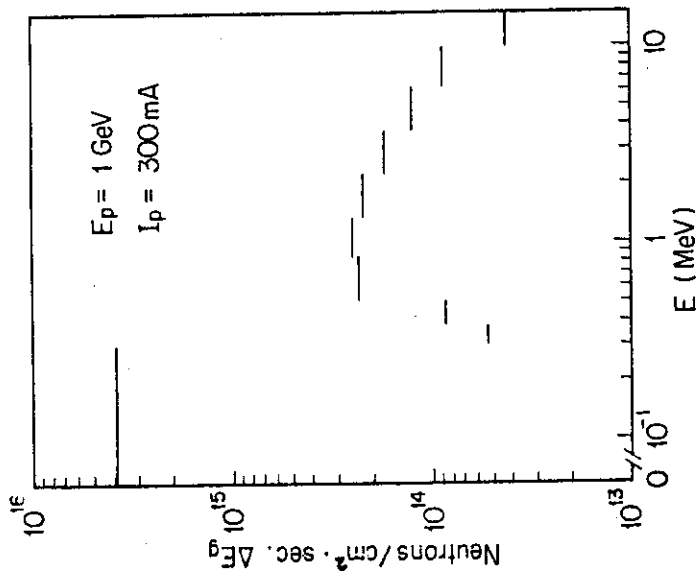


Fig.2.11.2 Neutron spectrum in $\text{LiF}\cdot\text{BeF}_2\cdot\text{ThF}_4$ (67-18-15)

2.12 High Resolution Electron Microscopy of Simple Defects in a (110) Silicon Crystal

T. Nishida and K. Izui

For high resolution electron microscopy we have undertaken the calculations of atomic images for a simple vacancy cluster included in a silicon crystal oriented in (110). The preliminary researches were performed about physical and electron optical parameters of crystal thickness and defect size, and aperture radius and defocus of objective lens to find a good representation of the cluster. The multislice formulation of the dynamical theory of electron diffraction could be also used on a superlattice structure extended for containing a defect by assuming the periodic continuation at its boundaries in the lateral dimension^{1),2)}. We had already described the outlines of the formulation of a divacancy cluster model without relaxation and the application of the multislice method to defect imaging calculations, presenting some simulated images³⁾. In the present paper the imaging conditions for gaining high resolution images of the atomic defect are investigated in further detail, taking into accounts the influences of relaxation of neighbouring atoms, the accelerating potential and the number of a defect layer.

a) Divacancy cluster images with relaxation of neighbouring atoms

It is well known that the lattice atoms in the neighbourhood of a defect should be displaced due to the relaxation motion. Then on our defect model the nearest neighbouring atoms around a divacancy which is at the center of (3×3) supercell are slightly moved to the direction of the divacancy within the slice on which the crystal potential is projected. Fig. 2.12.1 shows the divacancy cluster images with and without relaxation in the thickness of ten slices under two optical conditions of ideal lens ($\Delta f=0$, $C_s=0$) and Scherzer focus ($\Delta f=500\text{\AA}$, $C_s=0.7\text{mm}$) at 100 KV, where Δf and C_s denote the amount of defocus and the spherical aberration coefficient. From the good agreement among these figures it is considered that Scherzer focus gives the clear images of the vacancy cluster with relaxation. The relaxed atoms in Fig. 2.12.1 (d) have the slight displacements toward a divacancy similar to that of the defect model. Their peak intensities are reduced to the lower values than ones of the peak intensity on the normal lattice because there are a little discrepancies

between the positions of lattice atoms and relaxed atoms on each slice which is superposed in the depth direction.

b) Effects of the accelerating potential on the defect image

The images of four slices of divacancy ($4V_2^R$) in a crystal of ten slices are examined at 100 KV with $C_s = 0.7$ mm and at 500 KV and 1 MV with $C_s = 1$ mm for Scherzer focus defined at each potential as shown in Fig. 2.12.2 (a) ~ (c). At 500 KV and 1 MV the vacancy cluster images have higher contrasts 22% and 28% respectively than the contrast 15% at 100 KV although the resolution of host lattice become poor with increasing the potential. The position and the contrast reduction of relaxed atoms are sufficiently recognized on the images at higher potentials also.

c) Dependence of image contrast on the number of a defect layer

The amounts of decreases in the image intensity at the position of divacancy are calculated for the images of the clusters with several slices including the defect for Scherzer foci 377 Å and 295 Å at 500 KV and 1 MV respectively. As seen in Fig. 2.12.3 (a) the contrasts at the divacancy position are 9, 22 and 52% for 2, 4 and 8 slices of divacancy layer at 500 KV. This rapid increase of the contrast seems to be less marked with increasing the accelerating potential to 1 MV as illustrated in Fig. 2.12.3 (b). As the detectable limitation of the contrast is commonly about 5%, " $2V_2^R$ " cluster may be recognized by direct observation at 500 KV but could not be observed at 1 MV. In the images of " $4V_2^R$ " and " $8V_2^R$ " clusters at both potentials the relaxed atoms in the nearest neighbouring of divacancy are more clearly distinguished than host lattice atoms.

Further researches of defect images due to the effects of both chromatic aberration of objective lens and slight misorientation of the specimen will be discussed in the near future.

References

- 1) Field P.M., Cowley J.M.: "Computed Electron Microscope Images of Atomic Defect in F.C.C. Metals", Acta Cryst., A34, 103 (1978).
- 2) Spence J.C.H.: "Approximation for Dynamical Calculation of Micro-diffraction Pattern and Images of Defects", Acta Cryst., A34, 112 (1978).
- 3) Nishida T., Izui K., Furuno S., Otsu H.: "High Resolution Structure Images of a Simple Defect in a Silicon Crystal Oriented in (110)", JAERI-M 9032, 39 (1980).

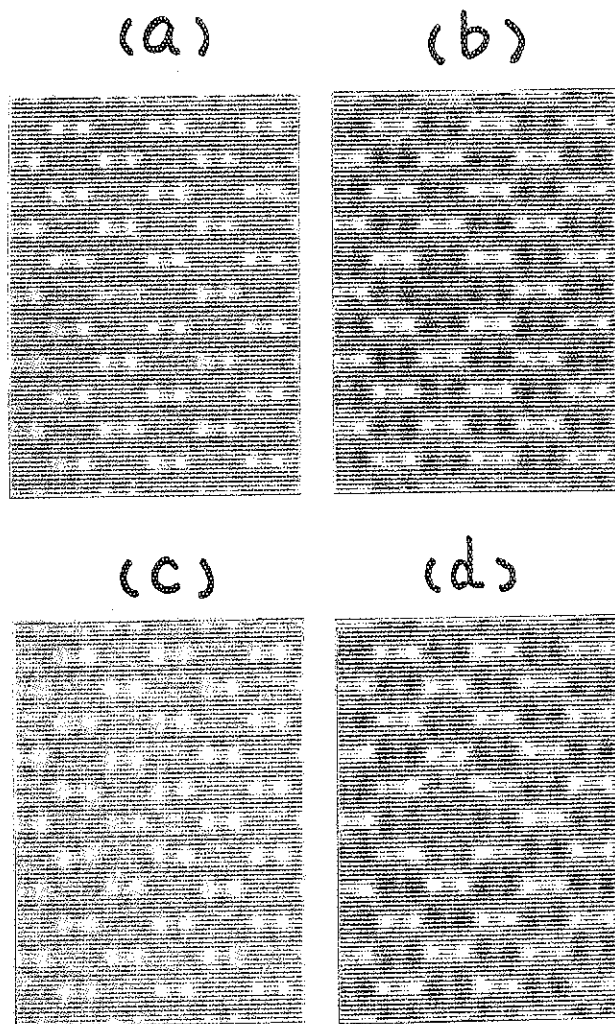


Fig. 2.12.1 Simulated images of a vacancy cluster of four defect slices in a crystal thickness of 10 slices at 100 KV under the conditions (a) ideal lens ($\Delta f=0$, $C_s=0$) and (b) Scherzer focus ($\Delta f=500\text{\AA}$, $C_s=0.7\text{mm}$) without relaxation, and (c) ideal lens and (d) Scherzer focus with relaxation.

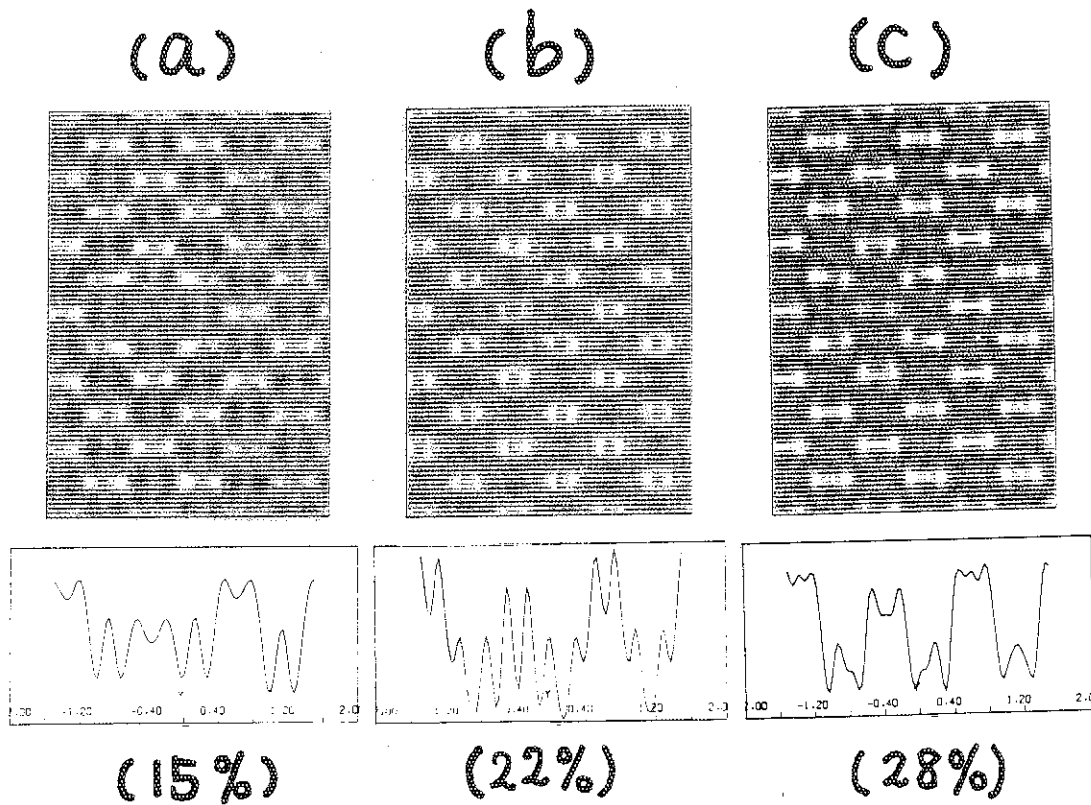


Fig. 2.12.2 Variation of " $4V_2^R$ " cluster image at the accelerating potentials (a) 100 KV, (b) 500 KV and (c) 1 MV for Scherzer foci 500\AA , 377\AA and 295\AA respectively. In the lower part of each figure, the image intensity profile along the line passing on a divacancy and the value of the defect contrast are shown.

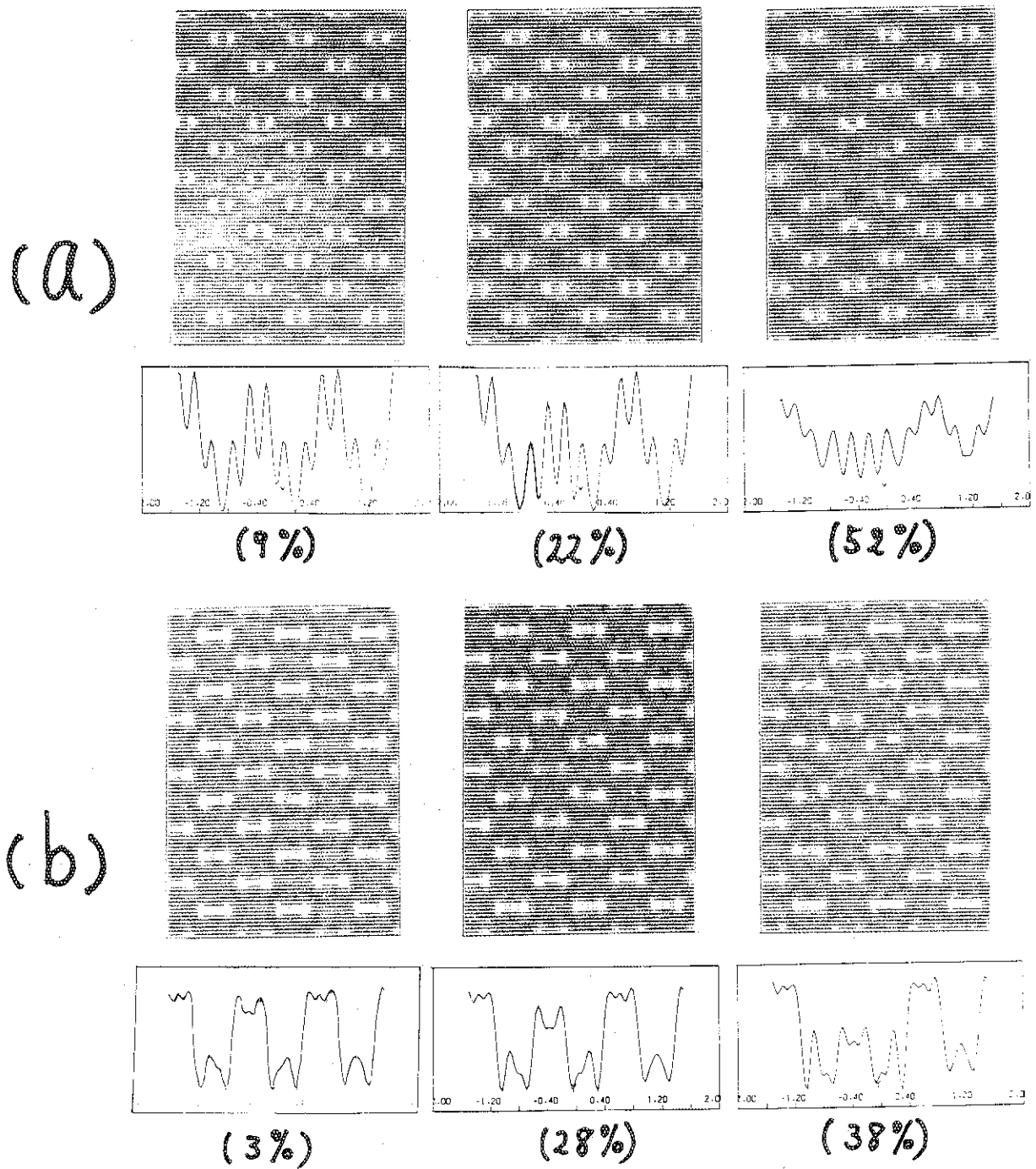


Fig. 2.12.3 Effect of the number of divacancy layer on the defect image contrast. The clusters are imaged for Scherzer focus at (a) 500 KV and (b) 1 MV and contain 2, 4 and 8 slices of divacancy layer in a crystal of ten slices respectively from the left figure to the right one. The percentage value given below each figure denotes the contrast of the cluster.

3. Integral Experiment and Analysis

3.1 Measurement of Reactivity Worths of Control Rods in Enriched Uranium Graphite Moderated Core Related to VHTR

F. Akino, M. Takeuchi, K. Kitadate, H. Yoshifuji and Y. Kaneko

As core design for the Experimental Very High Temperature Gas Cooled Reactor (VHTR) progresses, evaluation of design precision has become increasingly important. For a high precision design, required are adequate group constants based on accurate nuclear data, as well as calculation method. We, therefore, assembled SHE-14 and SHE-B2 cores, which are simulation cores for VHTR⁽¹⁾, using a graphite-moderated 20%-enriched uranium Semi-Homogeneous Experimental Critical Facility⁽²⁾ (SHE), and obtained experimental data useful in evaluating design precision. The VHTR is designed to accommodate burnable poison and control rods for reactivity compensation for fuel burn-up. Accordingly, the experimental control rods which are similar to those to be used in VHTR were prepared, and their reactivity values were measured in SHE-14, and SHE-B2 cores. The experimental control rods were made by filling an aluminium tube, 1 mm thick and about 1150 mm long, with neutron absorbing pellets of 50 mm in outer diameter, 30 mm in inner diameter and 50 mm in height.

The absorbing pellets were made by sintering B_4C powder with natural graphite powders; their gross density and boron content are 1.42 g/cm^3 and 30 w/o or 10 w/o, respectively.

Measurements were made for various configurations of experimental control rods; for example, a configuration of simulating the typical case considered in VHTR design is shown in Fig. 3.1.1. Reactivity worths were measured by Revised King-Simmons' pulsed neutron method⁽³⁾.

Theoretical analysis was performed according to two-dimensional diffusion theory for two groups and two regions. In calculating the control rod reactivity worths, we employed either of the following two methods:

1. a method using differential-logarithmic boundary conditions for the control rod surface or
2. an absorbing area method calculating the group constants of the control-rod containing cell using LAMP⁽⁴⁾ code system for both thermal

and fast neutron groups

The measured values and the calculated ones by the two methods agree with each another within 6~9%. Further, it was clearly indicated that the experimental control rods in the central column interact each other so as to increase the reactivity worths.

References

- 1) Aochi T., et al.: JAERI-M 6895 (1976).
- 2) Kaneko Y., et al.: JAERI 1257 (1978).
- 3) Akino F., et al.: J. Nucl. Sci. Tech. 17(8) p.593 (1980).
- 4) Tsuchihashi K.: JAERI 1259 (1979).

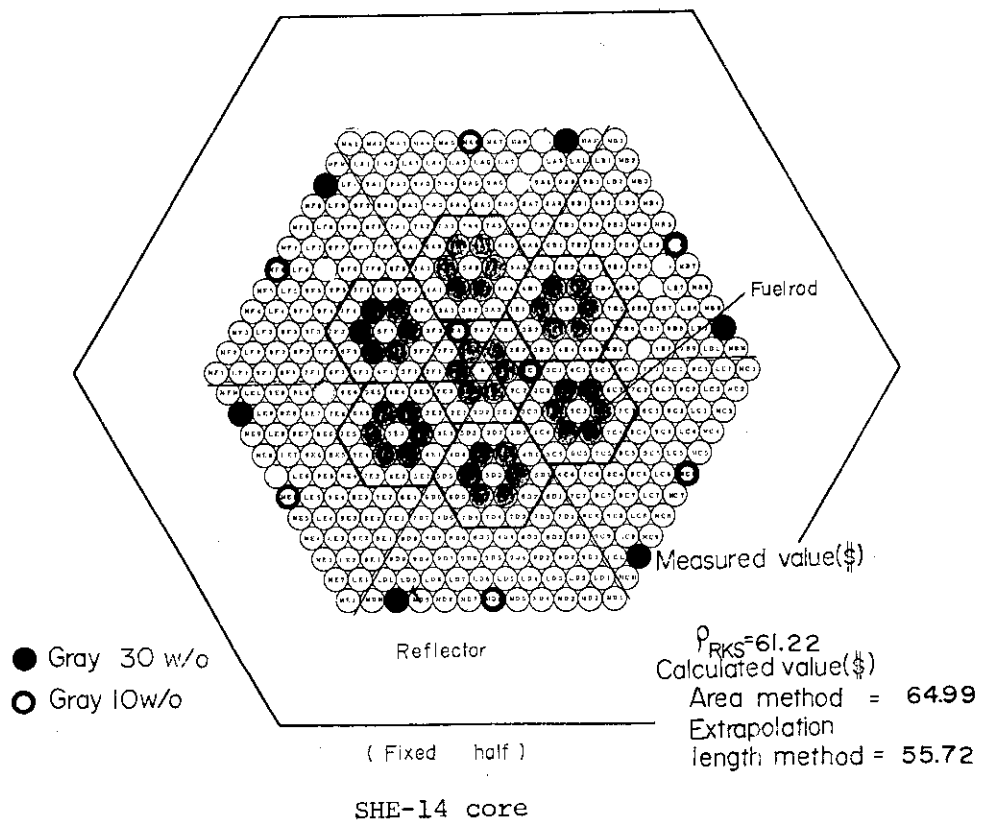


Fig. 3.1.1 Measured and calculated reactivity worths for the experimental control rods arrangement simulating the those in VHTR.

3.2 Reconstruction Program of SHE for Experimental VHTR

Y. Kaneko, Y. Gotoh and T. Asaoka

1. Object

Reconstruction program of SHE, Semi-Homogeneous Experimental Critical Facility, was approved by Japanese government. The object of the program is to obtain experimental verification for the design accuracy of Experimental VHTR fueled with low enriched uranium. Nuclear safety aspect is required to be solved from view point of operation licence before the start up of Experimental VHTR will be initiated. Therefore, reactivity worths of control rods or burnable poison rods as well as the critical mass of the simulation core of Experimental VHTR and its other important core physics parameters will be measured using the reconstructed SHE facility. Measurements of the reactivity temperature coefficients are also to be made.

2. Specification of reconstruction

Core geometry : horizontal half machine type

hexagonal prism in shape

height and length, 2.4 m for each

Core lattice : pin in block type same as Experimental VHTR

Core temperature : room temperature to 200°C throughout the whole core including reflector

Single fuel rod will be heated up to 800°C

Fuel : 2, 4 and 6 w/o enriched uranium, 275 kgU in total

coated particle fuel compacts as the same size of Experimental VHTR

BISO or TRISO

3. Schedule

Design of the reconstructed SHE facility has started from spring of this year. After safety examination by government, the reconstructed core will be assembled in 1984.

3.3 Heating Apparatus for Measurement of Reactivity Temperature Coefficient in SHE

H. Yasuda, K. Kitadate and M. Takeuchi

A core heating apparatus has been equipped in the SHE, and used for measurement of reactivity temperature coefficient of the SHE in the range from room temperature up to 100°C.

The heating apparatus consists of 30 KW power source, 38 electric heaters of nickel-chrome, 20 thermo-couples, temperature regulator, voltage controller and air cooler. The heater is a cartridge type with 9.5 mm dia. and 1200 mm long, and has a capacity of 500 W. The heaters are inserted in the SHE along the axis. Two of them are positioned at the center of the core, and the rest 36 elements are located in the inner part of the reflector region covered by the peripheral heat insulator. Maximum electric capacity is 20 KW, and it is controlled by the voltage controller. The lower part of the reflector adjacent to the table of the movable bed of the SHE is cooled by compressed air to prevent heat transfer from the core to the bed. Experimental arrangement of SHE core are shown in Fig. 1. It took about two days to raise the core temperature from room temperature to 100°C. The temperature rising characteristics are shown in Fig. 2, and the temperature distribution in core radial direction is shown in Fig. 3. Temperature slightly decreases in lower region of the core due to the effect of cooling air, but in core region, fairly flat temperature distribution is obtained.

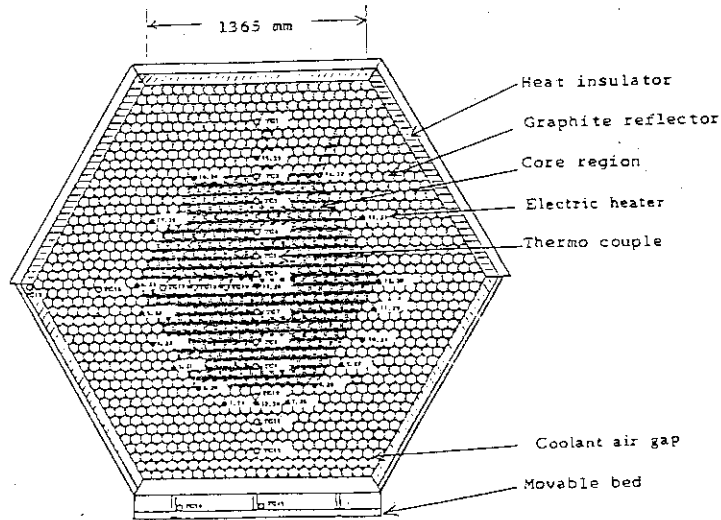


Fig.3.3.1 Experimental arrangement of SHE core

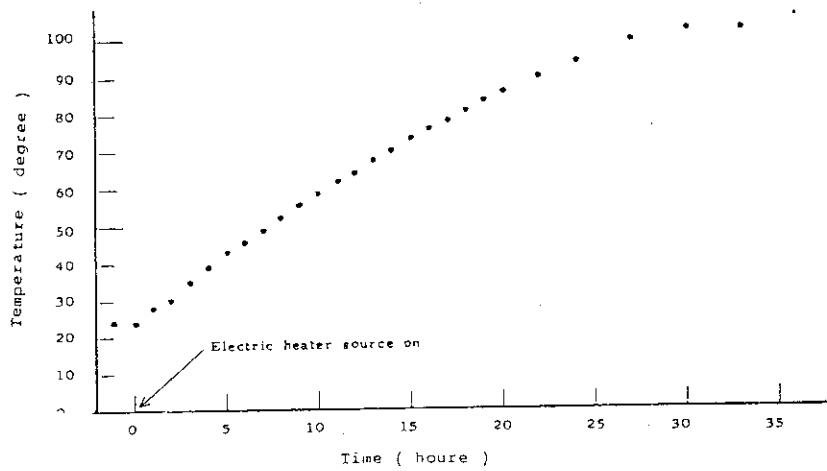


Fig.3.3.2 Characteristics of temperature rise

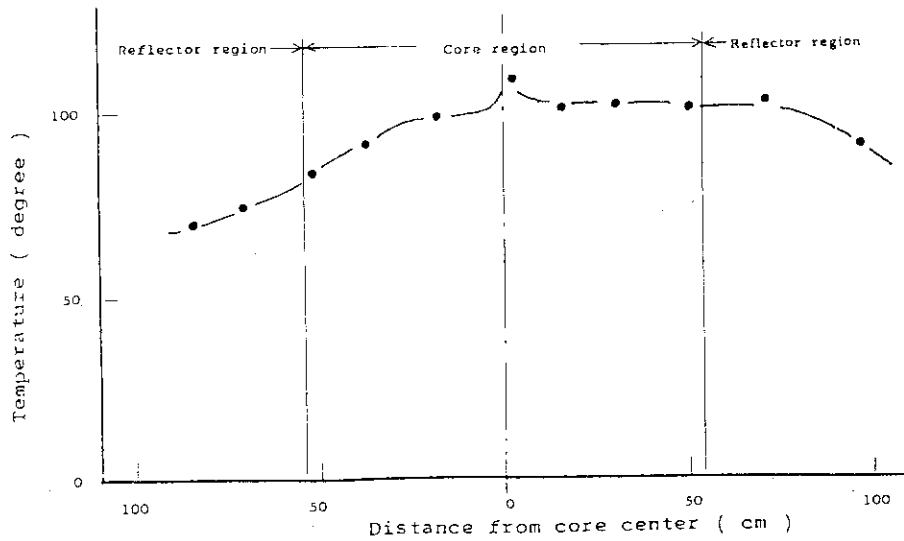


Fig.3.3.3 Temperature distribution of core

3.4 Analysis of Fuel Slumping Experiment on FCA Assembly VIII-2

M. Nakano and H. Tsunoda*

Analysis has been made of the reactivity change due to fuel slumping in the central region of FCA Assembly VIII-2. The assembly consisted of a central test region simulating the prototype FBR "MONJU" in axial dimensions and composition, and a uranium driver region¹⁾. Axially symmetric and asymmetric displacements of fuel were made in the central 3×3 drawers (equivalent radius 9.3 cm) with sodium expelled. Four configurations studied are illustrated in Fig. 3.4.1. The compacted fuel is formed by removal of stainless steel spacers resulting in the increase of fuel density by a factor of two, while the void region consists of the stainless steel spacers. For each configuration, axial fission rate distributions of ^{238}U and ^{235}U were measured by traversing micro fission chambers of depleted and enriched uranium in the center drawer and off-center one adjacent to the slumping region ($r = 15.6$ cm).

The analysis was made using JAERI-Fast Set Version II²⁾. In order to examine the adoptability of calculational methods used in analysing core disruptive accident, RZ calculation was carried out with the transport (Sn), conventional and modified diffusion methods, using the cell averaged 25 group cross sections prepared by the collision probability method.

The calculated reactivity change for the respective fuel displacement is compared with the experiment in Table 3.4.1. The prediction with the conventional diffusion calculation is quite poor when neutron streaming effect is large. Considerable improvement is achieved by applying the modified diffusion coefficient derived by J. Rowlands³⁾ for the void region. The transport calculation with S_4P_0 approximation predicts the reactivity change fairly well, the C/E value being about 0.8 even in the case of A3 configuration. However, there still remains the trend of underestimation which increases with extension of the fuel slumping region to the core edge.

Reactivity components calculated with the exact perturbation theory are shown in Fig. 3.4.2. The use of the modified diffusion coefficient reduces the leakage component nearly half for the A2 and A3 configura-

* Mitsubishi Research Institute, Inc.

tions, and it gives almost the same results as those obtained with the S_4P_0 transport calculation. However, the prediction of the non-leakage component is not improved by the modified diffusion calculation.

The axial distributions of ^{235}U and ^{238}U fission rate measured in each assembly are compared with the calculation. Agreement is good for ^{235}U fission rate distribution, although a little discrepancy is observed in the fuel slumping region. The conventional diffusion theory does not represent the measured ^{238}U fission rates both in the fuel compacted and voided region. No significant improvement is achieved by the use of the modified diffusion method, although it considerably improves the prediction of reactivity change. The results obtained by the transport theory with S_4P_0 approximation fairly well agree with the measured ones.

References

- 1) Nakano M., Tsunoda H. and Hirota J.: Reactor Engineering Division Annual Report, 47-49, JAERI-M 9032 (1980).
- 2) Takano H., et al.: JAERI Fast Reactor Group Constants Set, Version II, JAERI 1255 (1978).
- 3) Collins P.G., Ingram G. and Codd J.: Proc. Int. Symp. Fast Reactors, Tokyo, Oct. 16-19, A40 (1973).

Table 3.4.1 Calculated and experimental reactivity changes for the fuel slumping

Pattern	Calculation ($10^{-4}\Delta k/k$)			Experiment ($10^{-4}\Delta k/k$)	C - E ($10^{-4}\Delta k/k$)		
	Conv. D	Mod. D	S_4P_0		Conv. D	Mod. D	S_4P_0
A1	3.3	3.6	4.5	5.3 ± 0.3	-2.0	-1.7	-0.8
A2	6.1	8.5	10.5	12.6 ± 0.4	-6.5	-4.1	-2.1
A3	1.4	9.0	11.9	15.2 ± 0.4	-13.8	-6.2	-3.2
S	-6.4	-6.4	-3.9	-4.1 ± 0.3	-2.3	-2.3	+0.2

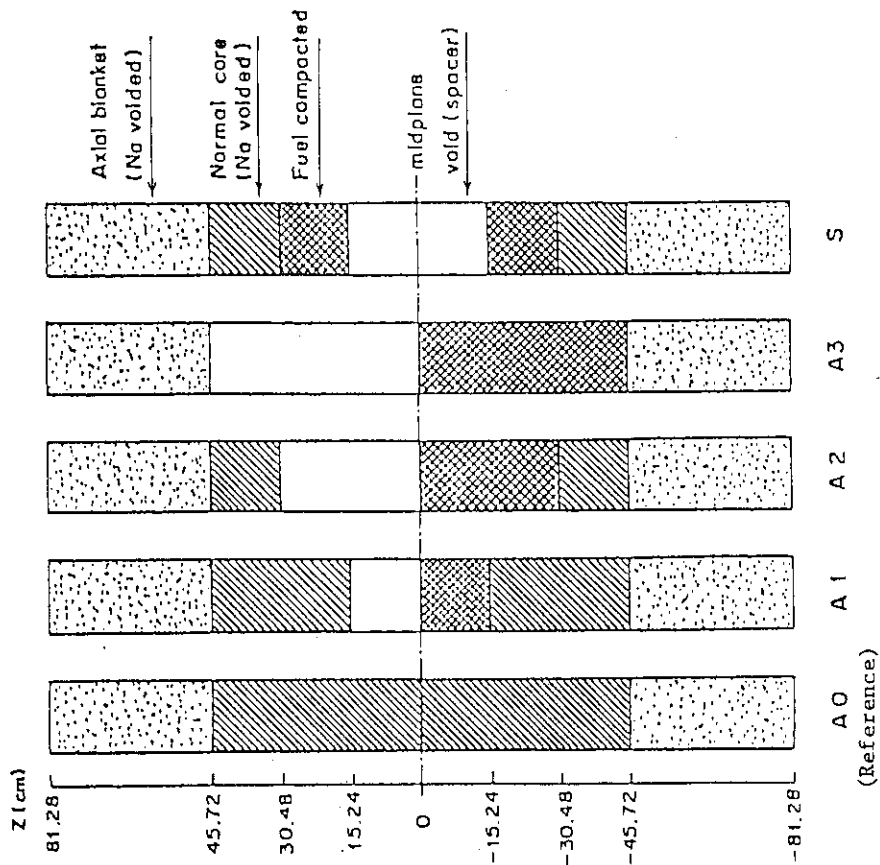


Fig. 3.4.1 Configurations of the central 3x3 drawers used in the slumping experiment

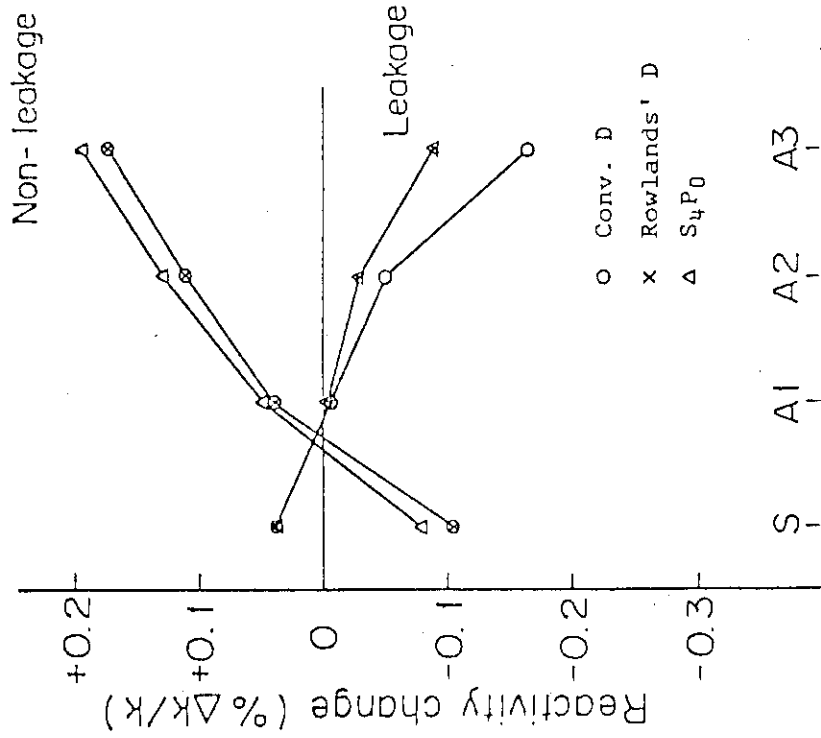


Fig. 3.4.2 Leakage and Non-leakage components for the fuel slumping in the central 3x3 drawers

3.5 Integral Experiments for Actinides Cross Section Evaluation (I)

T. Mukaiyama, M. Ōbu and H. Kuroi

Actinide transmutation study using fast critical assembly FCA

One of the major problems which may govern the very future of the nuclear power is the risks from the high-level, long-lived radioactive wastes. Among the radioactive wastes, most of fission products decay to innocuous levels in a relatively short time span of about 500 years, whereas the radiological hazards of actinides continue for a hundred thousands years. In order to alleviate the long-term radiological hazard of actinide nuclides, it has been proposed to recycle actinides in a suitable system to transmute them into fission products which are a shorter-term hazard. From the neutron economy point of view, the actinide recycle concept may be acceptable especially with the fast reactors because the most of actinide isotopes possess appreciable fission cross sections in the high energy region.

The study of the transmutation physics at JAERI is concentrated mainly on the following three fields, 1) Optimization of the transmutation system, 2) Evaluation of actinide elements nuclear cross section data by the integral experiments at FCA and 3) Risk-benefits-cost analysis of the partitioning-transmutation system.

Evaluation of actinide elements nuclear cross section data by the integral experiments¹⁾

The assessment of the actinide recycle concepts requires the reliable fission and capture cross sections of actinides over the whole energy spectrum of potential recycling systems.

The status of the cross section data is much less satisfactory. Some of the major actinide cross section data possess the uncertainty up to 50%^{1),2)}. Nuclear cross section data can be evaluated by the integral data using the method based on the least square fitting of the integral data³⁾. The realistic integral data for the evaluation of actinide cross sections are the small sample reactivity worth and the fission rate ratios because of the high radioactivity of actinides and the difficulty of obtaining pure samples.

The actinide production and transmutation study of the Actinide Burning Reactor "ABR" shows that ^{237}Np , ^{238}Pu , ^{240}Pu , ^{241}Am , ^{243}Am and

^{244}Cm are the ruling nuclides in the "ABR"4).

The integral measurements are under way at the Fast Critical Assembly FCA. These measurements will be performed in six to seven standard core configurations⁵⁾ which cover the wide variety of neutron spectra.

Actinide samples for worth measurements

Oxide actinide powder is encapsulated into double concentric stainless steel capsules shown in Fig. 3.5.1.

The small sample reactivity worth is to be measured for ^{237}Np , ^{238}Pu , ^{240}Pu , ^{241}Am and ^{243}Am samples. The quantity of each nuclide is 15 ~ 20 g. The isotopic content of the sample element is 99.2% for ^{237}Np , 91% for ^{238}Pu , 98% for ^{240}Pu , 97% for ^{241}Am and 100% for ^{243}Am . ^{243}Am isotope is extremely expensive (2 million U.S. \$ for 20 g). However U.S. Department of Energy, taking note of the importance of this experiment, agreed to loan this sample to JAERI with the condition that the information resulting from the use of this sample would be provided to DOE.

Actinide Fission Chamber

Fission chambers of parallel-plate type are provided to measure the central fission rates of ^{237}Np , ^{238}Pu , ^{239}Pu , ^{242}Pu , ^{241}Am , ^{243}Am and ^{244}Cm relative to fission in ^{235}U . The chamber consists of the body of a thin stainless steel wall, the collector of a circular disk and the polished platinum disk of 0.2 mm thick and 36 mm diameter, which is deposited with the fissile material in a circular area of 25 mm diameter, as shown in Fig. 3.5.2. The gas filled in the chamber is a mixture of 97% Ar and 3% N_2 at 1 atmosphere pressure.

The fissile masses in deposit are absolutely determined by α -spectrometry. For most of nuclides, weights deposited are adjusted in the range of about 40 ~ 90 μg to make the accurate determination of α -assay and to hold a suitable flux level for fission rate measurements. However, for the nuclides with much higher α specific activities, e.g. ^{244}Cm , ^{238}Pu and ^{241}Am , the masses of deposit are limited to less than 10 μg to reduce α -background.

The typical pulse height distribution of ^{244}Cm obtained in IX-I core⁵⁾ is shown in Fig. 3.5.3. Characteristics of low α pile-up are obtained for all chambers prepared. Errors of fission pulse rates introduced by those chambers are assigned from the uncertainties of α -assay, fissile impurities in the deposits, an individuality of the chambers and counting statistics measured in suitable power levels. It is

shown from the preliminary experiment that the actinide fission rates can be measured within errors of $\pm 2 \sim \pm 4\%$.

References

- 1) Mukaiyama T. et al.: "Evaluation of Actinide Cross Sections by Integral Experiments in Fast Critical Assembly FCA", Proceedings of International Conference on Nuclear Cross Sections for Technology (Knoxville, 1979), p.552, NBS SP594 (1980).
- 2) Mukaiyama T., Koyama K. and Kuroi H.: "Generation of Actinide Isotopes Cross Section Set for Fast Reactor Calculations using Data from ENDL and ENDF/B-IV", JAERI-M 8310 (1979).
- 3) Mitani H. and Kuroi H.: J. Nucl. Sci. Technol, 9, 388 (1972).
- 4) Mitani H., Koyama K. and Kuroi H.: "Sensitivity Analysis for Actinide Production and Depletion in Fast Reactors", JAERI-M 8133 (1979).
- 5) Nakano M., Koyama K. and Kuroi H.: Section 3.7 of this report.

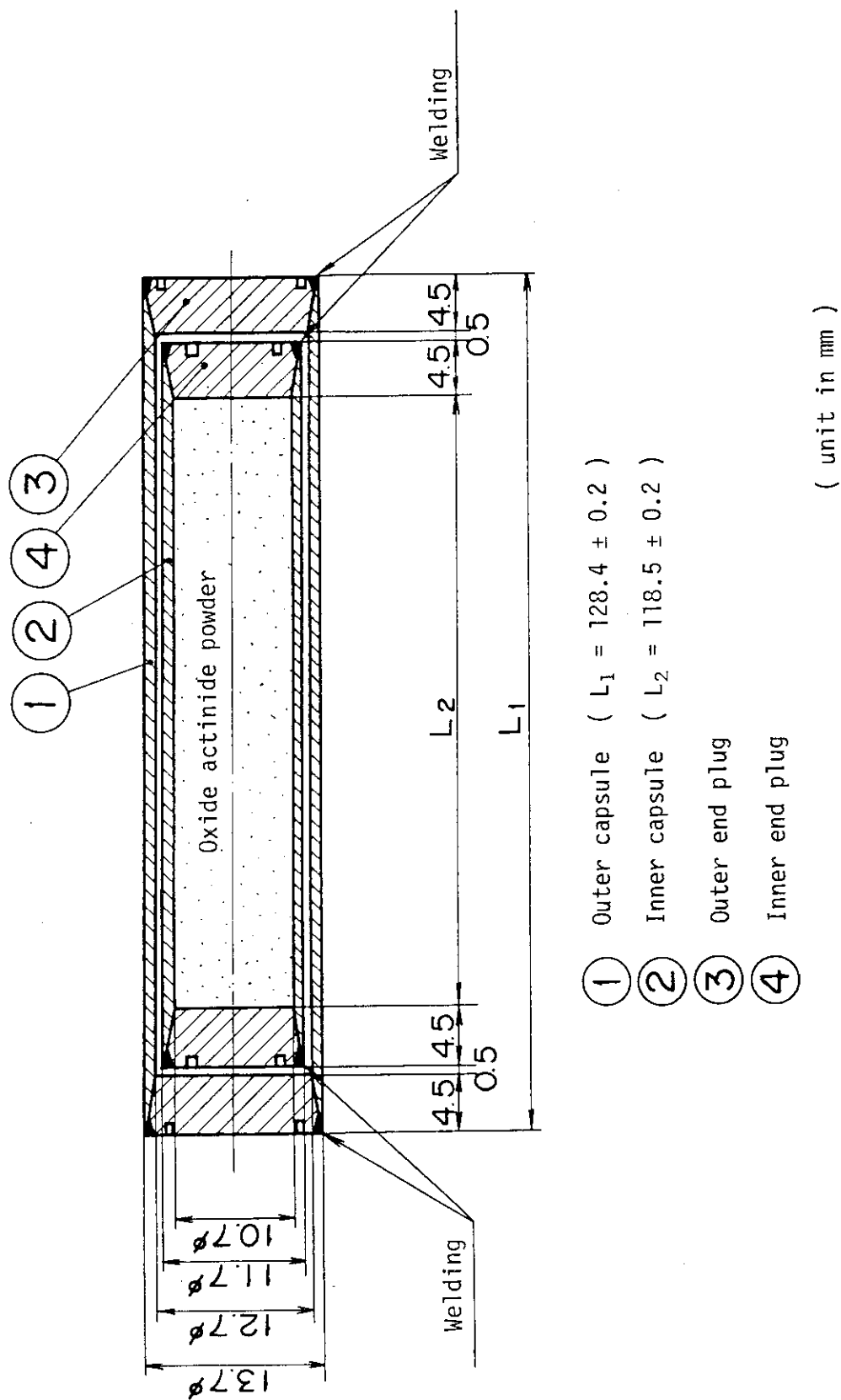
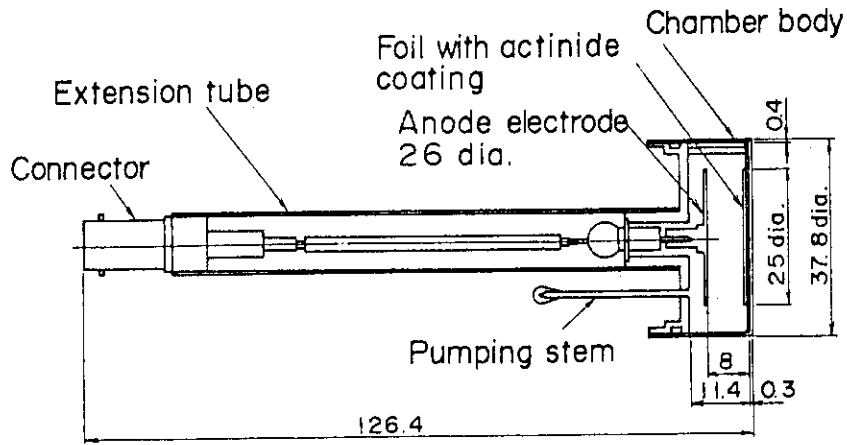


Fig. 3.5.1 Actinide sample for worth measurement



Dimensions in mm

Fig.3.5.2 Configuration of fission chamber

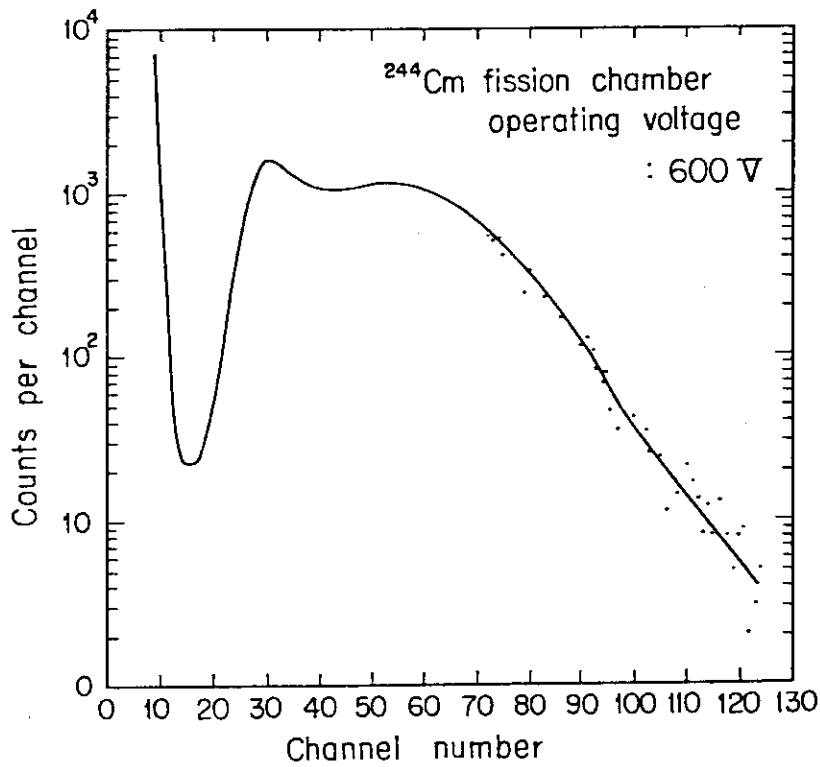


Fig.3.5.3 Fission pulse height distribution of ^{244}Cm

3.6 Integral Experiments for Actinides Cross Section Evaluation (II) FCA Standard Cores

M. Nakano, K. Koyama and H. Kuroi

Recently, reliable cross section data of actinide elements are getting more widely needed for evaluating problems relating on fuel cycle and waste dispersal alternatives. The improvement of cross section data is achieved by collaborating differential and integral measurements. The small perturbation and the fission rate ratio are the realistic integral data of the actinide elements because of the high radio activity of actinides. In contrast with the differential measurements, the integral measurements are very accurate, but the information with respect to the energy dependency is not so straightforward. Therefore, the choice of appropriate variety of neutron spectra where integral measurements are taken place is most important to obtain a successful result for improving the cross section data.

A series of integral experiments for evaluating actinide cross section data is now in progress on FCA Assembly IX. The assembly IX consists of six different version of cores to cover a wide range of neutron spectra. The core composition of these six cores given in Table 3.6.1 have been selected considering the following factors:

- a) Each configuration of core should be simple in its composition and geometry for making analysis reliable.
- b) Available amount of actinide sample for perturbation measurements is limited up to 20 gr. Therefore, core configurations are selected so as to be its critical mass less than 200 kg of fissile material.
- c) In order to minimize temperature drift during the perturbation measurements plutonium is not used as core fuel. Only 93% enriched uranium metal fuel is used and each one of graphite or stainless steel is used as a diluent material for shifting neutron spectrum appropriately.

Typical results of calculated fission rate ratio to be measured in these cores are given in Table 3.6.1. As seen in the Table, measured data will well represent neutron spectrum dependency.

Before starting integral measurements of actinide elements, basic parameters of the core including criticality and fission rates and sample

reactivity worths of standard materials have been measured on the selected cores of FCA IX. The C/E values of criticality are given in Table 3.6.2. The calculation was made by the transport theory with S_4P_1 approximation using the group constants generated from 1950 group library AGLI-2 for each core. The calculation predicts the measured criticality within $\pm 1\%$.

Integral measurements of actinide elements are now in progress. The experiment using fission chambers and sample materials of the separated isotope¹⁾ will be finished in December 1981.

Reference

1) Mukaiyama T., Ōbu M. and Kuroi H.: 3.5 of this report.

Table 3.6.1 Core composition and calculated fission rate ratio at the center of FCA Assembly IX

Assembly	IX-1	IX-2	IX-3	IX-4	IX-5	IX-6
<u>Core composition (v/o)</u>						
93% EU	5.3	10.6	15.9	10.6	15.9	15.9
C	79.4	74.1	68.8	0.0	0.0	0.0
Stainless Steel	10.8	10.8	10.8	84.9	79.6	27.9
Void	4.5	4.5	4.5	4.5	4.5	56.2
<u>Fission rate ratio</u>						
Np237/U235	0.23	0.36	0.45	0.40	0.48	0.59
Pu239/U235	1.06	1.08	1.14	1.15	1.21	1.27
Pu238/U235	0.67	0.88	1.00	1.00	1.10	1.20
Am241/U235	0.29	0.38	0.43	0.31	0.38	0.48
Am243/U235	0.18	0.28	0.35	0.27	0.34	0.43

Table 3.6.2 C/E value of the criticality of FCA Assembly IX

Assembly	C/E
IX-1	0.992
IX-3	0.999
IX-4	1.007
IX-6	1.005

4. Shielding

4.1 PALLAS-TS : A One-Dimensional Neutron Transport Code for Analyzing Fusion Blanket Neutronics¹⁾

T. Suzuki, Y. Ishiguro and Y. matsui*

The code PALLAS-TS has been developed for analyzing fusion blanket experiments. A 120-group library²⁾ of neutron group constants was prepared from the ENDF/B-IV nuclear data file using the process code PROF-GROUCH-GII³⁾. The energy range is from 16.487 MeV to 0.32241 eV, and the data of 29 nuclides were processed. Elastic and inelastic (discrete levels) scatterings were treated in anisotropic model, while inelastic scattering in the continuum level region and (n, 2n) and/or (n, 3n) reactions were assumed to be isotropic in the laboratory system. For the 121st (thermal) group, the constants needed are to be prepared for each problem by a cell calculation code like SRAC⁴⁾ and are input by cards.

The time independent transport equation is solved for one-dimensional, plane or spherical, multi-regional geometry. Special implementation can be summarized in the following three points:

- (1) Elastic and inelastic (discrete levels) scatterings are treated in anisotropic model without Legendre's polynomial expansion, that is, the group-to-group transference kernels are exactly obtained by direct numerical integration of the double-differential cross sections.⁵⁾
- (2) Spatial and angular distribution of neutron flux in each group is obtained by integrating directly the transport equation along the path traveled by neutrons. As the directions of these paths at each spatial mesh point, the Gaussian quadrature set for 20 points are used.⁶⁾
- (3) A usual multigroup model is adopted in calculation of spatial and angular flux distribution so as to make it possible to use iteration technique with neutron rebalancing in each group at each iteration stage.

Results of test calculation for a 4-region system consisting of lithium and carbon (Table 4.1.1) were compared with the experimental

* Japan Information Service Co., Ltd., Tokyo

values⁷⁾ with a 300 kV Cockcroft-Walton accelerator (PNS) (Table 4.1.2). The overestimate of the fission rate distribution of ^{235}U in the region of carbon may be attributed to the thorough neglect of the resonance self-shielding factors. The underestimate of the fission rate distributions of ^{232}Th and ^{238}U in the same region can be attributed to the fact that the data concerned with the anisotropic scatterings of L_i are insufficient in the ENDF/B-IV nuclear data file especially in the high energy region near 14 MeV.

The present code is the first trial of incorporating the multigroup model to the direct integration method for solving the transport equation. It is observed that computing time by this code is shorter than that of S_n method (Table 4.1.3). Therefore, it is expected for this code to be extended to deal with 2- and 3-dimensional geometries, and to be equipped with the gamma rays transport calculations, and thus, to form a general purpose radiation transport or radiation shielding code system (the BERMUDA code system).

References

- 1) Suzuki T., Ishiguro Y., Matsui Y.: "PALLAS-TS: A One-Dimensional Neutron Transport Code for Analyzing Fusion Blanket Neutronics", JAERI-M 9492 (1981) (in Japanese).
- 2) "Reactor Engineering Division Annual Report of Fiscal 1979", JAERI-M 9032, p.9 (1980).
- 3) Hasegawa A.: to be published.
- 4) "Reactor Engineering Division Annual Report of Fiscal 1979", JAERI-M 9032, p.19 (1980).
- 5) Takahashi A., et al.: J. Nucl. Sci. Technol., 16[1], 1 (1979).
- 6) Takeuchi K.: "Study on a Numerical Approach to the Boltzmann Transport Equation for the Purpose of Analyzing Neutron Shields", Report of Ship Research Institute, Vol.9, No.6, (1972) (in Japanese).
- 7) Maekawa H., Seki Y.: J. Nucl. Sci. Technol., 14[2], 97 (1977).

Table 4.1.1 Composition and outer radius of each region

region	1	2	3	4
nuclide r_0	10.00cm	34.14cm	55.29cm	70.00cm
${}^6\text{Li}$	0.	2.507-3	0.	0.
${}^7\text{Li}$	0.	3.128-2	0.	0.
C	0.	0.	7.345-2	0.
C_r	1.827-3	3.165-3	1.827-3	1.224-3
Fe	6.652-2	1.117-2	6.652-2	4.457-3
Ni	7.964-4	1.449-3	7.964-4	5.336-4

Table 4.1.2 Comparison between calculated values (C) of fission rate distribution by PALLAS-TS and experimental values (E) at PNS

σ_f	${}^{232}\text{Th}$			${}^{235}\text{U}$			${}^{238}\text{U}$		
	C	E	C/E	C	E	C/E	C	E	C/E
r (cm)									
4.6	1.434-3	1.66-3	0.864	1.001-2	1.29-2	0.776	4.588-3	5.93-3	0.774
10.1	3.109-4	2.85-4	1.091	3.159-3	3.04-3	1.039	1.018-3	1.01-3	1.008
15.6	1.105-4	1.16-4	0.953	1.818-3	1.72-3	1.057	3.719-4	3.85-4	0.966
Li 21.1	5.694-5	5.62-5	1.013	1.432-3	1.27-3	1.128	1.950-4	1.88-4	1.037
26.6	2.933-5	3.23-5	0.908	1.308-3	1.13-3	1.158	1.022-4	1.07-4	0.955
32.2	1.824-5	1.95-5	0.935	1.513-3	1.18-3	1.282	6.442-5	6.20-5	1.039
37.7	1.039-5	1.35-5	0.770	4.523-3	2.31-3	1.958	3.703-5	4.20-5	0.882
C 43.3	5.707-6	7.66-6	0.734	4.968-3	2.80-3	1.774	2.046-5	2.38-5	0.860
48.8	3.445-6	4.72-6	0.730	3.783-3	2.18-3	1.735	1.237-5	1.33-5	0.930

Table 4.1.3 Comparison of CPU time between PALLAS-TS and ANISN on FACOM/M200

	PALLAS-TS			ANISN	
	kernel and flux	kernel only	flux only	case 1	case 2
groups	119	119	119	100	4
mixtures	4	4	4	1	1
geometry	sphere	---	sphere	infinite cylinder	sphere
mesh intervals	82	---	82	10	50
n of S _n	20	20	20	6	12
l of P _l	∞	∞	∞	3	∞
ε(ρ) (pointwise)	10 ⁻³	---	10 ⁻³	10 ⁻⁴	?
source prob.?	yes	---	yes	yes	yes
CPU(sec)	845.8	525.0	331.9	101.9	55.0
core(KB)	1584	1584	1612	?	?
lines ^(*)	16629	843	13833	?	?
I/O access ^(*)	11131	4302	14311	?	?

(*) These are dependent on times of usage of the restart option in case of PALLAS-TS.

4.2 PALLAS-2DCY : A Code for Direct Integration of Transport Equation in Two-Dimensional (R, Z) Geometry

K. Takeuchi* and N. Sasamoto

The PALLAS-2DCY computer programme solves the energy and angular dependent Boltzmann transport equation with general anisotropic scattering in cylindrical geometry. Principal applications are to neutron or gamma-ray transport problems in forward mode. The code is particularly designed and suited to the solution of deep penetration radiation transport problems with external source.

The code has been designated based on a method of direct integration of the transport equation¹⁾²⁾, in which the equation is solved by integrating along a flight path of radiation in the direction of motion at each discrete ordinates angles. The specific features of this method are that (1) the radiation flux is calculated at each energy mesh ($n/cm^2 \cdot sec \cdot (sr) \cdot MeV$) without using any conventional iterative technique used widely in Sn method for obtaining group flux at each energy group, and (2) the scattering calculations are made directly using the differential scattering cross section for neutron and the Klein-Nishina formula for gamma rays³⁾. Thus a Legendre polynomial expansion approximation used widely in Sn method is not applied to the calculation of radiation scattering. As a result PALLAS-2DCY can provide always positive and physically meaningful angular and scalar fluxes. Besides, (3) no supplementary difference equations are required to obtain a solution to the flux, which makes users free from bothering about choice of such modes as "diamond difference", "step function" and "weighted difference" equations. By virtue of no use of average flux, PALLAS-2DCY can be applied to even such problems as violently varied angular and spatial distributions of radiation flux⁴⁾. In contrast, two-dimensional Sn codes calculate the transport equation based on the average flux for a cell with each pair of associated cell face fluxes in the five-dimensional finite cells defined in terms of location, direction, and energy phase space variables.

The weak points in the present PALLAS-2DCY code are that (1) it has been written in the fixed dimensioning, which restricts the numbers of

* Ship Research Institute

energy meshes, material regions, nuclides, angular meshes, spatial meshes to be input, and that (2) it is inadequate to deal with a coupled neutron-gamma nuclear data in the present PALLAS library: The present code can deal with only a neutron or a gamma-ray transport problem. Besides, (3) a subroutine for calculation of neutron monoenergy source problems has not been completed, though gamma-ray monoenergy source problems can be calculated. Since the PALLAS-2DCY calculates the radiation flux based on an assumption of continuous source energy, a monoenergy source must be dealt with in a special routine. Finally, (4) the present PALLAS-2DCY program is not completed for general use, and for this reason considerable effort should be made for this purpose.

The neutron cross sections required by PALLAS-2DCY are taken from the PALLAS library. On the other hand the gamma-ray cross sections must be prepared by users, in which only linear attenuation coefficients and pair production cross sections may be prepared at all the energy meshes specified by users and gamma-ray scattering cross sections are not required by virtue of direct use of the Klein-Nishina formula.

An analytic first collision source option is not available in the present code. Analytic first collision source options will be available in the PALLAS-2DCY-FC code under development for a variety of source geometries such as a point, line, disk and cylindrical volume sources. The original PALLAS-2DCY code was written for CDC-6600 computer in 1973⁵⁾ to calculate fast neutron transport in shields. Revisions have been made to the old version so as to calculate thermal neutron and gamma ray transport in shields and also to deal with not only a cylindrical volume source but also various boundary source problems.

References

- 1) Takeuchi K.: J. Nucl. Sci. Technol., Vol.8, No.3, 141 (1971).
- 2) Takeuchi K.: "Study on a Numerical Approach to the Boltzmann Transport Equation for the Purpose of Analyzing Neutron Shields", Report of Ship Res. Inst. Vol.9, No.6, (1972) (in Japanese).
- 3) Sasamoto N., Takeuchi K.: Nucl. Tech. Vol.47 (1), 189 (1980).
- 4) Sasamoto N., Takeuchi K.: Nucl. Sci. Eng., 71, 330 (1979).
- 5) Takeuchi K.: "PALLAS-2DCY, A Two-Dimensional Transport Code", Papers Ship Res. Inst. No.47 (1973).

4.3 Transport Calculation of Gamma Rays Including Bremsstrahlung by the Discrete Ordinates Code PALLAS

K. Takeuchi*, S. Tanaka and M. Kinno**

For the transport calculation of gamma rays including bremsstrahlung, an improvement is made in the PALLAS-PL, SP discrete ordinates direct-integration code to enable evaluation of bremsstrahlung¹⁾. The electrons resulting from Compton scattering, pair production, and photoelectric effect are individually evaluated based on the primary gamma-ray flux calculated with the code. Bremsstrahlung production is then calculated by applying the continuous slowing down model. For this purpose, both the electron stopping power and the differential cross section for bremsstrahlung production are evaluated.

Comparisons of PALLAS calculations with experiments are made to test the validity of this code and method. As a result, the following facts were concluded:

1. The fairly good agreement obtained between PALLAS calculations and experiments, as evidenced in Fig. 4.3.1. These results justifies (a) the accurate treatment of transport calculation of gamma rays, (b) the techniques introduced for calculating the electron stopping power and the differential cross section of bremsstrahlung production, and (c) the continuous slowing down model applied to the electron flux calculation.
2. It is essential for the accuracy of the transport calculation of bremsstrahlung to take into account the energy distribution of the pair-produced electrons as well as the bremsstrahlung.
3. In the case of transport of higher energy gamma rays in heavy materials, such as lead and tungsten, it has been confirmed that the contribution of bremsstrahlung photons to buildup factors is too large to disregard.

* Ship Research Institute

** Fujita Corporation

References

- 1) Takeuchi K., Tanaka S., Kinno M.: "Transport Calculation of Gamma Rays Including Bremsstrahlung by the Discrete Ordinates Code :PALLAS", Nucl. Sci. Eng., 78, 273 (1981).

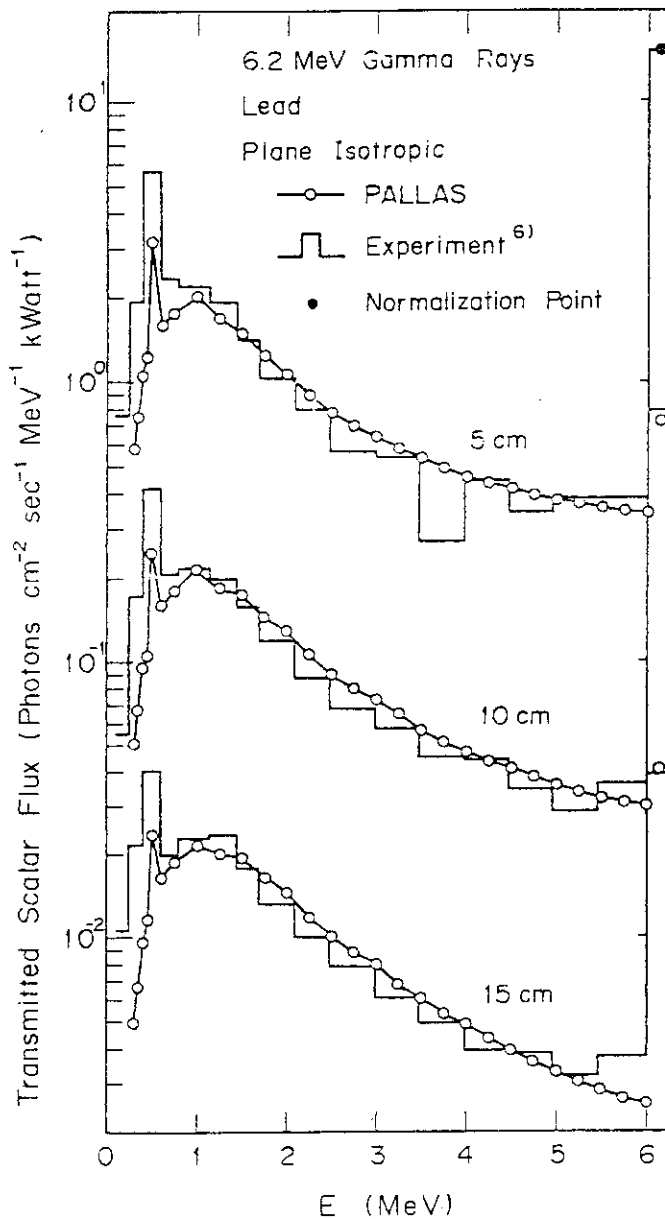


Fig.4.3.1 Comparison of the energy spectrum of gamma rays from a 6.2 MeV plane isotropic source transmitted through 5-, 10-, and 15-cm thick lead layer calculated by the PALLAS code with experiment

4.4 EELOSS : A Program for Calculation of Electron Energy Loss Data

S. Tanaka

A computer code EELOSS¹⁾ has been developed to obtain the electron energy loss data required for shielding and dosimetry of beta- and gamma rays in nuclear plants. With this code, the following data are obtainable for any energy from 0.01 to 15 MeV in any medium (metal, insulator, gas, compound, or mixture) composed of any choice of 69 elements with atomic number 1 - 94 :

- a) Collision stopping power,
- b) Restricted collision stopping power,
- c) Bremsstrahlung production cross section.

The influence of variance of physical data values used in code for the calculations of collision energy loss was examined in a series of calculations, and it is confirmed that the density effect is strongly influenced by the ionization potential, atomic energy level of orbital electrons, and oscillator strength, but the uncertainty in the collision stopping power is within a few percent. Larger uncertainty is attributed to the bremsstrahlung production cross sections in the energy region below 2 MeV because of the large error in the semi-empirical correction factor to the screening effect in the Born approximation in that energy region. However, the influence of this correction factor is much smaller in the energy region above 2 MeV, and consequently the uncertainty in the bremsstrahlung production cross sections also decreases. Fig.4.4.1 shows the comparison between the present calculations and experiments of the bremsstrahlung production cross section of 2.5 MeV electrons. The availability of bremsstrahlung production cross section data and stopping power data obtained by the EELOSS code is demonstrated by the comparison of calculated gamma-ray spectrum with measured one in Pb layer, where electron-photon cascade is included implicitly. As a result, it is concluded that the uncertainty in the bremsstrahlung production cross sections is negligible in the practical shielding calculations of energy less than 15 MeV, since the bremsstrahlung production cross sections increase

with the electron energy and the uncertainty for them decreases with increasing the electron energy. Furthermore, the accuracy of output data of the EELOSS code is evaluated in comparison with experimental data, and as seen in Table 4.4.1 satisfactory agreements are observed concerning the stopping power.

Reference

- 1) Tanaka S. : "EELOSS : The Program for Calculation of Electron Energy Loss Data", JAERI-M 9151 (1980).

Table 4.4.1 Comparison of total stopping power for electrons

T_0 (MeV)	Medium	$-\frac{1}{\rho} \left(\frac{dE}{dX} \right)_{tot} \cdot \text{MeV/g} \cdot \text{cm}^{-2}$		
		Exp.	Berger's data	Present cal.
2.8 ± 0.08	Be	1.45 ± 0.06	1.51	1.50
	C	1.53 ± 0.08	1.68	1.64
	Fe	1.43 ± 0.10	1.51	1.47
	Pb	1.32 ± 0.10	1.44	1.39
	H ₂ O	1.83 ± 0.10	1.92	1.89
4.7 ± 0.14	Be	1.73 ± 0.12	1.56	1.56
	C	1.89 ± 0.16	1.75	1.72
	Fe	1.94 ± 0.19	1.66	1.63
	Pb	2.04 ± 0.22	1.73	1.68
	H ₂ O	2.43 ± 0.20	2.00	1.97

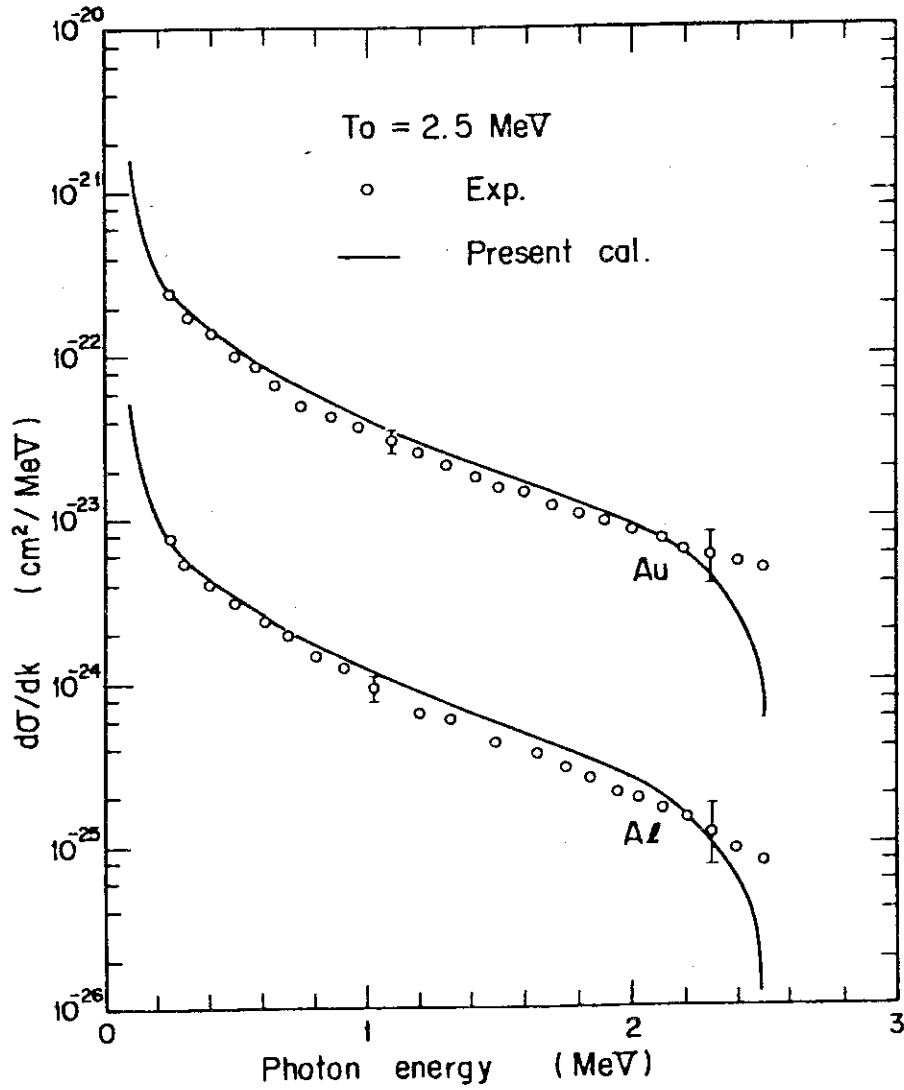


Fig.4.4.1 Comparison of bremsstrahlung production cross section between the present calculations and measurements for 2.5 MeV electrons in Al and Au

5. Reactor and Nuclear Instrumentation

5.1 Development of High-Temperature Neutron Detectors

N. Wakayama, H. Yamagishi, H. Itoh, T. Tomoda* and S. Fukakusa*

High-performance and high-temperature fission counter-chambers and gamma-compensated ionization chambers were developed to be used as in-vessel neutron sensors for VHTR, HTGR and large scale LMFBR, and accelerated neutron irradiation life tests were carried out at 600°C for the fission counter-chambers in 1975 to 1977 in the material testing reactor JMTR and research reactor JRR-3.¹⁾ Following these tests, a long-term real-time in-reactor operating reliability test was started for the same type fission chambers FX-2A and FX-3 in research reactor JRR-4 in December 1978.²⁾

At the beginning of February 1981, the total test period for these chambers in the reactor and the high-temperature operating time at 600°C reached to 774 days and 9697 hours (404 days) respectively. Detailed performance inspections for these chambers were carried out four times during this period and no notable change of operating characteristics has been found in these inspections. Figure 5.1.1 shows the stability of the integral bias curves of a fission counter-chamber FX-3 under the test in this period.

Simulating a reactor accident arisen in the end period of mission time of the neutron detector being used, over-heat operating test has been carried out previously for a fission chamber FX-3 after its irradiation life test.³⁾ As the next over-heat operating test, a new chamber just manufactured has been tested with same manner assuming the reactor accident arisen in the beginning period of the use of the chamber.

An FX-3 chamber was used for this test and the chamber was operated about 510 hours at 700°C and 92 hours at 800°C. No change of performance of the chamber was observed through this test even in the operating characteristics of the chamber at 800°C. Figures 5.1.2 and 5.1.3 show the pulse height distribution and integral bias curves of the chamber measured at the operating temperature of 25°C, 600°C, 700°C and 800°C.

As concerns the high-temperature gamma-compensated ionization cham-

* Mitsubishi Electric Corporation

ber (CIC), accelerated irradiation life test for two CICs manufactured as experimental basis has been initiated in the reactor JRR-4 under the test condition of temperature of 400°C and neutron flux density of around 1.5×10^{11} n/cm²s. Figure 5.1.4 shows a result of the output lineality measurement for these CICs at 25°C and 400°C for the neutron flux density range of 10^2 to 1.6×10^{11} n/cm²s.

References

- 1) Wakayama N., Yamagishi H., Tomoda Y., Kawashima K.: "Development of Fission Chambers for High-Temperature Reactors", Symposium proceedings on Nuclear power Plant Control and Instrumentation, Vol.II, IAEA-SN-226/32, 243 (1978) IAEA.
- 2) Wakayama N., Yamagishi H., Itoh H., Tomoda T., Fukakusa S.: "Reactor Eng. Div. Annual Report (Apr. 1978 - Mar. 1980)", JAERI-M 9032, 98 (1980).
- 3) Wakayama N., Yamagishi H., Itoh H., Tomoda T., Fukakusa S.: "Reactor Eng. Div. Annual Report (Apr. 1978 - Mar. 1979)", JAERI-M 8393, 77 (1979).

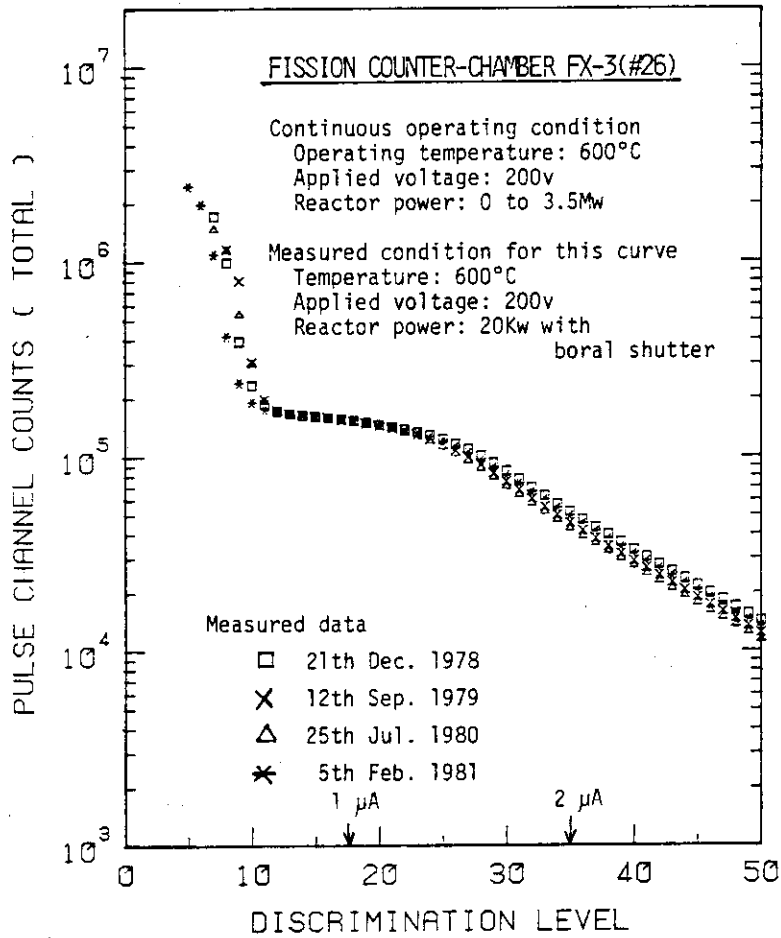


Fig.5.1.1 A result of long-term, high-temperature and in-reactor operating test of fission counter-chamber developed. -Integral bias curves measured at the periodic inspections

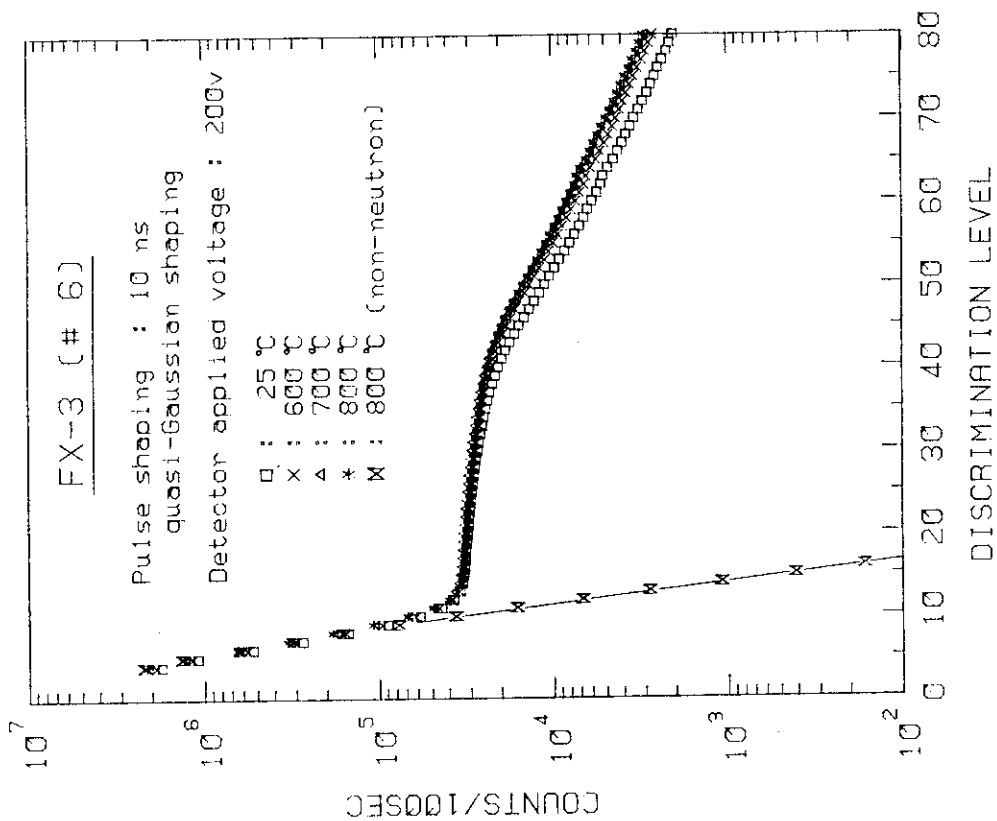


Fig.5.1.1.3 Integral bias curves of the FX-3 chamber at the operating temperature up to 800°C

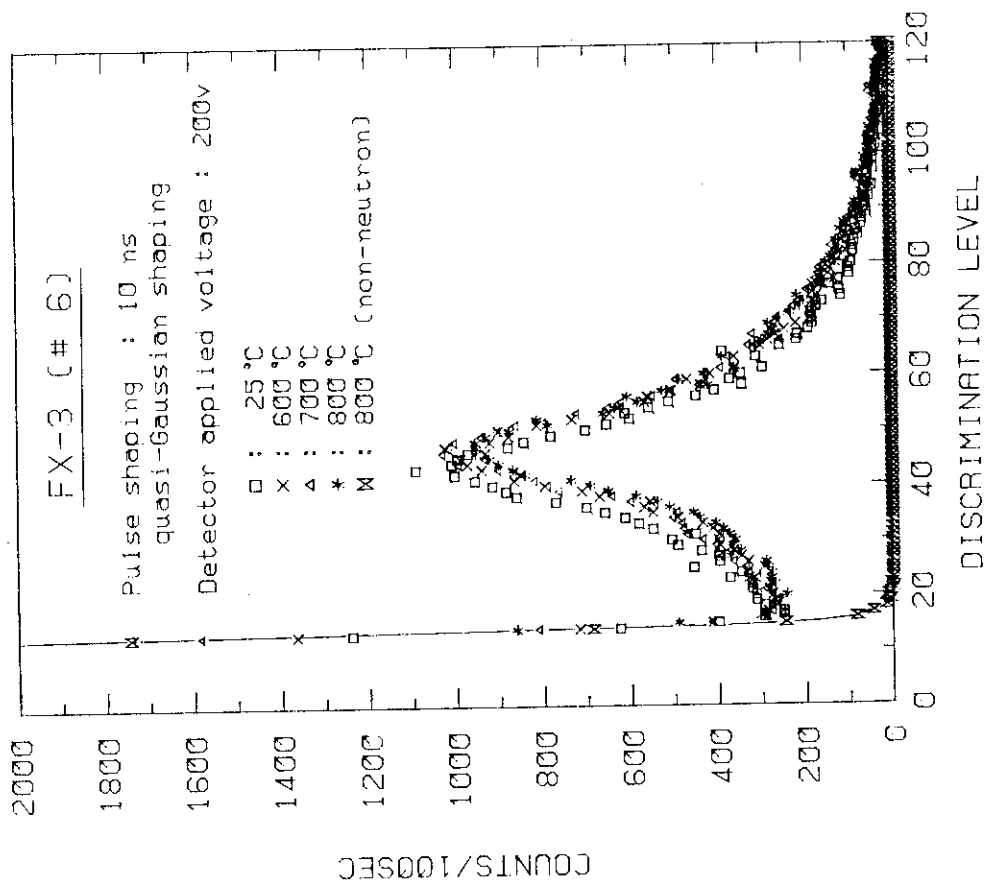


Fig.5.1.1.2 A result of the over-heat test for a fission counter-chamber, model FX-3. -Pulse height distributions at various operating temperature up to 800°C

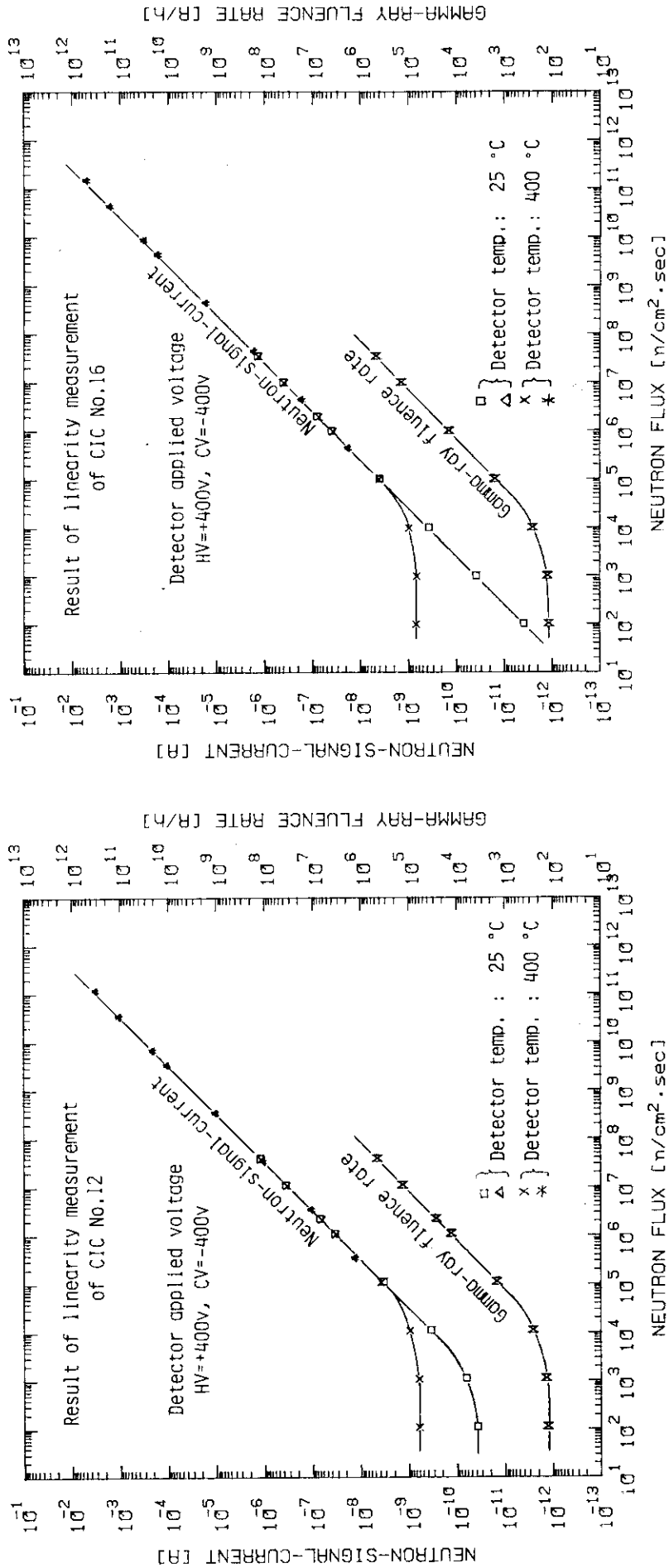


Fig.5.1.4 A result of output linearity measurement for compensated ionisation chambers BCX-2/#12(left) and BCX-2/#16(right) at 25°C and 400°C

5.2 Development of High-temperature Thermocouples for VHTR

K. Ara, M. Yamada and N. Wakayama

As a part of development of high-temperature thermocouples for measurement of helium-gas temperature at the outlet of fuel region in the multi-purpose VHTR, the CA composite-type stranded W-Re alloy thermocouples were fabricated and tested. Figure 5.2.1 shows the general concept of the thermocouple structure¹⁾. The couple of stranded WRe5-26 wire elements is adopted to make itself flexible for adapting to the difference of thermal expansion between the wire and the Al_2O_3 insulator. The double-sheath structure is also one of important points of this thermocouple. The inner sheath is made of a getter material and works as a chemical protector for the element wires against active impurity gases being contained in the charged helium gas and liberated from the insulator. The outer sheath is a mechanical and chemical protector for the inner sheath against the incore environment of high-temperature helium gas containing somewhat reducing impurities.

The fabrication of three thermocouples were carried out, and one of the finished TCs is shown in Photo. 5.2.1. They have the double sheath of Mo(outer) and Ta(inner), and the stranded WRe5-26 element of dia. 0.076 mm x 7 wires; the outer diameter is 4.8 mm and the length of WRe/TC part is 500 mm. These TCs were tested in the electric furnace, shown in Photo. 5.2.2, where the inside of furnace core was filled with helium gas. The hot-junctions were heated up to 1000 °C and the compensating-junctions to 600 °C. This conditions were kept for about 3000 hours, and the electromotive forces were recorded into a data processor and converted to temperature indications. Then, the temperature indications were compared with that of the reference PtRh/TC. All TCs showed very stable emf characteristics and kept good insulations between the element and the sheath. One of the results is shown in Fig. 5.2.2. At the next stage of development program, the performances of these TCs will be examined at more elevated temperatures.

Reference

1) Ara K., Wakayama N.: JAERI-M 7844, pp.137-140 (1978).

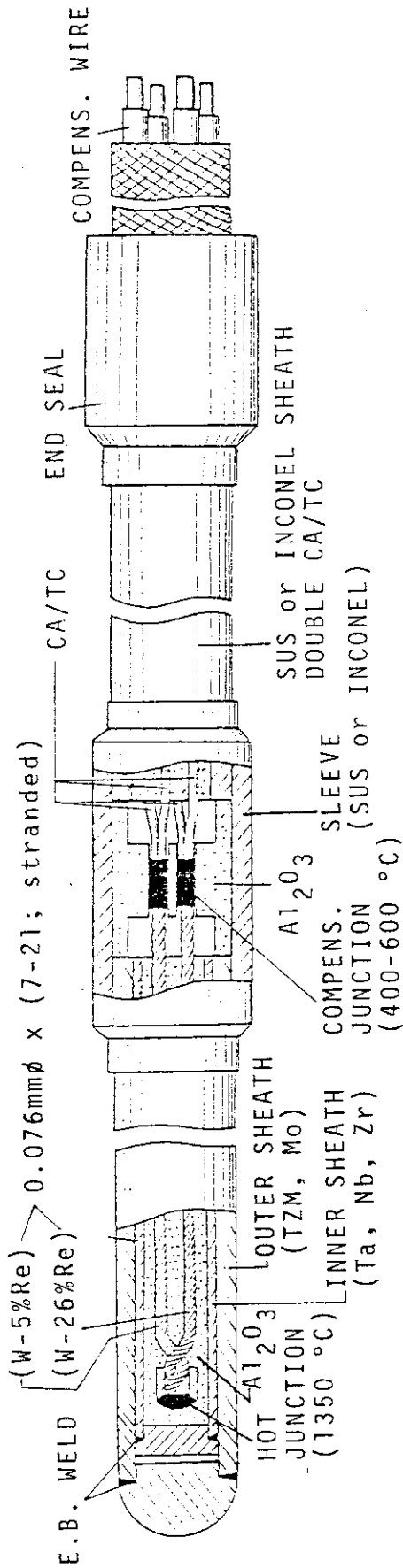


Fig. 5.2.1 Structure of thermocouple

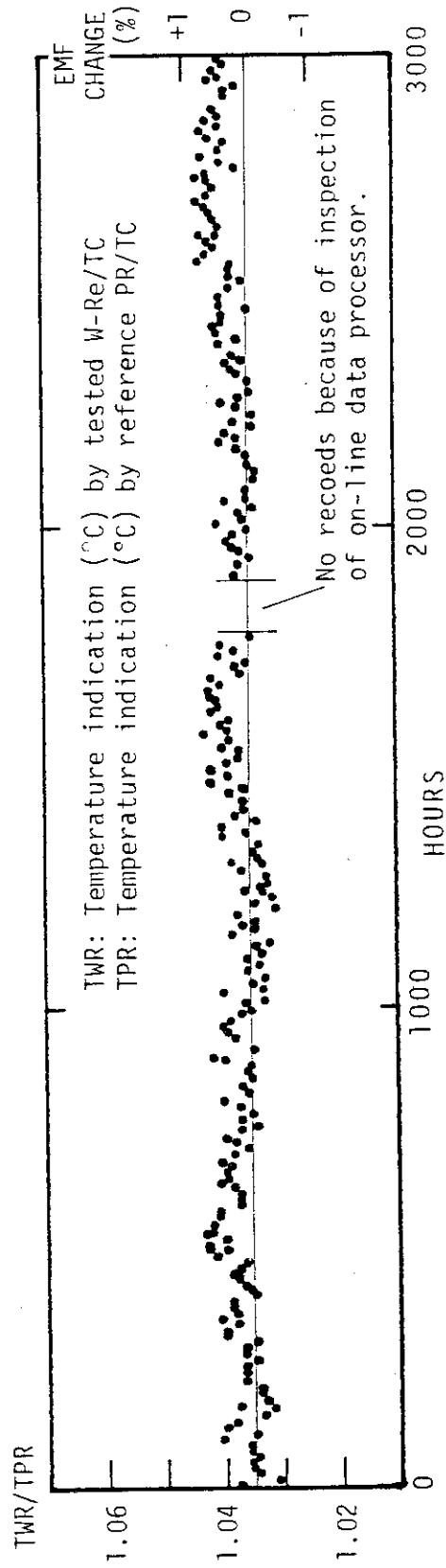


Fig. 5.2.2 Test result of fabricated thermocouple

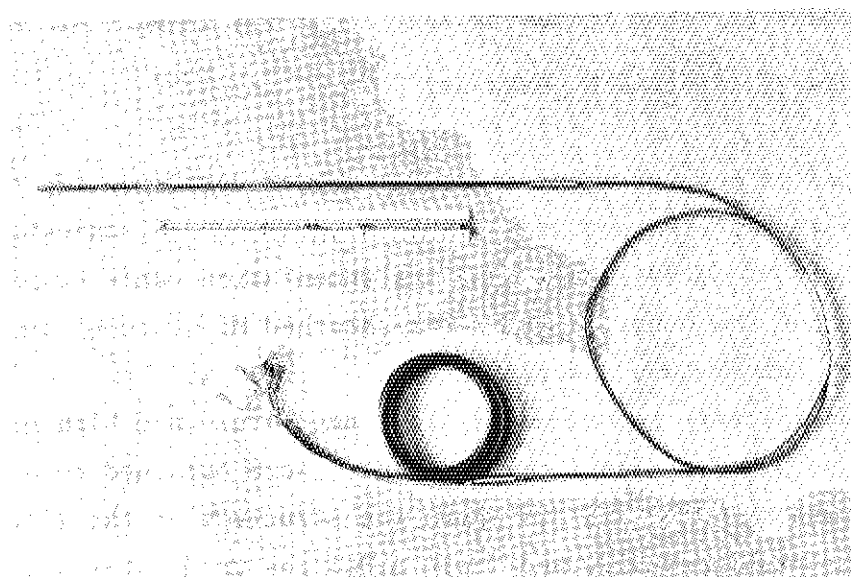


Photo. 5.2.1 Fabricated thermocouple

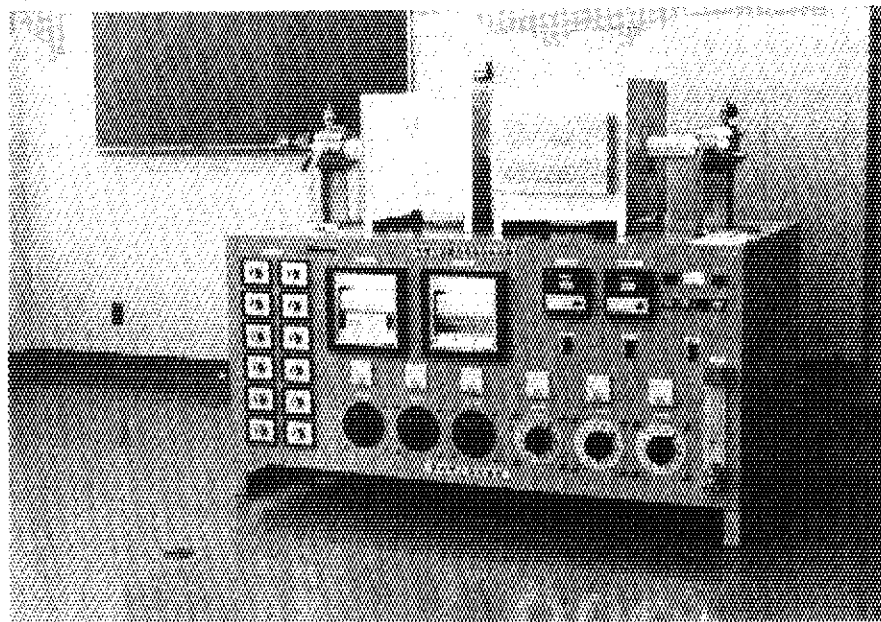


Photo. 5.2.2 Electric furnace for heating test of high-temperature thermocouple

5.3 Development of Cable Insulator and Cables for LMFBR Instrumentation

T. Kakuta, K. Ara and N. Wakayama

Two types of new tri-axial cables have been developed for small-signal transmission in high-temperature and high-radiation environments around the primary circuit of LMFBR. One is the instrumentation cable having enough flexibility, and the other is the metal-sheathed MI-cable to be used as a cable of high-temperature neutron detector.

These cables were tested under high-temperature and high gamma-radiation environments, and fundamental data were obtained to evaluate their performances. Figure 5.3.1 shows the structure of the flexible tri-axial instrumentation cable, and Table 5.3.1 the used materials. The cables showed excellent insulation characteristics under gamma-irradiation of 1.1×10^{10} R, retaining good transmission characteristics and electrical performances. It was also shown, through the flame resisting and vertical-tray flame test, that the cables can keep their functions during a fire for enough time. The results are shown in Fig. 5.3.2.

The MI-cable having the structure shown in Fig. 5.3.3 was made of the materials in Table 5.3.2. Its insulation resistances were examined under high-temperature and gamma-irradiation. The results are shown in Fig. 5.3.4. Also, it was confirmed that the breakdown-pulse-noise inception voltage is over 600 V, even at 550 °C. The transmission characteristic changes very little with temperature up to 550 °C and is very uniform at every part of the cable. The cable can be applied to transmission of small signals in nuclear instrumentation.

Table 5.3.1 Materials of the flexible tri-axial instrumentation cable

	Materials			Size
	79-01	79-02	79-03	
Inner conductor	Poly imide enamelled Ag-plated Cu wire		Ag-plated Cu wire	0.9 mm Dia.
Inner insulator	Glass fiber winding and braid (Poly imide impregnate)	Glass fiber winding and braid (Non impregnate)		5.0mm O.D. 2.0mm Thick.
	Glass fiber tape Glass fiber braid			
Outer conductor	Ag-plated Cu wire braid Ag-plated Cu tape			0.14mm Dia. 0.1 mm Thick.
Outer insulator	Glass fiber tape Glass fiber braid			0.4mm Thick.
Armour	SUS wire braid			0.32mm Dia.
Diameter	—	—	—	8 mm O. D.
Weight	150 kg/km	140 kg/km	140 kg/km	—

Table 5.3.2 Materials of the MI cable

	Material	Size (mm)	
		O. D.	Thick.
Center conductor	Oxygen free Cu	0.95	
Inner insulator	SiO ₂ - fiber	2.90	0.98
Inner sheath 1S	Cu	3.90	0.50
Outer insulator	SiO ₂ - fiber	5.40	0.75
Outer sheath 2S	SUS - 304	6.40	0.50
Insulation density	≈ 60 %	—	

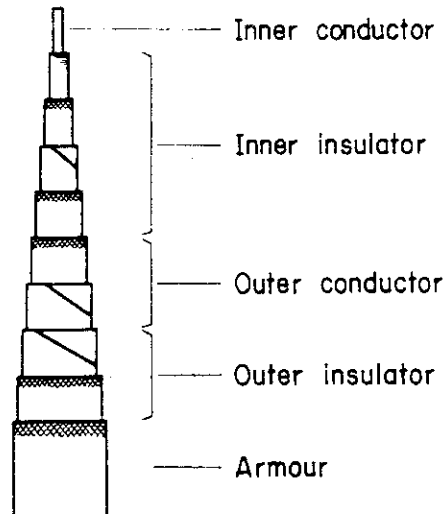


Fig. 5.3.1 Structure of the flexible tri-axial instrumentation cable

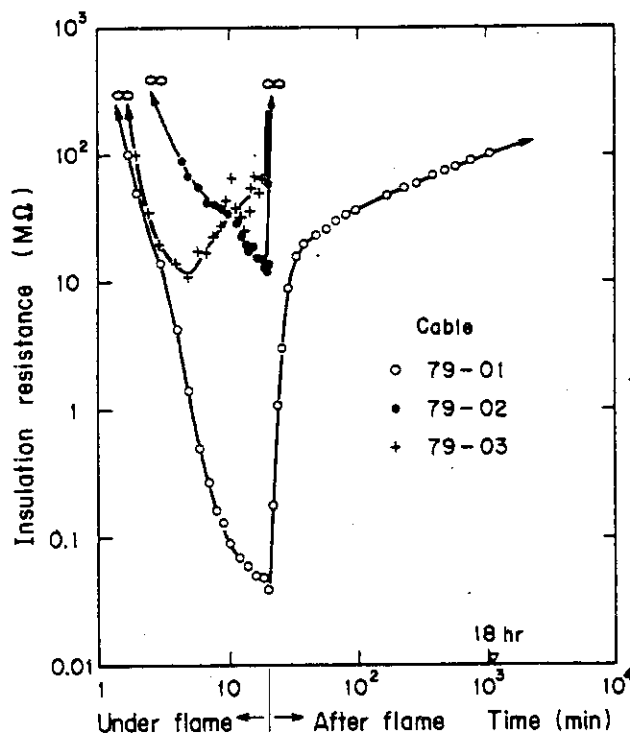


Fig. 5.3.2 Insulation resistances measured at the vertical-tray flame test

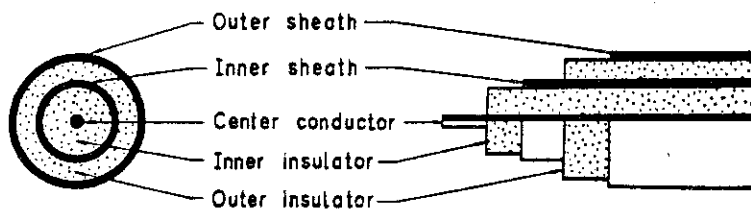


Fig. 5.3.3 Structure of the MI cable

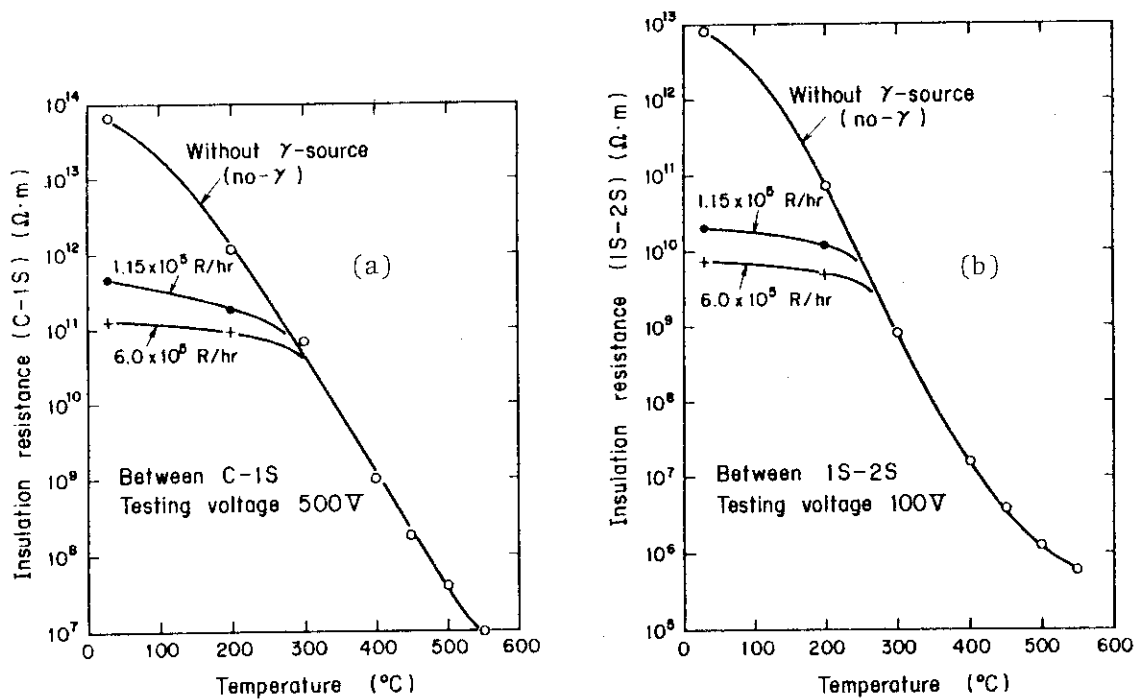


Fig. 5.3.4 Insulation resistances of the MI cable under high-temperature and gamma-radiation environments.

5.4 Development of Fuel Failure Detection System

M. Katagiri, H. Terada and N. Wakayama

In the very high temperature gas-cooled reactor (VHTR) using c.p.f. fuels, a sensitive fuel failure detection system is required to prevent immediately the increase of fuel failure in the anomaly of the reactor core. However, there are several difficult problems which should be solved. One problem is that there exists considerable high background-count due to long life FP-nuclides in the primary He-coolant. The other problem is that the amount of FP-nuclides in the He-gas changes depending on fuel temperature, reactor power, fuel burn-up and so forth. Because of those problems, the conventional FFD-system which is generally used in ordinary GCR is not available to detect the fuel failure in VHTR. In case the conventional FFD-system is used in VHTR, it is estimated that the detection limit of fuel failure is not lower than around ten percent of all fuel elements in the monitoring region.

Following ideas are considered to solve the problems:

- 1) Selective detection of short life FP-nuclides,
- 2) Regional monitoring of the primary He-coolant gas,
- 3) Diagnosis of fuel failure by means of criterion for state equation representing FP-release from the particle fuels.

A new FFD-system was designed on the basis of these ideas; and it is expected that detection limit of fuel failure for the VHTR will be improved up to one percent failure of the inventor at least. The new FFD-system is mainly consist of a filter, time-delay pipings and a wire precipitator. It is planned to examine the feasibility and performance of this FFD-system, coupling to sampling lines of the gas-sweep capsule which is a kind of an irradiation facility for c.p.f. fuels in JMTR. Figure 5.4.1 shows the system construction of the fuel detection experiment.

The purpose of the experiment is to determine the state equation for the FP-release as functions of fuel temperature, reactor power, burn-up rate of the fuels and so forth, and to find the method to judge the fuel failure.

Up to the present step, the each component and system assembly have been already completed, and now the FFD-system is running in test operation at the laboratory. The FFD-system will be connected with the gas-sweep capsule of JMTR in the next July (1981) and then the experiment will be started.

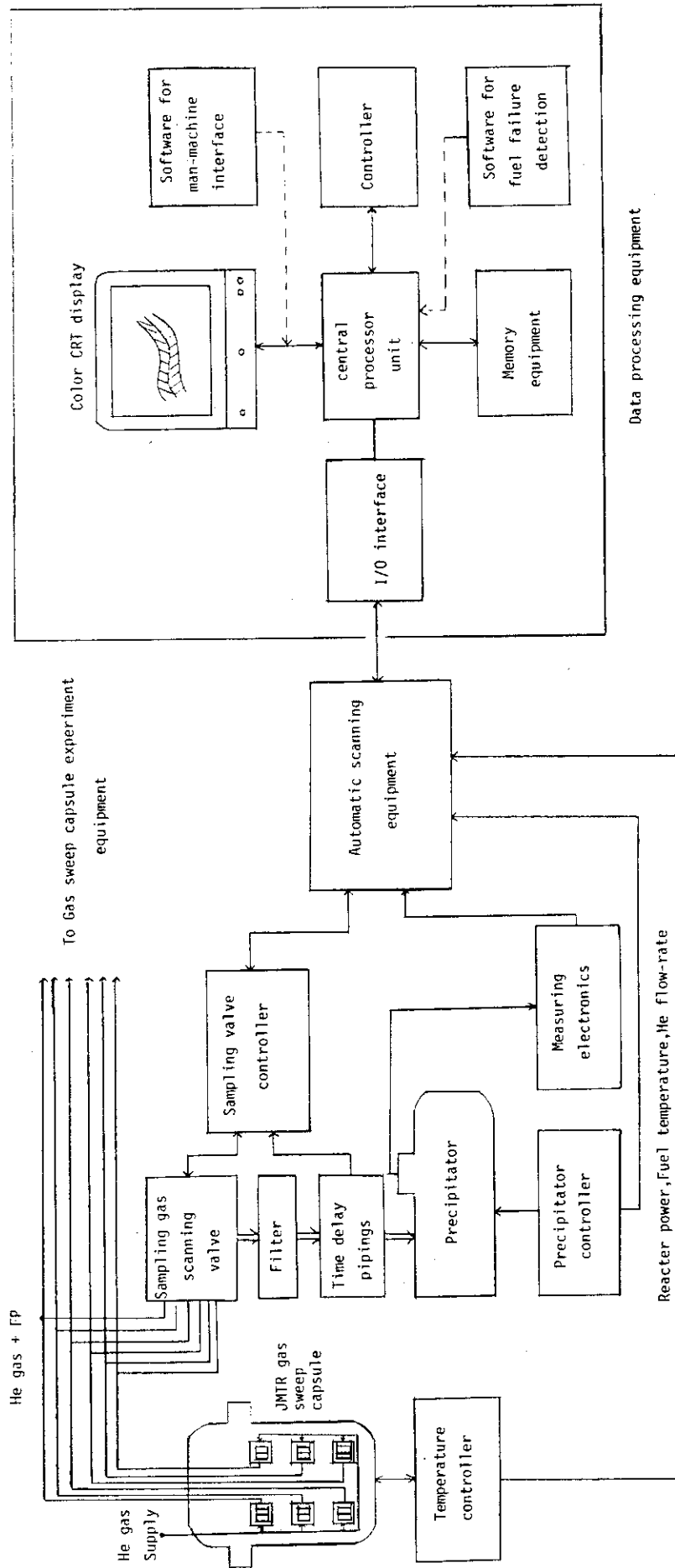


Fig. 5.4.1 System construction of the fuel failure detection experiment

5.5 Development and Test of Cover-gas On-line Gamma-ray Monitors

E.Sakai, K.Kubo*and H.Yoshida

In order to obtain basic data for the use of fuel failure detection systems to be used in the experimental FBR "JOYO" and for designing those systems for the prototype FBR "MONJU", the experiments have been continued using the Cover-Gas Monitor Test Facility located in JRR-3 nuclear reactor 1)2). The performance of a Ge(Li) on-line gamma-ray spectrometer system combined with a cover-gas reservoir or a room temperature charcoal chamber and a fixed-wire type precipitator system were tested using the helium cover-gas of JRR-3 which contained gaseous fission products of 10^{-1} to 10^{-3} $\mu\text{Ci}/\text{cm}^3$ concentrations as well as ^{41}Ar .

The main results obtained are as follows:

- (1) Each of CRT terminal and dot printer were added to the on-line gamma-ray spectrometer system. Some of the programs necessary to the experiments were newly developed³⁾ and some of the problems associated with the present system were analyzed.
- (2) The static adsorption coefficients of Kr at 25°C, 20°C, 10°C and 0°C were measured as $54\text{cm}^3/\text{g}$, $115\text{cm}^3/\text{g}$, $167\text{cm}^3/\text{g}$ and $248\text{cm}^3/\text{g}$, respectively, for 5000ppm Kr in He standard gas flowed through 50g of charcoal TSURUMI COAL 2GM packed in a 100cm^3 chamber.
- (3) The saturated enrichment factors of ^{41}Ar , ^{88}Kr and ^{135}Xe were found to be about 8, 48 and 800, respectively, for cover gas flowed through the room temperature charcoal chamber (50g TSURUMI COAL 2GM in 100cm^3) installed in the CGMIF. Thus, the ratios of Kr-88/Ar-41 and Xe-135/Ar-41 improved by 6 times and 100 times, respectively.
- (4) The output counting rates from the fixed-wire type precipitator system showed a very good response to the rare-gas fission products in JRR-3 cover-gas. Some improvements necessary to the system of practical use were suggested.

The details of the experiments were described in a report⁴⁾.

References

- 1) Sakai, E., Kubo, K.: Development and test of cover-gas on-line gamma-ray monitor (I), SJ 250 79-06, (April 1979) (in Japanese).
- 2) Sakai, E., Kubo, K., Yoshida, Y.: Development of cover-gas on-line gamma-ray monitor (II), SJ 250 80-27 (June 1980) (in Japanese).

* Visiting engineer, on leave from Toshiba Corporation

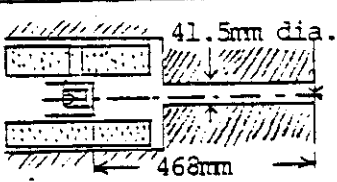
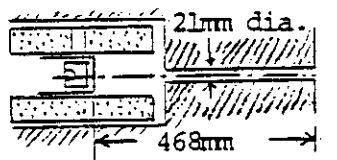
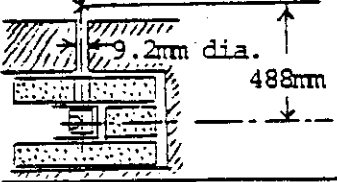
- 3) Yoshida,H., Kubo,K., Sakai,E.: Program development for Canberra Industries 8100/QUANTA system, in Section 5.10 in this annual report.
- 4) Sakai,E., Kubo,K., Yoshida,H.: Development and test of cover-gas on-line gamma-ray monitor (III), SJ 250 81-07 (March 1981) (in Japanese).

5.6 Performance of an Anticoincidence-shielded High-purity Ge Gamma-ray Spectrometer System

E.Sakai

An anticoincidence-shielded high-purity germanium gamma-ray spectrometer was built combining a 10"dia. x 10" long NaI(Tl) scintillation annulus (Horiba Model 440AH U6MP s/n 30623, 10.7% energy resolution for 661.7keV gamma-rays) having a 70mm dia. through hole, a 2.5"dia. x 3" long NaI(Tl) scintillation plug, and a closed-end high-purity Ge detector(PGT 45 x 45 s/n 340, 1.78keV FWHM, 11.5% relative peak detection efficiency, 44:1 peak-to-Compton ratio for 1332.5keV gamma-rays) in a 15cm thick lead shield as shown in Fig.5.6.1. This system can be used to analyze gamma-ray beam incident from the sources placed at the outside of the shield as well as to analyze the sources placed at the inside of the shield. The performance of various types of the spectrometers was investigated. Some of the results were as follows.

(1) The performance of the spectrometers of the three configurations for measuring gamma-ray beams is summarized in the following table.

Configuration	Gamma-ray energy		
	661.7keV	834.8keV	1274.5keV
	FWHM(keV) 1.40 P.D.E. ($\frac{\text{cts}}{\gamma}$) 8.0×10^{-5} P/C _m 540	1.50 6.8×10^{-5} 560	1.80 4.5×10^{-5} 580
	FWHM(keV) 1.45 P.D.E. ($\frac{\text{cts}}{\gamma}$) 4.2×10^{-5} P/C _m 950	1.52 3.5×10^{-5} 1019	1.70 2.5×10^{-5} 900
	FWHM(keV) 1.47 P.D.E. ($\frac{\text{cts}}{\gamma}$) 1.00×10^{-5} P/C _m 1024	1.60 8.5×10^{-6} 960	1.77 5.25×10^{-6} 1110

Figures 5.6.2, 5.6.3 and 5.6.4 show the examples of the pulse height distributions of gamma-rays obtained with normal and anticoincidence modes. In Fig.5.6.2 which obtained from a 834.8keV gamma-ray beam from ⁵⁴Mn through the 21mm dia. collimator hole, the peak-to-Compton minimum ratio improved to 1019 while the Compton edge is noticeable. Figure 5.6.3 was obtained from a 661.7keV gamma-ray beam incident from the side through

the 9.2mm dia. hole and exhibited little Compton edge with a peak-to-Compton minimum ratio of 1024 although the gamma-ray peak detection efficiency decreased to one fourth of that obtained from the beam through the 21mm dia. hole. The peak-to-Compton ratios of about 1000 obtained by this spectrometer are almost comparable to those reported by Camp¹⁾ and Aarts et al²⁾. Figure 5.6.4 shows the pulse height distributions of ¹⁵²Eu(+ ¹⁵⁴Eu) gamma-rays through the 21mm dia. hole. A comparison of the figure of merit³⁾ measurements using anticoincidence mode under ²²Na gamma-ray background for the three different diameter holes gave the best value for 41.5mm hole and the worst for 9.2mm hole even though the peak-to-Compton ratio was the worst for the 45mm hole since the peak detection efficiency played an important role for the figure of merit.

(2) The performance of the anticoincidence spectrometer for low level activity measurements was also tested by placing gamma-ray sources in a space between the Ge detector and the NaI(Tl) plug. The peak-to-Compton ratios were 609 and 636 for 661.7keV and 834.8keV gamma-rays from ¹³⁷Cs and ⁵⁴Mn, respectively; the peak detection efficiencies were 1.2×10^{-2} and 1.0×10^{-2} counts/gamma. The detection limit³⁾ of ¹³⁷Cs for 1000min counting was 0.72pCi(3 sigma) for a point source and 1.9pCi(3 sigma) for a 1367cm³ volume source of 0.344g/cm³ density as shown in the next table.

MINIMUM DETECTABLE DISINTEGRATION RATE, D_m (dps)

$$D_m(E_1) = \frac{A_m}{\epsilon(E_1)f_1t} \left([2bR(E_1)(B_{C2}(E_1) + B_N(E_1)) + \frac{A_m^2}{4}]^{1/2} + \frac{A_m}{2} \right)$$

b=2 for FWTM

¹³⁷Cs; $E_1=661.660\text{keV}$, $f_1=0.853$, $R(E_1)=1.59\text{keV}$

$t=6 \times 10^4\text{s}=1000\text{min}$, $B_{C2}(E_1)=0$

Source	$\epsilon(E_1)$ cts/ γ	$B_N(E_1)$ cts/keV in 1000min	Minimum detectable disintegration rate			
			$A_m=1(100\% \text{ error})$	$A_m=3$	$A_m=10$	
Point	Normal	1.72×10^{-2}	25	1.5×10^{-2} dps (0.40pCi)	4.8×10^{-2} dps (1.3pCi)	2.11×10^{-1} dps (5.7pCi)
	Anticoincidence	1.72×10^{-2}	6	7.6×10^{-3} dps (0.21pCi)	2.7×10^{-2} dps (0.72pCi)	1.47×10^{-1} dps (4.0pCi)
Volume (PL-50A)	Normal	6.4×10^{-3}	25	4.0×10^{-2} dps (1.1pCi)	1.3×10^{-1} dps (3.5pCi)	5.67×10^{-1} dps (15.3pCi)
	Anticoincidence	6.4×10^{-3}	6	2.0×10^{-2} dps (0.55pCi)	7.2×10^{-2} dps (1.9pCi)	3.95×10^{-1} dps (10.68pCi)

The spectrometer performance, especially very high peak-to-Compton ratio is very attractive in various types of measurements.

Cooperation of Katsumi Kubo, Toshiba Corporation, and Hiroshi Yoshida, JAERI, is deeply acknowledged.

References

- 1) Camp, D.C.: Proceedings of ERDA Symposium on X- and Gamma-Ray Sources and Applications, CONF-760539, 67(1976).
- 2) Aarts, J.M. et al: Nucl. Instrum. and Methods, Vol.172, 439(1980).
- 3) Cooper, J.A.: Nucl. Instrum. and Methods, Vol.82, 273(1970).

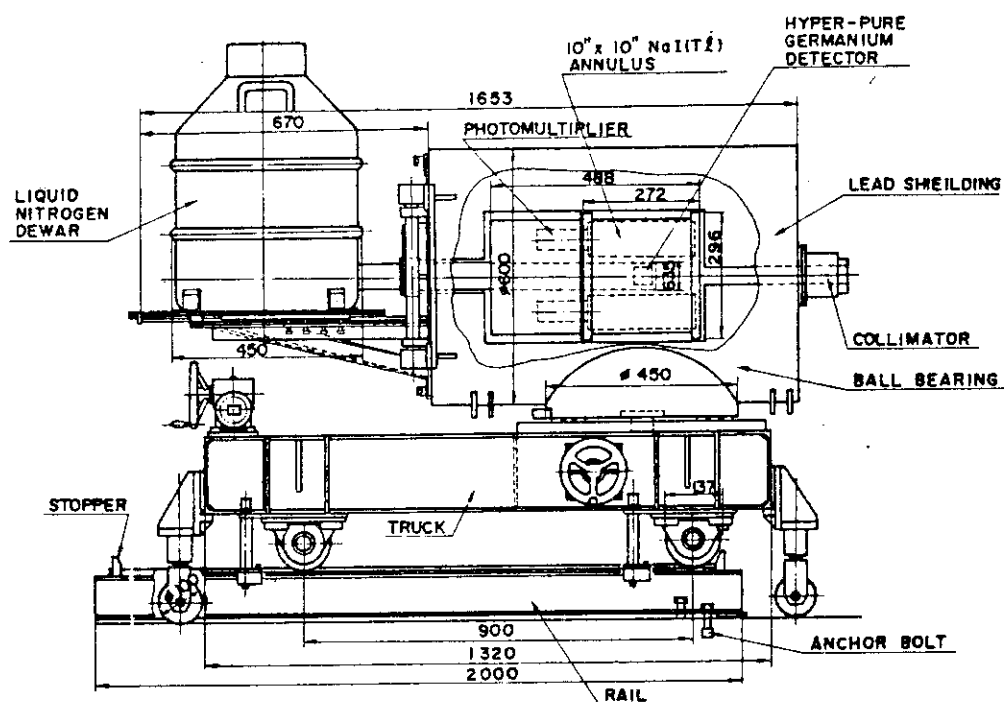


Fig.5.6.1 Anticoincidence-shielded high-purity Ge gamma-ray spectrometer system

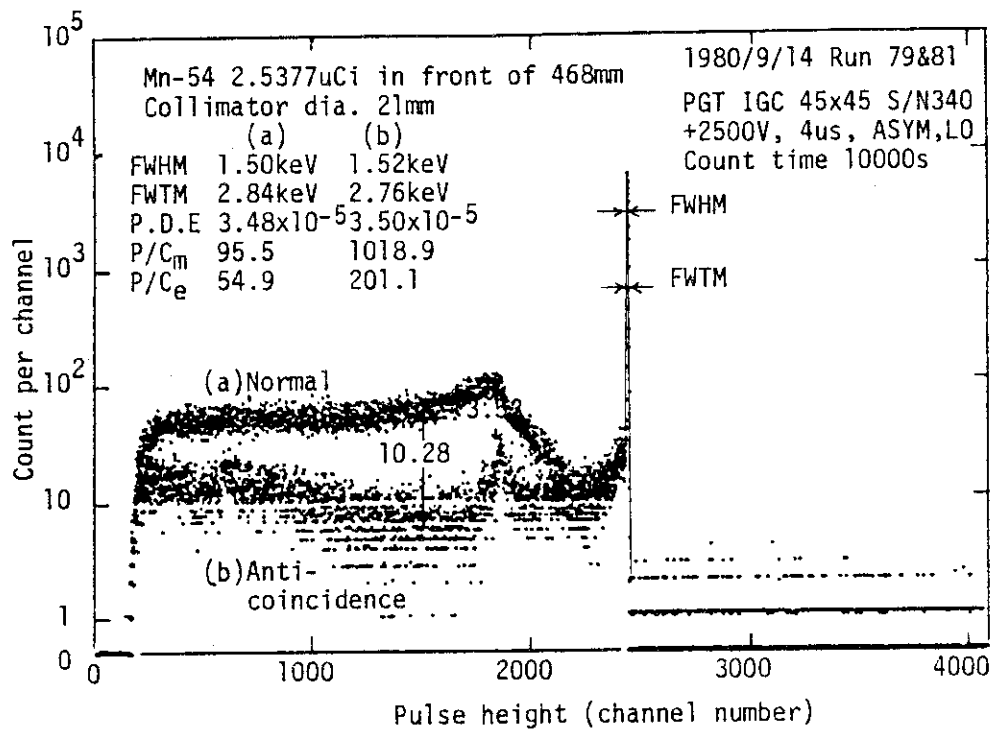


Fig.5.6.2 Pulse height distributions of a 834.8keV gamma-ray beam from ⁵⁴Mn obtained through a 21mm dia. front collimator hole in normal mode (a) and in anticoincidence mode(b)

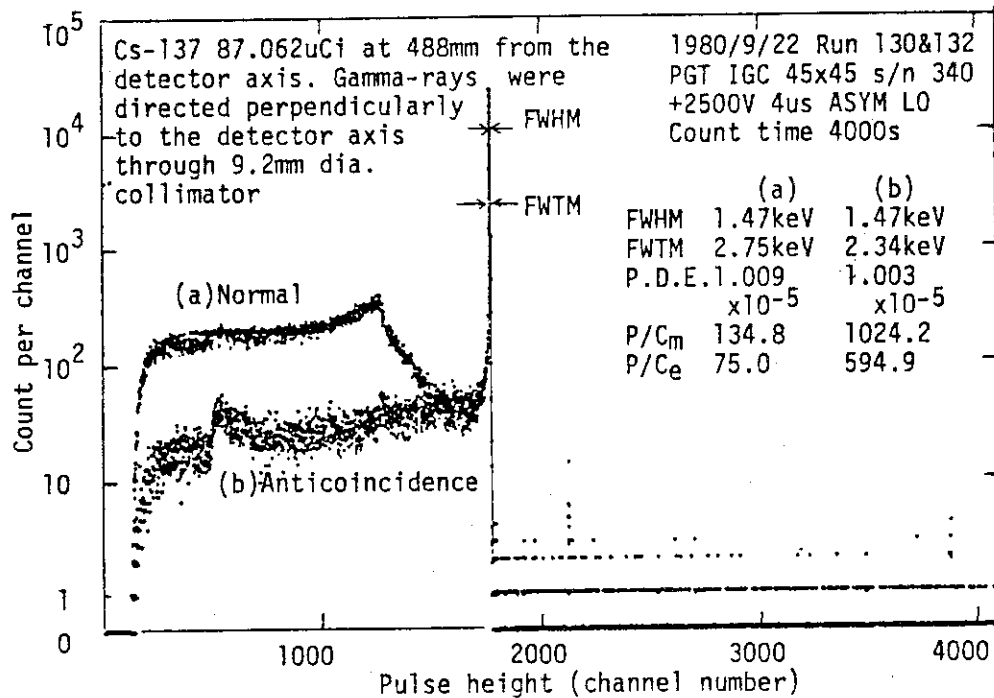


Fig.5.6.3 Pulse height distributions of a 661.7keV gamma-ray beam from ¹³⁷Cs obtained through a 9.2mm dia. side hole in normal mode(a) and in anticoincidence mode(b)

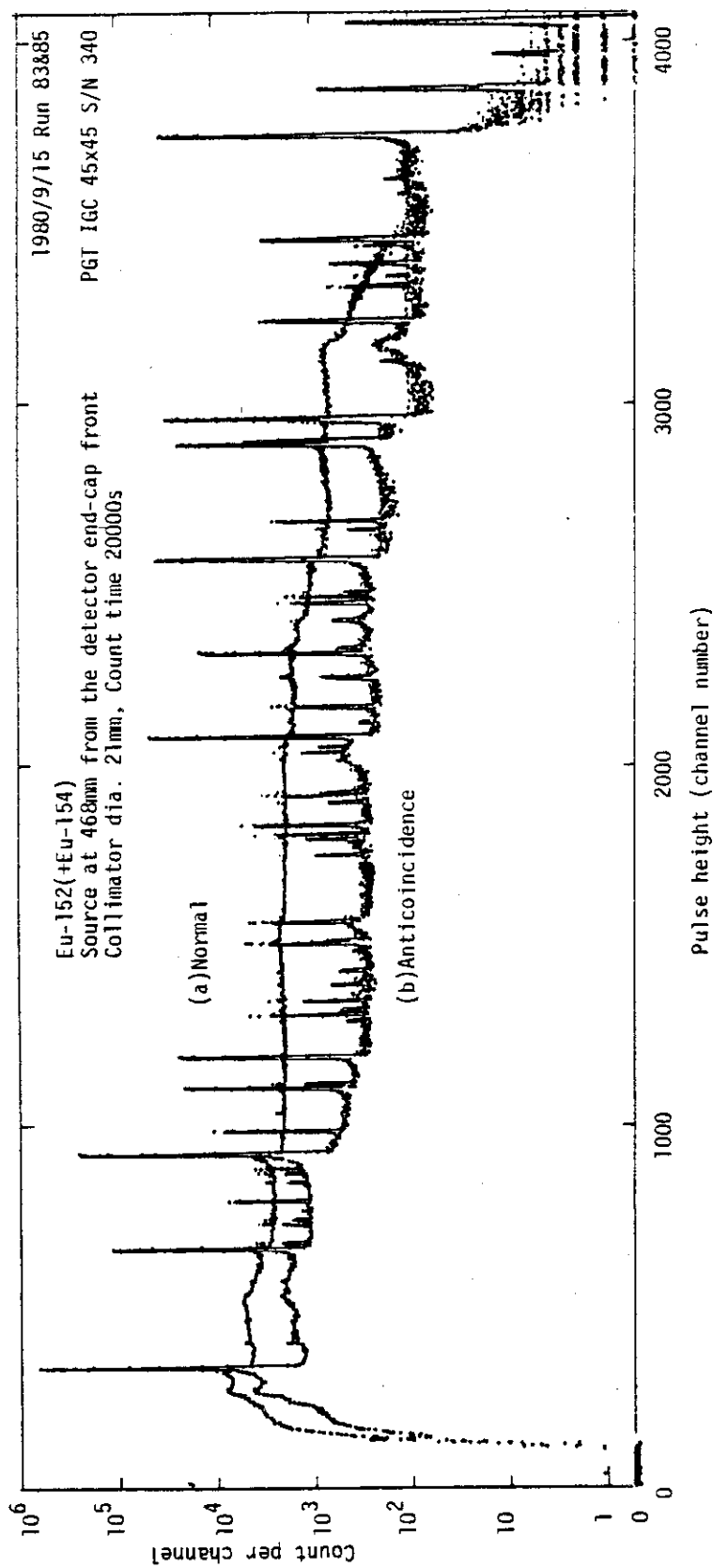


Fig.5.6.4 Pulse height distributions of ^{152}Eu (+ ^{154}Eu) gamma-rays through a 21mm (b) dia. front hole obtained in normal mode(a) and in anticoincidence mode

5.7 Performance of a High-purity Ge Gamma-ray Spectrometer System

Using a Closed-cycle Cryogenic Refrigerator

E.Sakai, Y.Murakami* and H.Nakatani*

Germanium gamma-ray detectors have been normally operated in the cryostats cooled by liquid nitrogen, and produced sometimes maintenance problems related to supplying liquid nitrogen. Recently, the requirement of maintenance free Ge spectrometer systems arises, especially in gamma-ray spectrometry application in nuclear industry. This report describes our experience on the use of a closed-cycle cryogenic refrigerator(Lake Shore Cryotronics, Inc. Model 21, down to 15K, 2W at 20K, $\pm 0.5K$) for cooling a small high-purity Ge detector(APTEC, Ltd., Model No.05005B, $50\text{mm}^2 \times 5\text{mm}$ planar charged particle detector, 10^{-10}A at 600V at 77K). The refrigerator and the detector were chosen simply by the fact that they were there at hand although Marler, et al.¹⁾ found that one type of the refrigerators manufactured by Air Products & Chemicals, Inc. was the most suitable cooler for this application.

First experiment was performed using a standard universal sample chamber supplied with the refrigerator as shown in Photo 5.7.1 in which the compressor unit(200VAC, 15A) and the thermometer/controller(Model DRC 70C) are seen at the right. The detector was mounted on a cold finger placed on the second stage cold station. One of the four glass windows was replaced by an aluminum plate having two feedthroughs for connecting the detector to a room temperature preamplifier(Canberra Industries, Model 2001) and a multichannel analyzer(Canberra Industries, Model 8100). It took about one hour to cool down to 77K. The observed energy resolutions degraded due to the periodic noises caused by the 167 cycles/min vibration of the cold head. The FWHM for a 1.3MeV gamma-ray peak was 10.5keV at an amplifier shaping time of $4\mu\text{s}$ although the FWHM of 3.2keV was observed during a shut down period of the cold head operation. The FWHM improved to 2.6keV at $0.25\mu\text{s}$ as the amplifier shaping time was reduced although this short shaping time is not appropriate for longer risetimes of the pulses generated by larger volume detectors. The FWHM for 60keV gamma-rays was 1.9 keV at $0.25\mu\text{s}$.

Second experiment was carried out using an ordinary design of an end cap-flange combination with the same room temperature preamplifier as shown in Photo 5.7.2. The contribution of the cold head vibration became more significant than that in the first experiment.

* Faculty of Engineering, Toyama University, 1-1, Nakagawasonomachi, Takaoka, Japan 933.

Third experiment was made with a cooled-FET preamplifier (Canberra Industries, Model 970C) using the same chamber as in the second experiment. The vibration effect was reduced to give 3.0keV FWHM for 1.3MeV gamma-rays at 4 μ s shaping while the vibration noises were still observed as shown in Figs.5.7.1, 5.7.2 and 5.7.3. The FWHM of 2.8keV was obtained at 0.25 μ s shaping as shown in Fig.5.7.4. The FWHM for 60keV gamma-rays was 3.3keV even at 0.25 μ s shaping time since the vibration effect enhanced at the higher gain setting of the amplifier used.

Possible methods to reduce the effects of vibration are as follows;

- a) Use of a pileup rejector to reject piled-up pulses.
- b) Use of a gating circuit in order to close the multichannel analyzer synchronously with vibration-induced noises.
- c) Recording gamma-ray pulses only at temporary shut down periods of the cold head operation.
- d) Use of an anti-vibration mount.

One design of anti-vibration mount was prepared, but the experiment is not yet performed.

Cooperation of Katsumi Kubo, Toshiba Corporation, is deeply acknowledged.

Reference

- 1) Marler, J.M., Gelezunas, V.L.: IEEE Trans., Vol.NS-20, No.1, 522(1973).

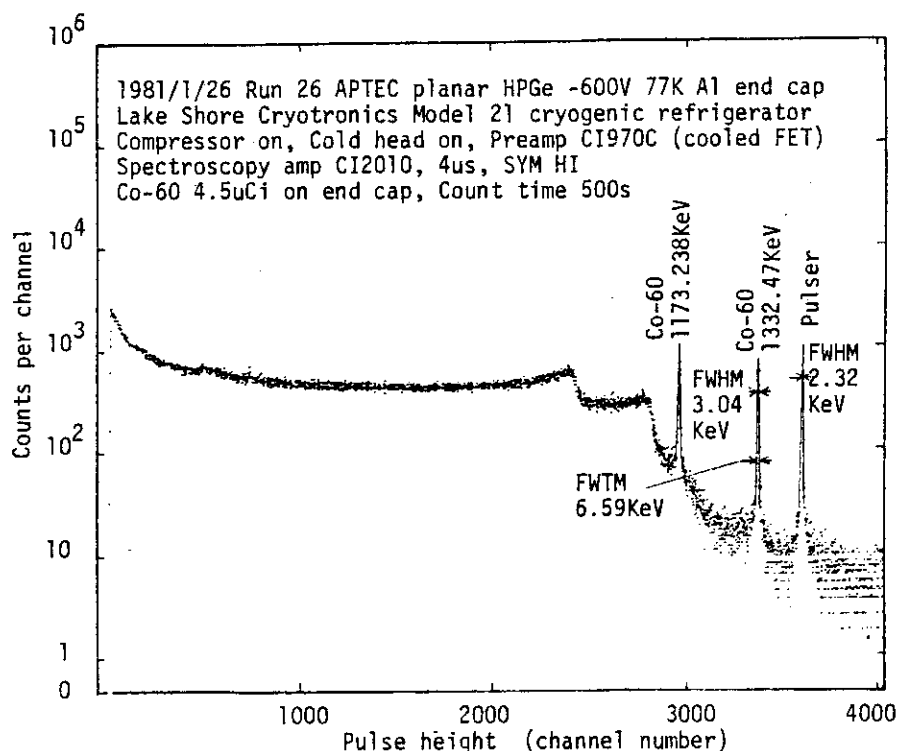


Fig.5.7.1 Pulse height distribution of ^{60}Co gamma-rays observed from a $50\text{mm}^2 \times 5\text{mm}$ planar high-purity Ge detector with a cooled-FET preamplifier. The detector was cooled by a closed-cycle cryogenic refrigerator. The shaping time of the amplifier was $4\mu\text{s}$.

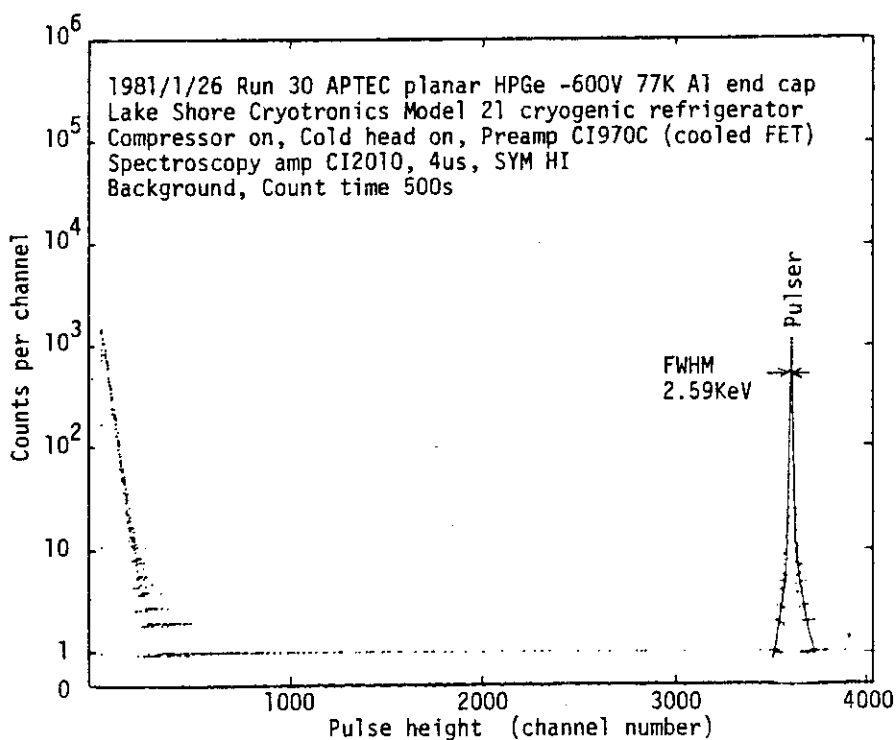


Fig.5.7.2 Background pulse height distribution observed from the same conditions as in Fig.5.7.1. The effect of the vibration is still noticeable at the lower pulse height and the pulser peak.

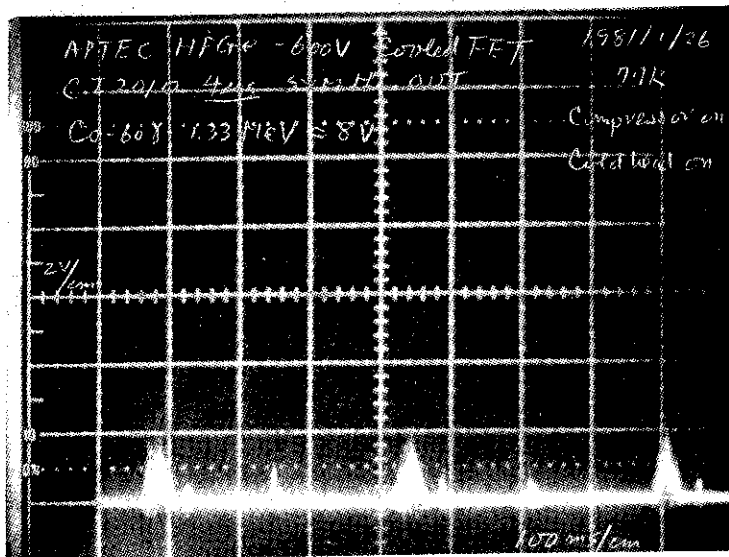


Fig.5.7.3 Noises observed at Canberra Industries Model 2010 spectroscopy amplifier(4 μ s, SYM, HI, Unipolar) output. Vertical and horizontal scales are 2V/cm and 100ms/cm, , respectively. Gamma-ray pulses of 1.3MeV correspond to an amplitude of about 8V .

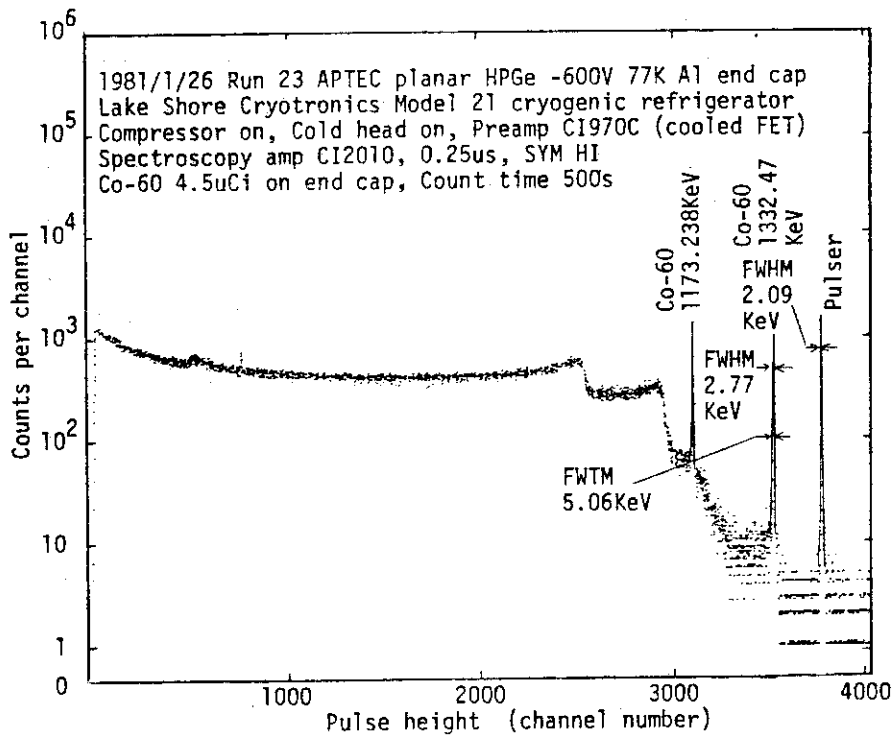


Fig.5.7.4 Pulse height distribution of ^{60}Co gamma-rays observed from the same detector with 0.25 μ s shaping time of the amplifier. The effect of the vibration reduced as compared with that in Fig.5.7.1

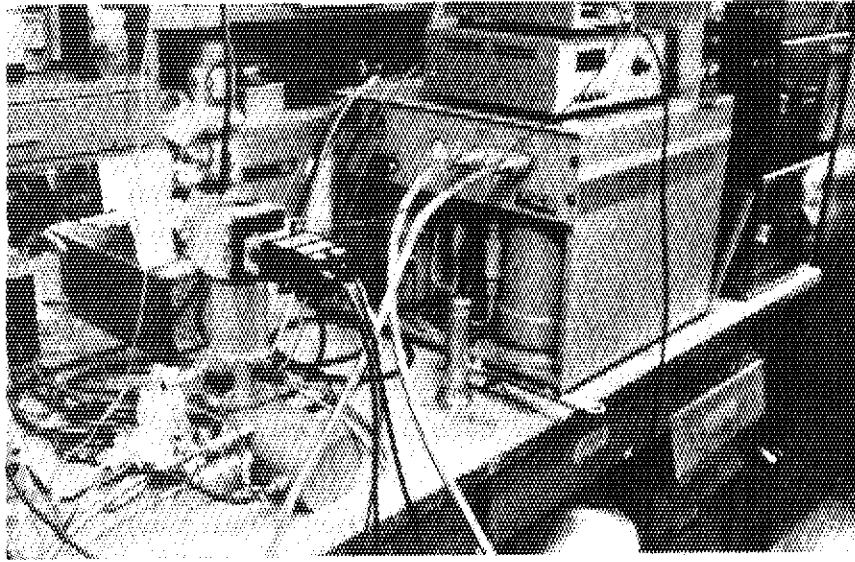


Photo 5.7.1 High-purity Ge gamma-ray spectrometer system cooled by closed-cycle cryogenic refrigerator, Lake Shore Cryotronics, Inc., Model 21. The detector was temporarily mounted in the standard universal sample chamber supplied with the refrigerator.

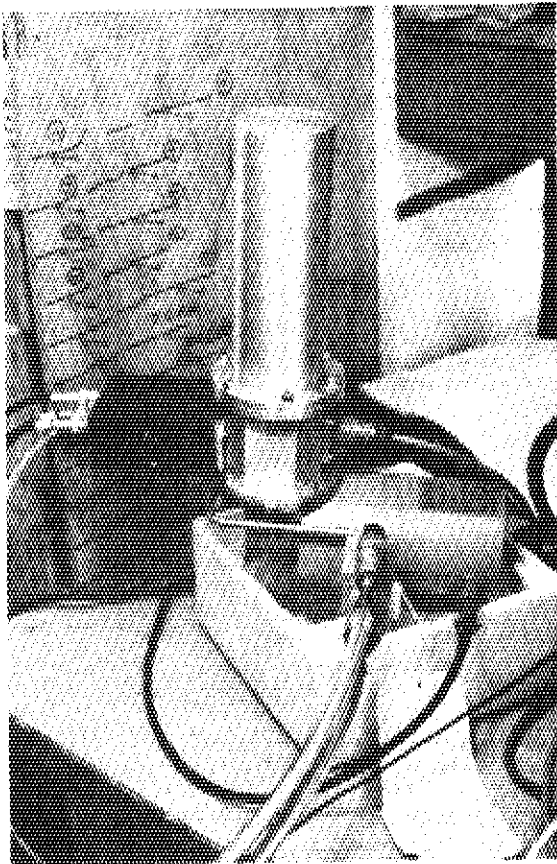


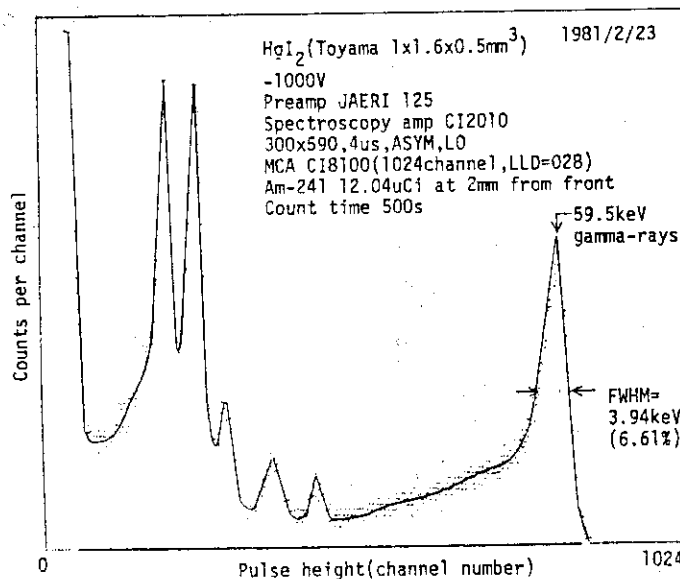
Photo 5.7.2 Refrigerator cold head with an ordinary design of aluminum end cap.

5.8 Fabrication of HgI_2 Nuclear Radiation Detectors

E.Sakai, T.Okubo*, K.Ichinose** and H.Nakatani**

We have been fabricated mercuric iodide (HgI_2) nuclear radiation detectors by putting aquadag electrodes to both sides of about 0.5mm thick crystals grown by a simple vapor transport method. The crystals were grown in a evacuated Pyrex ampoule in a two-temperature-region furnace. The crystals were cut with a laser edge and etched in KI solution¹⁾. Figure 5.8.1 shows a X- and gamma-ray pulse height distribution of ^{241}Am obtained from one HgI_2 detector (#1-3, 1mm x 1.6mm x 0.5mm, Humiseal 1B12 coated) two years and four months after the detector fabrication. The FWHM of 59.5keV gamma-ray peak is 4keV, compared with 5.8keV on the day of the detector fabrication.

This simple crystal growth method produces only small crystals with different characteristics, and large crystals are difficult to be grown. Also it is difficult to find the relation between the detector performance and the crystal growth condition. Thus, we decided to try the temperature oscillation method using a vertical ampoule²⁾. The growth apparatus was built. The first crystal growth using 50g material started the end of December 1980 and after one month an about 30g crystal of 30mm diameter with 25mm height was grown. The crystal was not a single crystal, but it had a single crystal in the center. The C-face of the crystal was determined by neutron diffraction to be slanting. The crystal is not yet tried as detectors.

Fig.5.8.1 Pulse height distribution of ^{241}Am X- and gamma-rays

* Reactor School student, on leave from Japan Nuclear Ship Development Corporation.

**Faculty of Engineering, Toyama University.

References

- 1) Nakatani, H*, Sakai, E., Katagiri, K.: Fabrication of HgI₂ nuclear radiation detectors, JAERI-M 8478 (September 1979) (in Japanese).
- 2) Schieber, M., Schnepfle, W.F., van den Berg, L.: Vapor growth of HgI₂ by periodic source or crystal temperature oscillation, J. Crystal Growth, Vol.33, 125 (1976).

5.9 Fabrication of Low Temperature Cryostats for Tandem Heavy-ion Accelerator

E.Sakai and Y.Kazumata*

Two cryostats were designed and fabricated for studying radiation damage behavior or doping behavior of metals, ceramics and semiconductors under irradiation of various heavy-ions accelerated by the newly built JAERI tandem accelerator.

One of the cryostats, type A, as shown in Photo 5.9.1, was designed for irradiation of samples at controlled temperatures between -196°C and $+100^{\circ}\text{C}$. The sample holder has eight faces, each of which can be set at the irradiation position by rotating the inner assembly with a pulse motor, thus eight samples can be irradiated without breaking vacuum. All the flanges are of ICF conflat types. Two inner assemblies were prepared in order to facilitate a short time of changing samples although the outer assembly is fixed in the accelerator beam-line. In the acceptance test, one charge of liquid nitrogen lasted more than 24hrs and the vacuum reached less than 10^{-8} torr at -200°C and 10^{-7} torr at $+90^{\circ}\text{C}$.

The other types of the cryostats, type B, as shown in Photo 5.9.2, was designed for irradiating at temperatures controlled between 4K and 373K. The sample holder and the inner assembly rotating mechanism are the same as those of type A cryostat although the type B cryostat has its own 100 liters/s turbo-molecular pump, gate valve and double dewars. The type B cryostat can be used in long-term experiments such as annealing measurements after disconnecting from the accelerator beam-line. The acceptance test showed that one charge of liquid helium lasted 7 hrs although 20hrs are expected if the windows of the thermal shield are closed. The vacuum reached less than 10^{-8} torr. A television camera can be used to see beam size, sample condition or vacuum gaze.

These cryostats will be used by various research groups in JAERI.

* Solid State Physics I Laboratory, JAERI.

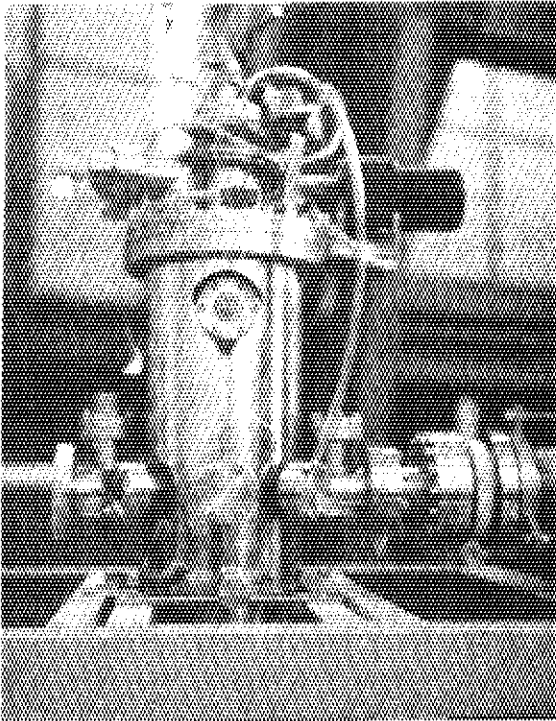


Photo 5.9.1

Type A cryostat for heavy-ion irradiation at temperatures between -196°C and $+100^{\circ}\text{C}$

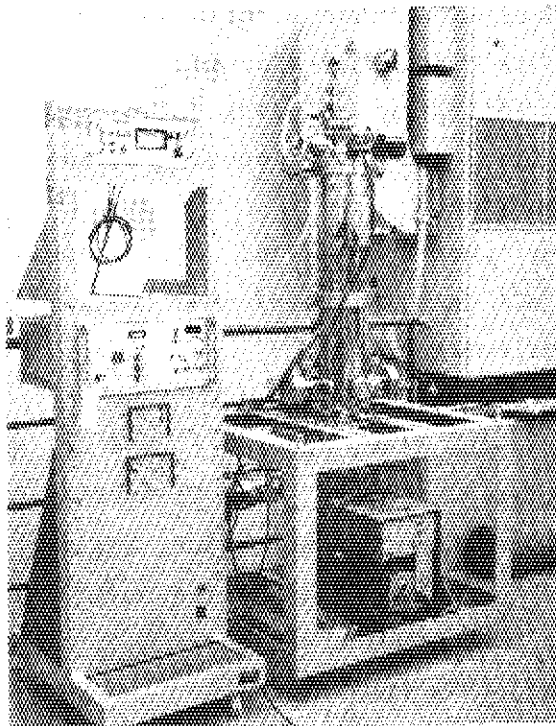


Photo 5.9.2

Type B cryostat for heavy-ion irradiation at temperatures between 4K and $+100^{\circ}\text{C}$. Vacuum gauge, temperature controller, inner assembly rotation controller and automatic liquid nitrogen filler are seen in the left hand rack

5.10 Program Development for Canberra Industries 8100/Quanta System

H. Yoshida, K. Kubo* and E. Sakai

The previous reports¹⁾²⁾ described the hardware construction and principal programs constructed with programming language 'CLASS' (Canberra Laboratory Automation Software System)³⁾ to collect and analyze gamma spectra data.

This report describes the programs which are revised or developed after the previous reports were published.

(1) Second revision of "COLECT" program: as described in the previous report,²⁾ this program accumulates the pulse height distribution of gamma spectra in the memory of MCA (multi-channel pulse height analyzer), copies those data on the disk, analyzes them and writes the resultant data of analysis on the disk. The main parts of the second revision are addition of the functions in which the value of time when each accumulation of gamma spectra stopped, and total counts of #1 to #4095 channel are also recorded on the disk. The content of #0 channel is excluded from totalizing because it stores duration time of data accumulation. The function of recording the start time of each data accumulation is originally adapted.

(2) Development of "CLTO" program: this program prints the list of start time, stop time of data accumulation and total counts recorded on the disk by the program "COLECT" above mentioned.

(3) Development of "COMPRT" program: when A_i , B_i and C_i are assumed as the values of i -th channel counts of MCA data [A], [B] and [C] written on the disk respectively, this program calculates

$$C_i = (A_i / B_i) \times (t_B / t_A)$$

and writes the resultant data as [C] on the disk, where t_A and t_B are collect time of data [A] and [B] respectively. If $B_i \leq 0$, C_i is set zero always. This program is used to calculate Compton reduction ratios of whole channels between data [A] which is accumulated in the normal mode and data [B] which is accumulated in the anticoincidence mode.

(4) Development of "CMPLST" program: this program prints the results of the program "COMPRT" above mentioned recorded on the disk for desired run

*Visiting engineer, on leave from Tokyo Shibaura Electric Corporation.

numbers and desired region of channels recorded on the disk. The time required for the printing of a 4096 channel data set is about 35 minutes.

(5) Development of "MTDSK" program: one of two MCA's of the System is sometimes used for off-line measurements and the data are recorded on the magnetic tapes(M.T.) only. This program is for transferring those data on the M.T. to a disk file in the form of those written by the program "COLECT". The user must type in data identification messages, the start time and stop time of each data accumulation because the data of M.T. contain only the counts of each channels.

(6) Development of "EFPLOT" program and revision of "CALIB" program: "EFPLOT" program draws a continuous curve of gamma-ray energy vs. photopeak detection efficiency characteristics which is calculated by the parameters obtained by "CALIB" program using the digital plotter. X(energy)-axis and Y(detection efficiency)-axis are expressed on a log scale. The points used to calibrate detection efficiency are plotted with combined triangle marks " ∇ " (see Fig. 5.10.1). "CALIB" program is revised to store the data of detection efficiency calibration points (up to 15 points) on the disk.

(7) Development of program "SPLST2": this program prints the list of every channel count of MCA recorded on the disk for desired run numbers and desired region of channels. The results of isotope analysis which are estimated by the program "COLECT" or "GAMMAY"²⁾ are also printed if they are recorded on the disk. The time required for the printing a 4096 channel data set is about 37 minutes.

References

- 1) Yoshida, H., Kubo, K., Sakai, E.: Reactor Engineering Division Annual Report (April 1, 1978 - March 31, 1979), 5.16, pp.128-130, JAERI-M 8383 (September 1979).
- 2) Yoshida, H., Kubo, K., Sakai, E.: Reactor Engineering Division Annual Report (April 1, 1979 - March 31, 1980), 5.13, pp.129-131, JAERI-M 9032 (September 1980).
- 3) Yoshida, H., Kubo, K.: Programming of Canberra Industries 8100/Quanta System - Program Development with "CLASS", JAERI-M 8694 (March 1980) (in Japanese).

DETECTOR: 8
GEOMETRY: 8
DATE: 5-DEC-80: MC-2
VOLUME: 100.00000 CC

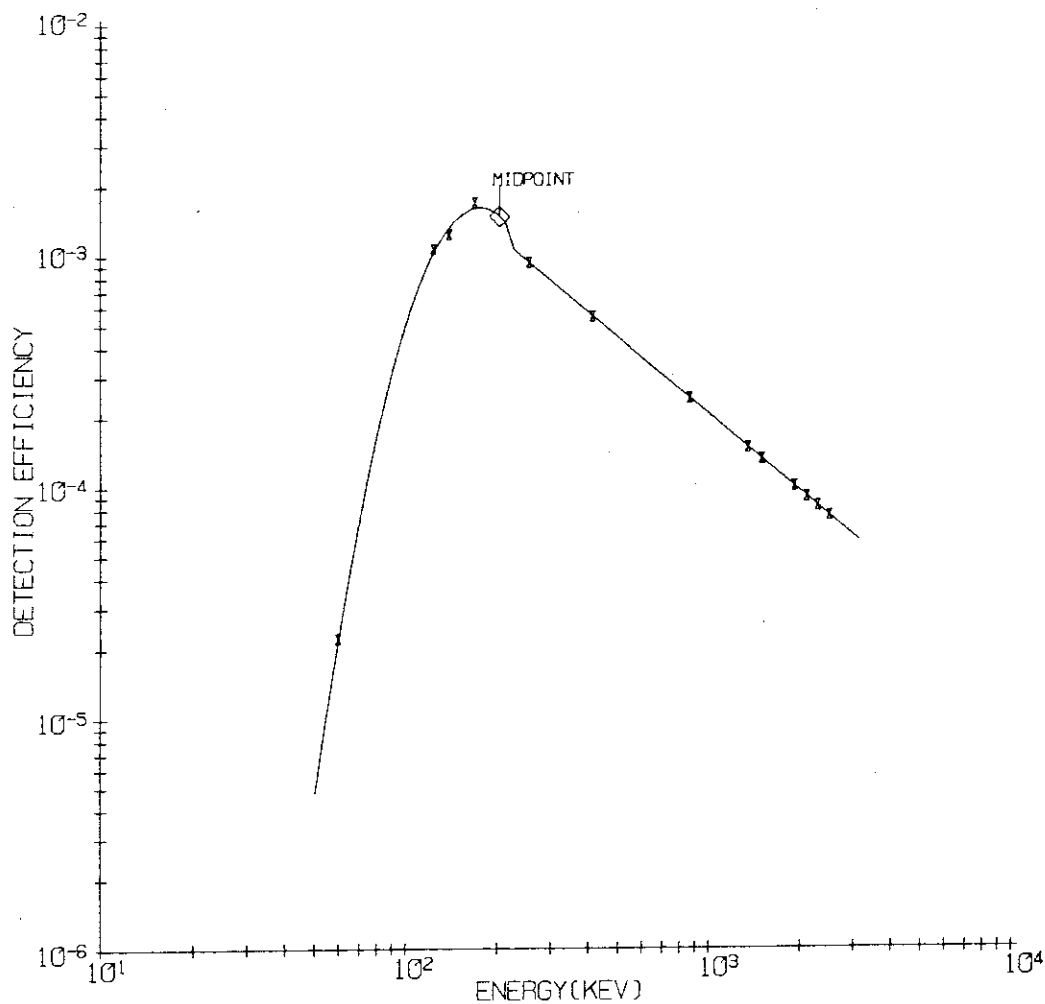


Fig. 5.10.1 Example of Gamma-ray Energy vs. Photopeak Detection Efficiency Curve Drawn by "EFPLOT" Program

5.11 Uncertainty Induced by Count Statistics in Enrichment Measurement with SAM-2 (II)

H. Gotoh

Suppose the case where a SAM-2 is calibrated against n (≥ 2) physical standards, a uranium sample is counted with the SAM-2 and the enrichment and its variance of the sample are derived. Assume that uncertainties in the enrichment of standards and in counting times are both negligible and that counts in channel 1 and 2 contain uncertainties.

Symbols C_{1j} and C_{2j} respectively stand for counts of channel 1 and 2 obtained against the j -th standard during an equal counting time T_j . The deviation of count C_{ij} from the corresponding true count Γ_{ij} is assumed to obey the normal distribution with zero mean and with variance σ_{ij}^2 ($i=1,2$; $j=1,\dots,n$). Symbols C_1 and C_2 respectively denote counts of channel 1 and 2 against the sample during an equal counting time T . Deviations of C_1 and C_2 from the corresponding true counts Γ_1 and Γ_2 are respectively assumed to obey the normal distribution with zero means and with variances σ_1^2 and σ_2^2 . Furthermore we assume the existence of two coefficients α and β and that the following relations are satisfied

$$E_j \cdot T_j = \alpha \cdot \Gamma_{1j} - \beta \cdot \Gamma_{2j}, \quad j=1, \dots, n$$

$$E \cdot T = \alpha \cdot \Gamma_1 - \beta \cdot \Gamma_2.$$
(1)

The indirect least squares procedure with constraints can be applied¹⁾. To obtain the most probable values a and b for α and β , we have to adopt an iterative method. A better approximate set of coefficients a_1 and b_1 can be derived from an approximate set of a_0 and b_0 :

$$a_1 = \frac{1}{\Delta_0} \cdot \left\{ \left(\sum_{j=1}^n \frac{C_{2j}^2}{a_0^2 \cdot \sigma_{1j}^2 + b_0^2 \cdot \sigma_{2j}^2} \right) \cdot \left(\sum_{j=1}^n \frac{C_{1j} \cdot E_j \cdot T_j}{a_0^2 \cdot \sigma_{1j}^2 + b_0^2 \cdot \sigma_{2j}^2} \right) \right. \\ \left. - \left(\sum_{j=1}^n \frac{C_{1j} \cdot C_{2j}}{a_0^2 \cdot \sigma_{1j}^2 + b_0^2 \cdot \sigma_{2j}^2} \right) \cdot \left(\sum_{j=1}^n \frac{C_{2j} \cdot E_j \cdot T_j}{a_0^2 \cdot \sigma_{1j}^2 + b_0^2 \cdot \sigma_{2j}^2} \right) \right\}$$

$$b_1 = \frac{1}{\Delta_0} \cdot \left\{ \left(\sum_{j=1}^n \frac{C_{1j} \cdot C_{2j}}{a_0^2 \cdot \sigma_{2j}^2 + b_0^2 \cdot \sigma_{2j}^2} \right) \cdot \left(\sum_{j=1}^n \frac{C_{1j} \cdot E_j \cdot T_j}{a_0^2 \cdot \sigma_{1j}^2 + b_0^2 \cdot \sigma_{2j}^2} \right) - \left(\sum_{j=1}^n \frac{C_{1j}^2}{a_0^2 \cdot \sigma_{1j}^2 + b_0^2 \cdot \sigma_{2j}^2} \right) \cdot \left(\sum_{j=1}^n \frac{C_{2j} \cdot E_j \cdot T_j}{a_0^2 \cdot \sigma_{1j}^2 + b_0^2 \cdot \sigma_{2j}^2} \right) \right\}, \quad (2)$$

where

$$\Delta_0 = \left(\sum_{j=1}^n \frac{C_{1j}^2}{a_0^2 \cdot \sigma_{1j}^2 + b_0^2 \cdot \sigma_{2j}^2} \right) \cdot \left(\sum_{j=1}^n \frac{C_{2j}^2}{a_0^2 \cdot \sigma_{1j}^2 + b_0^2 \cdot \sigma_{2j}^2} \right) - \left(\sum_{j=1}^n \frac{C_{1j} \cdot C_{2j}}{a_0^2 \cdot \sigma_{1j}^2 + b_0^2 \cdot \sigma_{2j}^2} \right)^2.$$

Variations σ_a^2 and σ_b^2 of a and b and the covariance γ_{ab} between them are given by

$$\sigma_a^2 = \frac{1}{\Delta_0} \cdot \left(\sum_{j=1}^n \frac{C_{2j}^2}{a^2 \cdot \sigma_{1j}^2 + b^2 \cdot \sigma_{2j}^2} \right),$$

$$\sigma_b^2 = \frac{1}{\Delta_0} \cdot \left(\sum_{j=1}^n \frac{C_{1j}^2}{a^2 \cdot \sigma_{1j}^2 + b^2 \cdot \sigma_{2j}^2} \right), \quad (3)$$

and

$$\gamma_{ab} = \frac{1}{\Delta_0} \cdot \left(\sum_{j=1}^n \frac{C_{1j} \cdot C_{2j}}{a^2 \cdot \sigma_{1j}^2 + b^2 \cdot \sigma_{2j}^2} \right).$$

The most probable enrichment of the sample is given by

$$\hat{E} = \frac{1}{T} \cdot (a \cdot C_1 - b \cdot C_2), \quad (4)$$

and its variance by

$$\sigma_{\hat{E}}^2 = \frac{1}{T^2} \cdot (a^2 \cdot \sigma_1^2 + b^2 \cdot \sigma_2^2 + C_1^2 \cdot \sigma_a^2 + C_2^2 \cdot \sigma_b^2 - 2 \cdot C_1 \cdot C_2 \cdot \gamma_{ab}). \quad (5)$$

The sum of the first two terms in eq.(5) represents the random error and that of the last three terms corresponds to the systematic error.

Reference

- 1) S. Brandt: Statistical and Computational Methods in Data Analysis (North-Holland Publishing Company, Amsterdam and London, 1970) Chap.9.

6. Reactor Control and Diagnosis

6.1 Simulation Study of Sodium Boiling Detection Methods

J. Shimazaki, Y. Fujii and Y. Shinohara

As a part of the work on the development of a diagnostic system for detecting anomalies in the core of an operating reactor, a study is being made on the methods of detecting abnormal reactivity and coolant boiling on the basis of computer simulation. The objective of the study is to obtain some basic information useful for developing sensitive methods of signal processing suitable for boiling detection.

Neutronic, acoustic and measurement noises are simulated on a hybrid computer using source noise data recorded on a multichannel magnetic data tape and a multivariable function generator which is used for generating basic void patterns. The function generator is driven by random signals in order to simulate the randomness in the time of bubble formation and also in size. The void patterns are chosen from experimentally observed bubble formation patterns.

The neutronic signal is generated using a reactor simulator, to the input of which is applied the reactivity caused by bubbles through the void coefficient of reactivity. At the output of the reactor simulator is added the measurement noise.

The acoustic signal is generated based on the second time derivative of the void signal. At the output of the acoustic signal simulation block is added a random signal which simulates the background noise including the measurement noise.

From the simulation results which were obtained parametrically for various noise conditions using correlation, spectral and coherence analyses, it has been confirmed that the cross-spectral and coherence analyses between neutronic and acoustic signals are effective methods for detecting boiling even when the signal-to-noise ratio is small provided that the void coefficient of reactivity is not practically zero. It has also been shown that detection capability can be improved to a certain extent by applying some nonlinear preprocessing of the measured signals.

6.2 Dynamic Model of the VHTR Plant for Analyzing Its Control System

J. Shimazaki, H. Usui and Y. Shinohara

The dynamic model of the Multi-Purpose Very High Temperature Gas-Cooled Reactor (VHTR) has been made to design and evaluate the control system efficiently. For the analysis of the VHTR dynamics and the design of the control system, it is needed to develop the dynamic model and the simulation method to reduce the computation time of the dynamic simulation under various kinds of disturbances and plant parameter changes. It takes about 10 minutes for one case of the VHTR dynamic simulation to use the plant simulation digital code¹⁾ (ICARUS-IIa) and about the same to the hybrid computer simulation²⁾. However the dynamic model developed can be used to one simulation within 10 sec CPU time on FACOM-M200 computer. And this model is applicable to the control design and evaluation through comparing and examining a lot of dynamic simulation results.

The VHTR plant consists of reactor core, reactor structure, intermediate heat exchanger (IHX), steam generator, thermochemical process, high temperature coaxial double piping and so on in order to analyze the VHTR dynamics. The dynamic model is made of the primary system of the VHTR plant in the form of state variable representation. As a one-dimensional distributed parameter model is needed for reactor heat transfer and IHX, the number of nodes in nodal approximation is determined though the simulation results of different nodes and of the continuous-space-discrete-time method using a hybrid computer. The model shown in Fig. 6.2.1 has four subsystems which are neutron kinetics part, reactor heat transfer part and two IHXs. A subsystem is in general represented by introducing state variable x_i , control variable u_i , output variable y_i , system matrix A_i , control transfer matrix B_i and output matrix C_i . The four subsystems are completely determined by defining the variables mentioned on the computer code which generates the matrices A_i , B_i & C_i . The dynamic simulation of the total system can be done after making the discrete-time model and connecting the subsystems.

One of the dynamic simulation results is shown in Fig. 6.2.2 when 10¢ in reactivity is applied. In this simulation, the discrete time interval is 5 sec and the simulation time 2000 sec. It takes about 2 sec of CPU time for one dynamic simulation to a given disturbance. The responses in Fig. 6.2.2 are consistent with the result on the hybrid

computer simulation. The new model and the simulation method developed have been shown to be useful for optimal parameter setting of a control system and for the design of control systems structure.

References

- 1) Esaki M., et al.: "ICARUS.1, A Computer Code for Transient Analysis of the Multi-Purpose High-Temperature Reactor Plant Performance", JAERI-M 5058 (1972).
- 2) Usui H., Kudo K.: "Hybrid Computer Simulation of the Dynamics of the Primary System of Experimental Multi-Purpose Gas-Cooled Reactor", JAERI-M 8974 (1980).

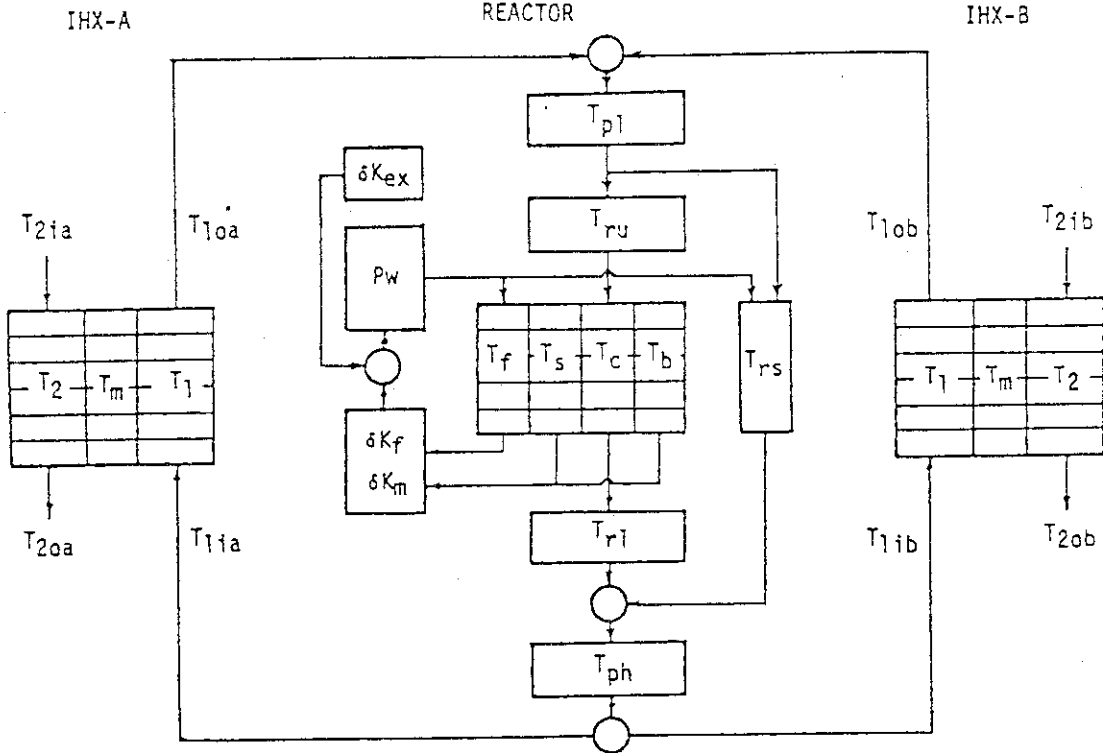


Fig.6.2.1 Schematic diagram of the simplified simulation of primary cooling system of VHTR

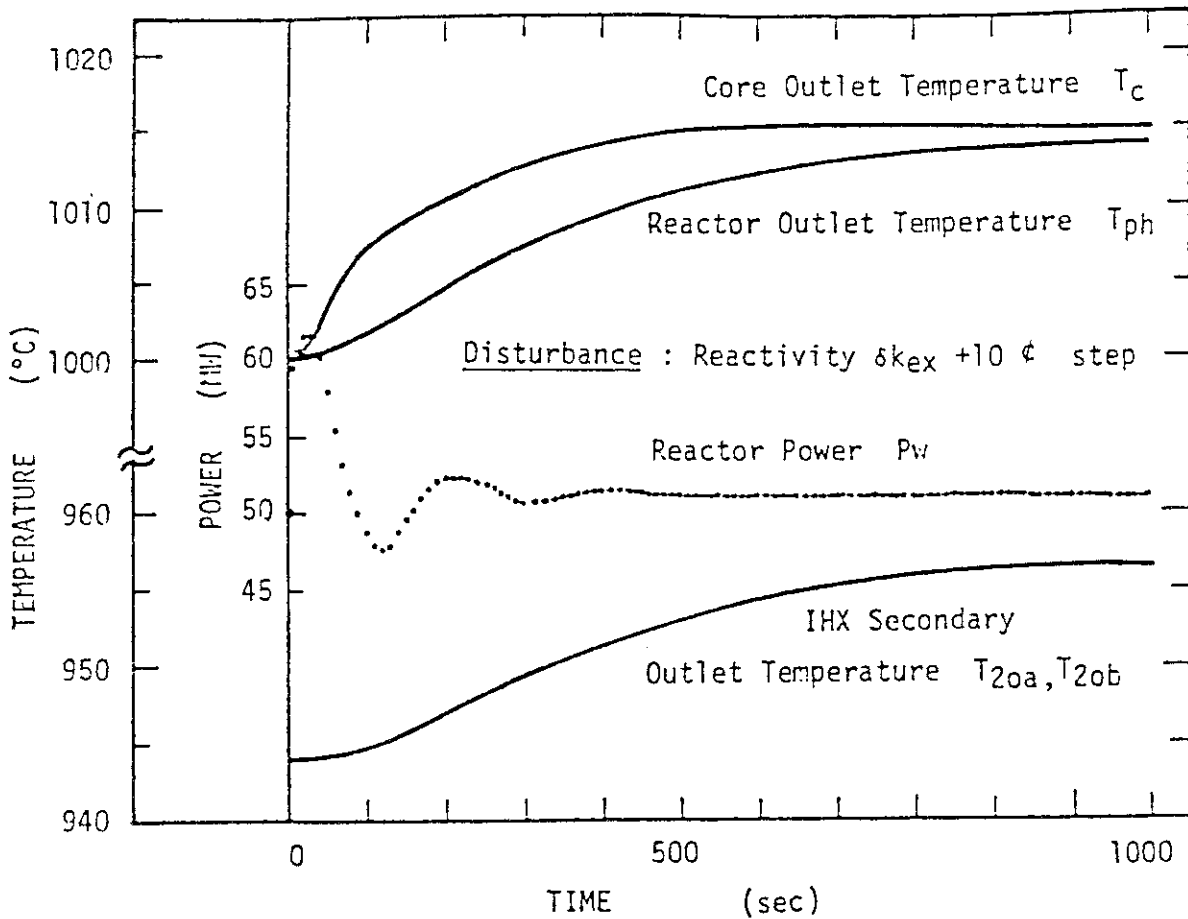


Fig.6.2.2 Response of reactor power and outlet temperature to +10¢ reactivity step input (VHTR primary cooling loop system)

6.3 Reactor Water Level Estimator of a BWR plant

J. Shimazaki and M. Yokobayashi

The reactor water level of a BWR plant is an important variable to be continually monitored for the safety of the reactor core. However the actual water level (mixture level) shows the different behavior¹⁾ with the measured water level especially in the case of large core flow change or pressure decrease. And it is necessary to estimate the actual water level from the measurement data of the reactor plant.²⁾ The water level in the reactor has been analyzed by using the water level estimator. It is also shown that the conventional level meter installed in the reactor plant has the dynamics of a dead time and first order time delay.

The dynamic model of water level estimation is made of seven dimensional state variables and seven input variables from fifteen dimensional state variable model already developed. The state variables are the reactor thermal power Q_c , the core average void fraction R_g , the core outlet quality X_c , the riser average void fraction R_{gr} , the riser outlet quality X_r , the reactor pressure P and the actual water level H_r . The input variables are the neutron flux N , the turbine steam flow W_{st} , the dump condenser steam flow W_{sd} , the recirculation flow W_o and the core inlet temperature T_{in} . The measured water level (meter level) H_m is not included in the state variables because it shows the dynamic response of the measurement device.

The water level estimator is designed by applying Kalman-Bucy filtering to the above-mentioned dynamic model. In the estimator, the measurement variable to be fed to the state variable model is the pressure only and the covariances of state and measurement variables are assumed to be 1-2% of their steady state values at normal power. In order to estimate the dynamics of the level meter, the water level corresponding to the meter level is calculated from the mixture level of the water level estimator, considering the pressure drop effect and the dynamic model of the level meter of $e^{-Ts}/(1+Ts)$ type.

Using the actual data obtained from JPDR-II dynamic experiments at 50% power, the characteristics of the water level estimator are analyzed as well as identifying the dynamics of the level meter. The input variables are shown in Fig. 6.3.1 when the setting value of the master controller of recirculation pump is changed as rectangular form. Fig. 6.3.2

shows the responses of the estimator. Adjusting the parameters of $e^{-Ts}/(1+Ts)$, the dynamics of the level meter is identified as $\tau = 2$ sec and $T = 0.5$ sec. The estimated water level given in Fig. 6.3.3 represents good consistence with the measured water level from the conventional level meter. This type of estimator has good characteristics of stability and response, comparing with the estimator designed by input variables without pressure feedback. As the experimental data used are from small disturbance (within 10% power change), the dynamic model is sufficient to be linear. Further work is still remained to develop a non-linear dynamic model for estimating the reactor water level corresponding to the large disturbances.

References

- 1) Shimazaki J., Yokobayashi M.: "Reactor Eng. Div. Annual Report (Apr. 1978 - Mar. 1979)", JAERI-M 9032, pp.135-137 (1979).
- 2) Shimazaki J., Yokobayashi M.: "Reactor Water Level Estimator of a BWR Plant", Annual Meeting of the Atomic Energy Society of Japan, D41.

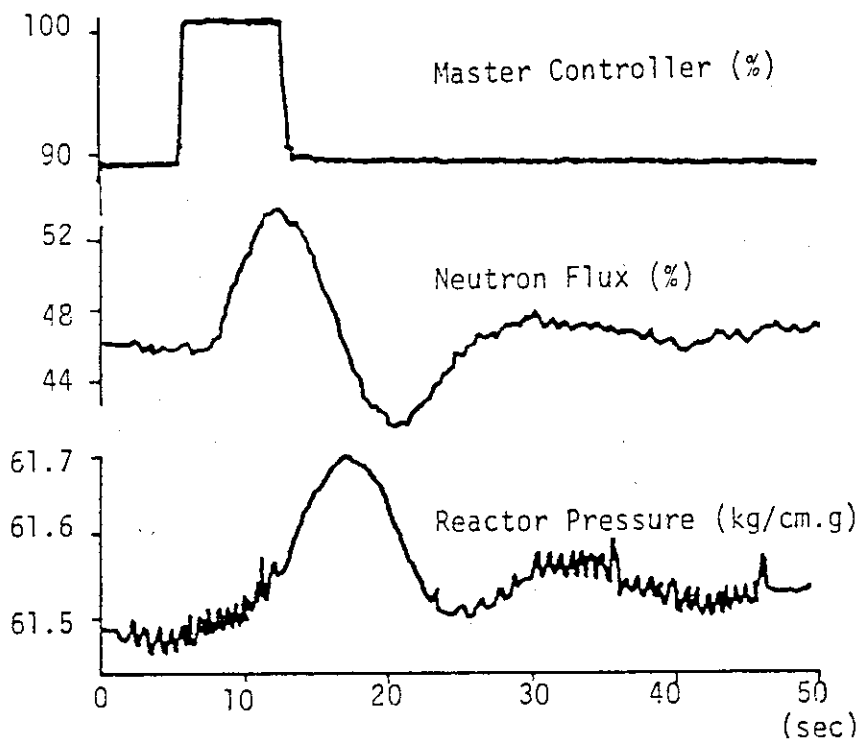


Fig.6.3.1 Input variables to water level estimator when master controller of recirculation pump is changed 10% rectangularly

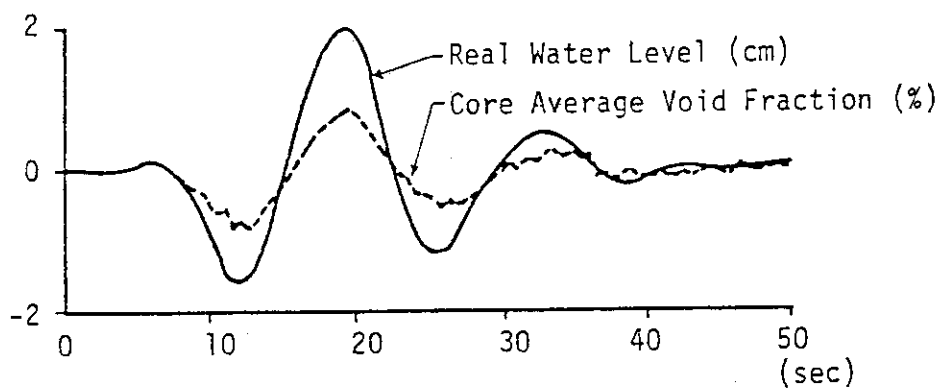


Fig.6.3.2 Response of water level estimator in the same condition

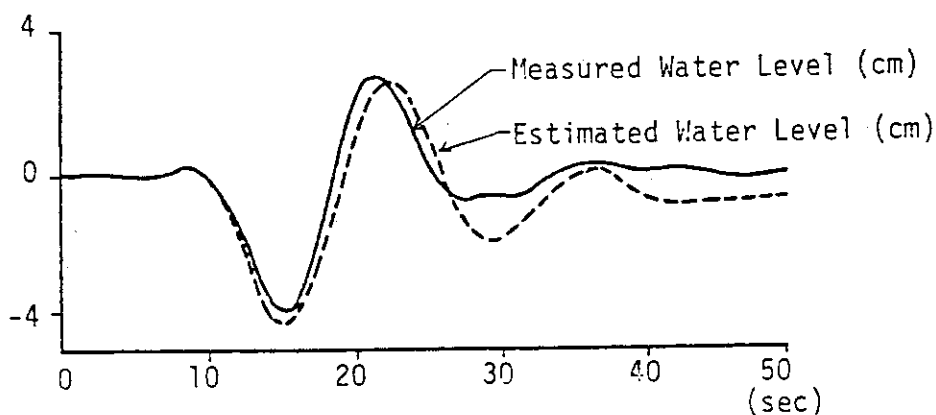


Fig.6.3.3 Estimated water level from the estimator in the same condition

6.4 A New Method for Leak Detection in OWL-1 Loop Based on Time Series Analysis of Dewpoint Signals

R. Oguma, K. Hayashi and T. Kitajima*

Introduction

The problem of early detection of abnormal water leakage from nuclear reactor plants is particularly important from the standpoint of reducing a release of fission products and the resultant contamination.

The present study is concerned with a new method aiming at the development of an on-line computer-based leak monitoring system for the OWL-1 (Oarai Water Loop No.1). The OWL-1 loop is an in-pile water loop of JMTR (Japan Materials Testing Reactor) used as an irradiation facility for testing materials. Most equipments of the OWL-1 loop system are contained in the loop cubicle of a volume about 115 m^3 . The cubicle is segregated by a thick concrete wall and is ventilated. A considerable amount of experience on leak monitoring has been accumulated at JMTR up to now through the tests carried out on different methods, in which the use of dewmeters is thought to be promising.¹⁾ In order to obtain a sensitive indication of leaks, here, time series analysis based on ARX (autoregressive model with exogenous variable) modeling²⁾ is applied to information processing of the signals from the dewmeters. The method is based upon the ability of the identified ARX model to estimate the current state on the ambient humidity, i. e., the change in the humidity caused by the water leakage would lead to deviation of the measured humidity from the estimation by the ARX model, thus detecting the leakage.

A simple digital filter composed of the identified ARX model and a Butterworth filter³⁾ was designed as an attempt to develop an efficient leak monitor, which was then applied to dewpoint recordings collected during the 43rd cycle of the JMTR operation.

In the present study, the ARX modeling was applied as a method for information processing to enhance the detection sensitivity to the change in physical state of interest.

Brief Description of the OWL-1 Cubicle and the Dewpoint Measurement

Figure 1 illustrates the air flow path to and out of the cubicle together with the location of the dewmeters. The dewmeters used here for measuring humidity of the supply and the exhaust air in the ventilation system is a Dewcel meter with assured measurement range of $-10 \sim 50 \text{ }^\circ\text{C}$. The signal's outputs of the dewmeters are sampled every 10 sec and are recorded on a chart recorder.

* Division of JMTR, Oarai Research Establishment

Method of Data Analysis

Given a set of sample records with sample size of N on the supply and exhaust dewpoint signals, $\{T_o(k), T_i(k); k=1, 2, \dots, N\}$, the ARX modeling technique can be conveniently applied to identify the dynamics model relating $T_o(k)$ and $T_i(k)$. The ARX model for these two variables at time k can be represented by

$$T_o(k) = \sum_{m=1}^M a(m)T_o(k-m) + \sum_{m=1}^M b(m)T_i(k-m) + e(k). \quad (1)$$

Once the ARX model was obtained, the exhaust dewpoint at time k can be estimated by inputting the supply dewpoint signals to the identified ARX model, i. e.,

$$\hat{T}_o(k) = \sum_{m=1}^M a(m)\hat{T}_o(k-m) + \sum_{m=1}^M b(m)T_i(k-m), \quad (2)$$

where $\hat{T}_o(k)$ denotes the estimate of $T_o(k)$. If a leak has occurred, the estimates of the exhaust dewpoint would deviate from the measurement value. Hence, monitoring the time behavior of the difference $\{T_o(k) - \hat{T}_o(k)\}$ would lead to efficient leak detection. The ARX modeling of Eq.(1) for a set of measurement dewpoint data can be achieved by applying the least squares fitting method.

Results of the Analysis

Figure 2 shows an example of the exhaust dewpoint estimation based on Eq.(2) for the normal data without leaks from the OWL-1 loop. The estimated values follow quite well the original measurement data in a sense of mean value, indicating the validity of the identified model.

A computer algorithm for an on-line leak monitor was developed on the basis of the model identification. This leak monitor consists of two steps of data processing; the first step for evaluating the difference signal $\{T_o(k) - \hat{T}_o(k)\}$ which includes the identified model, and the second for smoothing the difference signal. The latter is composed of Butterworth lowpass filter of the third order, with which one can cut off the signal's high frequency components not needed for leak monitor.

This leak monitor was applied to analyze the data collected when abnormal water leakage occurred at the OWL-1 loop. In Fig.3 the results of the leak monitoring are summarized together with the events observed during the loop operation. From the figure the followings can be pointed out;

- i) It is inferred that the leak from the loop became evident about one hour after starting the OWL-1 loop heating up (14 o'clock on March 12th).
- ii) Reaching steady condition of the loop operation, the leak rate estimated

also became steady.

- iii) Almost at the same time when the operator started to decrease the temperature and pressure of the loop, the estimated leak rate also began to decrease.
- iv) There is not much discrepancy between the confirmed and estimated time of the end of leak.

Especially iii) and iv) among these four features indicate the present analysis to be fairly reliable.

Considering the time history of the leak estimated by the leak monitor applied here, it is conjectured that the leak could have been detected by the present method, at least, when the loop operation attained P-mode^{*} stationary condition.

The results obtained in the present analysis indicate the potential usefulness of the method developed here for an early detection of water leakage.

References

1. "Operational Report on JMTR Irradiation Facilities in 43rd Cycle", Irradiation Section II, (1979)
2. Akaike H., Nakagawa T.: Statistical Analysis and Control of Dynamic Systems, (1972), Saiensu-sha
3. Rabiner L. R., Gold B.: Theory and Application of Digital Signal Processing, (1975), Prentice-Hall

* P-mode; coolant condition of pressurized water reactor

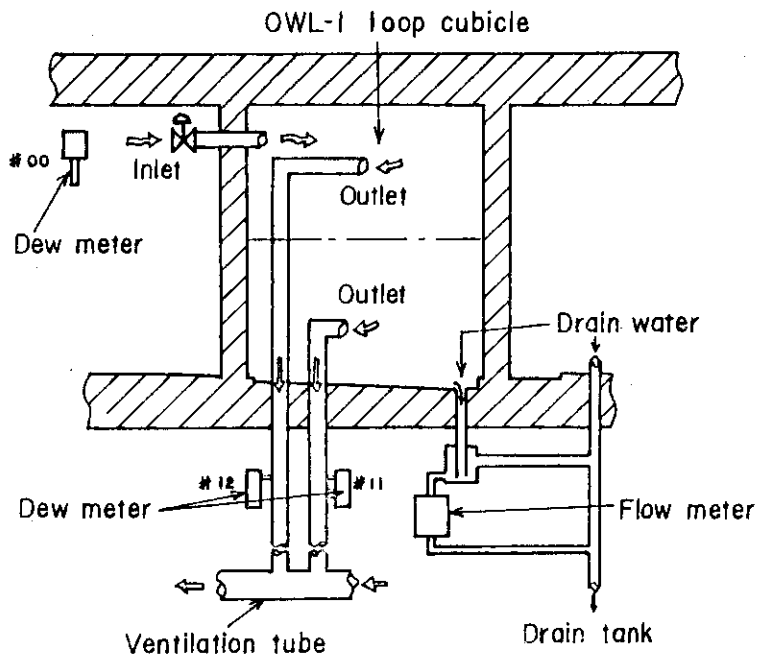


Fig. 6.4.1 Diagram showing air-flow paths for the cubicle ventilation and location of dewmeters.

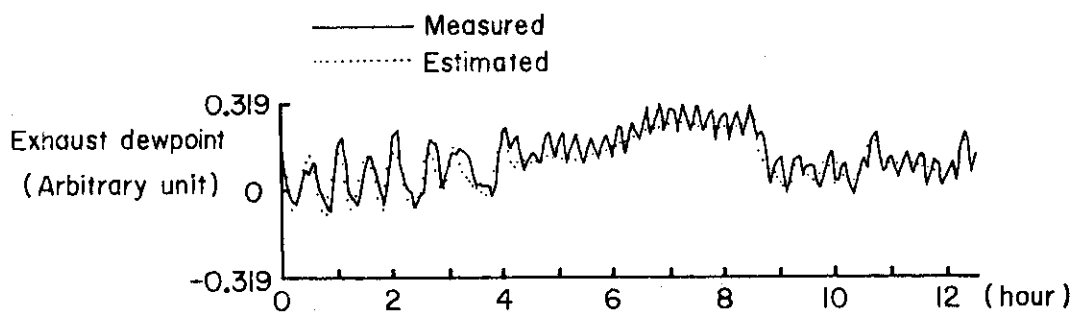


Fig.6.4.2 Typical example of the exhaust dewpoint estimation based on an identified dewpoint dynamics model.

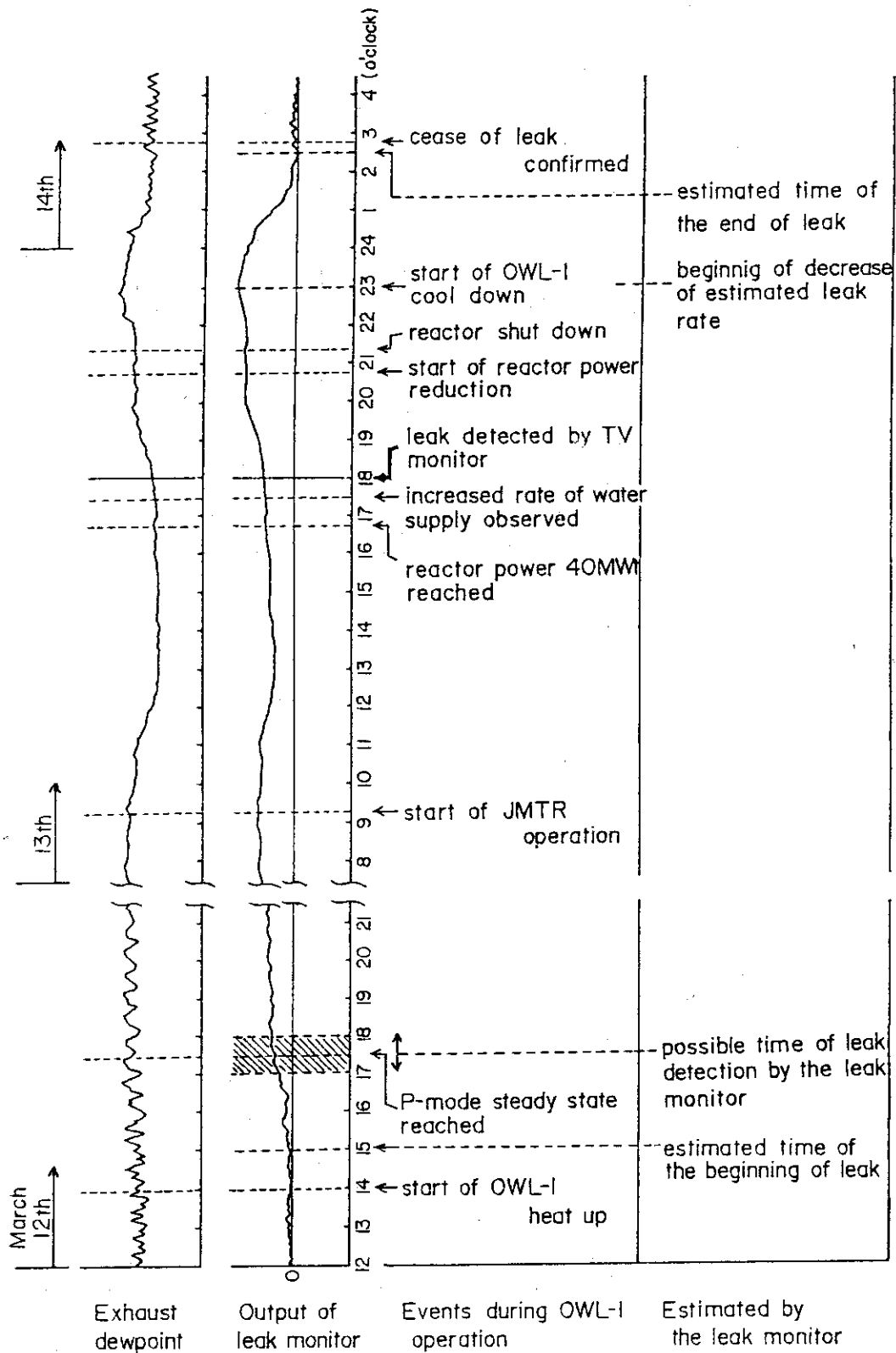


Fig.6.4.3 Evaluation of time history of the water leakage occurred during the 43rd cycle of JMTR operation by the leak monitor designed.

7. Fusion Reactor Technology

7.1 Construction of Accelerator System for Fusion Neutronics Source (FNS) --- Installation ---

J. Kusano, H. Maekawa, S. Sato*, T. Sakase*, C. Kutsukake,
S. Tanaka, Y. Oyama, Y. Ikeda and T. Nakamura

The FNS is a powerful 14 MeV neutron generator used for the fusion reactor blanket and shielding experiments. The installation of the accelerator system of the FNS began in early April of 1980. As the first step, alignment lines of the beam transport were determined and benchmarks were set on the walls and floors in the accelerator and target rooms. The packages of the accelerator components arrived at the JAERI site at the end of April. Immediately finishing the unpackage and the inspection of the contents, the assembling was started. The mechanical assembling and associated wiring proceeded fairly smoothly through May to June. The first high voltage test was done successfully at the end of May. The beam tests was started at the middle of June using high current ion source 740A and beam current of 5 mA was obtained immediately.

Then the works for increasing the current in both of the two beam lines followed, but the results were not so satisfactory as expected due to poor beam transmission to the target position. Small modifications and reassembling on the beam pulsing system and control console wiring were made from July to August and beam tests were started again. In spite of long time and careful adjustment, currents obtained were only 60 ~ 70% of the specified values i.e., 20 mA for 0° beam line and 3 mA for 80° one, respectively. Major cause of the results was guessed to be attributable to a larger emittance of the ion sources than that had been used in the original ion path calculations and it seemed no way to increase the beam without changing or adding optical components.

The installation schedule was revised in the middle of September and intensive beam diagnosis was performed by setting a view chamber and observing the beam shape and size at various positions between the acceleration tube and the target for different component arrangements. As a result, it was concluded that an additional quadrupole lens was

* Daini-Seikosha Co. Ltd.

needed for each line.

With the rearrangement of the beam transport system including the addition of lenses, the rated values of DC d^+ beams for 0° and 80° beam lines were finally achieved at the end of December, 1980 and at the middle of January, 1981, respectively. Successively, the pulsed beam adjustments began with the improved pulsing circuits that has been modified during DC beam tests.

The final acceptance tests was started from early March and was finished at the end of the month with successful results, which is described in section 7.2.

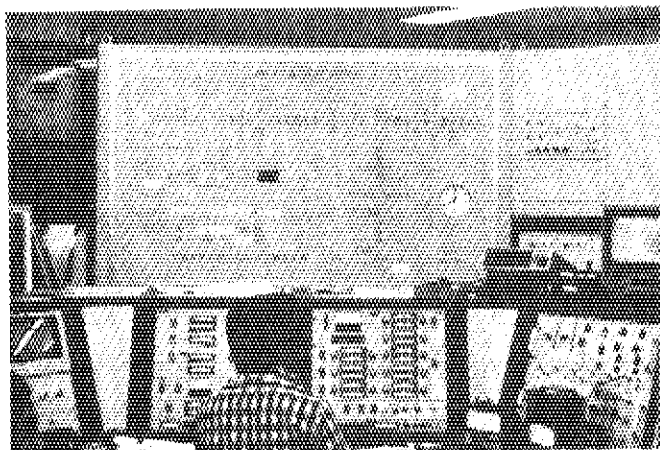


Photo 7.1.1 Diagrammatical display and control console

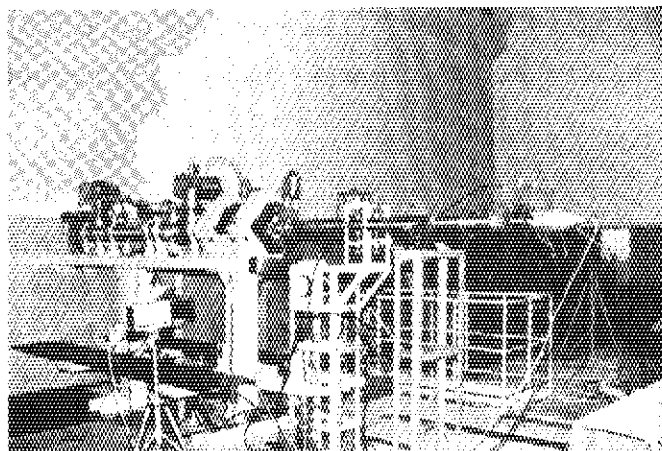


Photo 7.1.2 80 degree beam line in the first target room
Fast Faraday cup is mounted at the end of it to make
the test of pulsed beam.

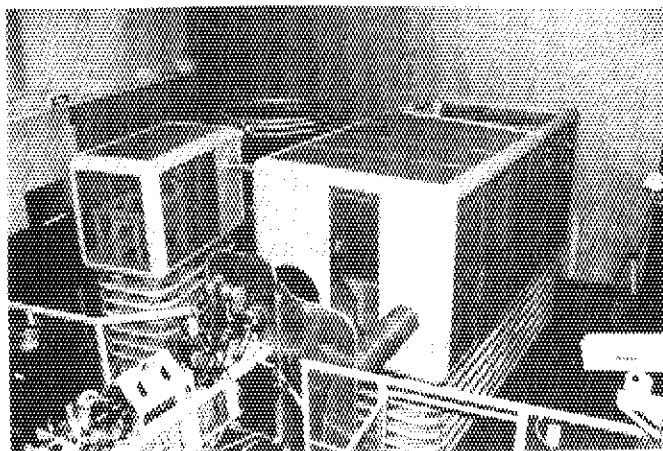


Photo 7.1.3 Overview of the high voltage area

7.2 Construction of Accelerator System for Fusion Neutronics Source (FNS) --- Performance Test ---

H. Maekawa, Y. Oyama, Y. Ikeda, J. Kusano, C. Kutsukake,
S. Takana, S. Sato*, T. Sakase* and T. Nakamura

After the installation of accelerator system for FNS had been completed, the performance test was started to corroborate its ability. All rated values of beam specifications had been determined at the prescribed target positions using D^+ ion beam. The beam sizes of them had also been defined within 15 mm ϕ at the target. They were confirmed by a collimator for a rotating neutron target (RNT) of 0 degree beam line and by an aperture for a dummy target and a fast Faraday cup (FFC) of 80 degree beam line. The sizes of collimator and aperture were 15 mm ϕ .

Method and results of performance test are described briefly as follows.

DC Beam Test

The beam currents at the target were measured by a calibrated ammeter. Layout of target systems are shown in Figs. 7.2.1 and 7.2.2. If the collimator of rotating target was biased, some beam hit it and secondary electrons are emitted to the target. Therefore, it was not biased in the test of 0 degree DC beam to obtain reasonable beam current. The dummy target assembly was used at the end of 80 degree beam line. The bias voltage of electron suppressor was 200 V. This value was determined to be enough to suppress the secondary electrons from the target. The beam current was also measured by a calorimetric method. The beam current I is given,

$$I = 4.186 \frac{F \cdot \Delta T}{V}$$

where I : beam current (mA),
 ΔT : temperature difference between outlet and inlet,
 cooling water ($^{\circ}C$),
 F : flow rate of cooling water (cm^3/s),
 V : acceleration voltage (KV).

* Daini-Seikosha Co. Ltd.

The results are summarized in Table 7.2.1 with the rated specifications. The values of electrical and calorimetric methods agree well each other within the experimental errors.

Pulsed Beam Test

Pulse width and peak current of sweep pulse mode were measured by a oscilloscope to observe the pulse shape from a Fast Faraday Cup (FFC) that was mounted at the end of 80 degree beam line. In case of bunched pulse mode, pulse width was obtained from the time distribution of D-D neutrons that were generated at FFC, i.e., self-target. Typical result is shown in Fig. 7.2.3. The peak current was evaluated from the pulse shape measured by the oscilloscope assuming the area, i.e., (pulse height) \times (FWHM), was equal to that of the time distribution.

The ON/OFF ratios were also measured by detecting D-D neutrons from a Ti-D target that was mounted on a air-cooled target assembly in stead of the FFC. Results of pulsed beam test are summarized in Table 7.2.3.

The performance test shows that FNS Accelerator System has achieved the expected beam specifications.

Table 7.2.1 Results of DC beam test

Beam-line	Ion source	Beam current at the target		
		Rated value	Measured value	
			Ammeter	Calorimeter
0 degree	740A	20 mA	23.4 mA	22.0 mA
80 degree	740A	10 mA	10.7 mA	11.0 mA
80 degree	820	3 mA	3.18 mA	3.21 mA

Table 7.2.2 Results of pulsed beam test

Mode	Pulse width		Peak current		On/Off ratio	
	Rated	Measured	Rated	Measured	Rated	Measured
Bunch	2 ns	1.55 ns	25 mA	45.4 mA	10^5	4.1×10^5
Sweep (min. width) (>50 ns)	30 ns	22 ns	3 mA	3.0 mA	10^4	1.9×10^5
	50 ns $\sim 8 \mu\text{s}$	Same as rated values	3 mA	3.0 ~ 3.4 mA	10^4	6.1×10^5

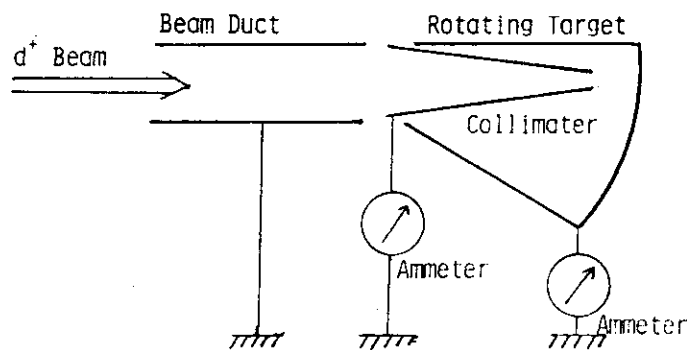


Fig.7.2.1 Rotating target used for the DC beam test on 0 degree beam-line

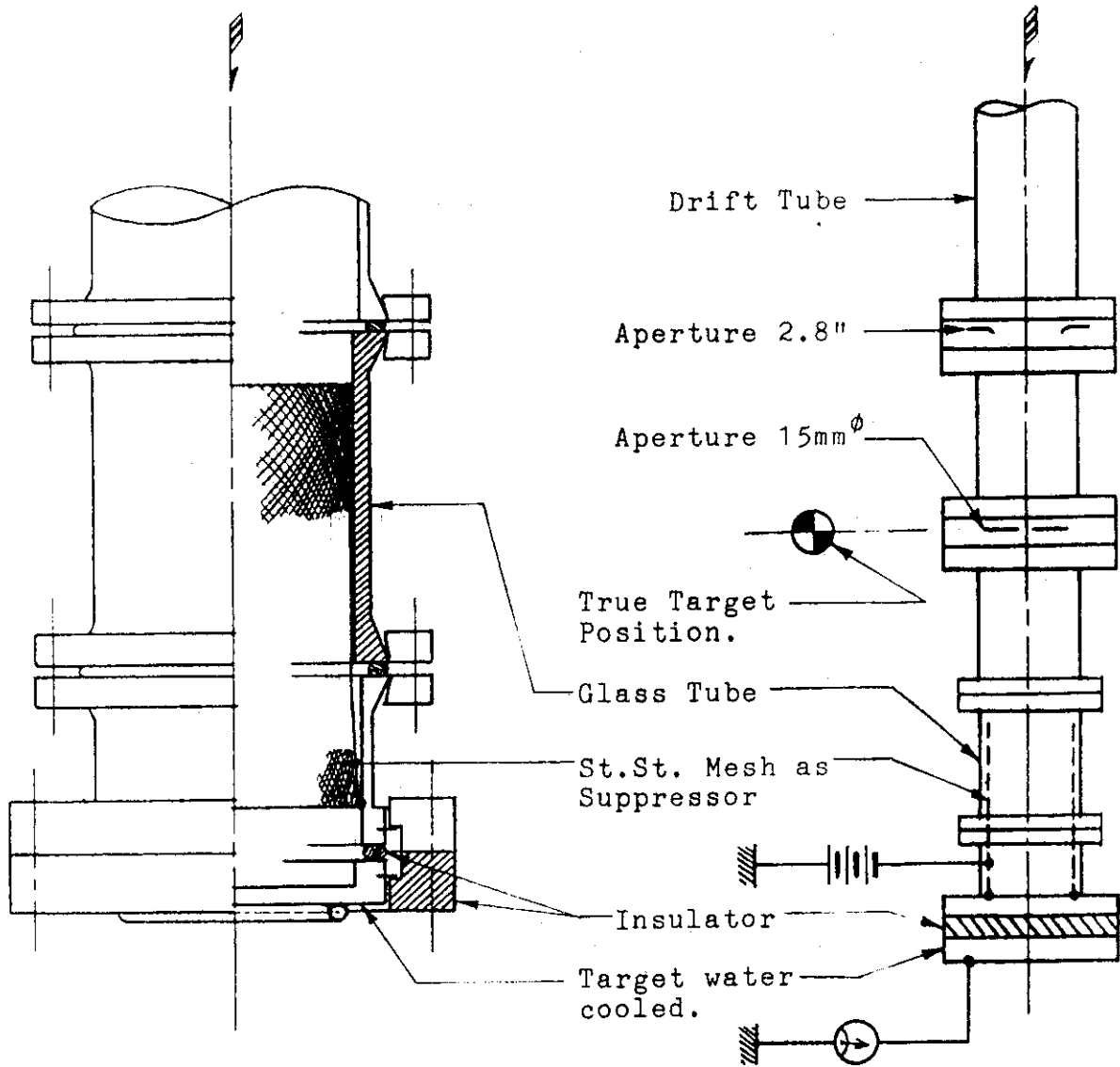


Fig.7.2.2 Dummy target used for the DC beam test on 80 degree beam-line

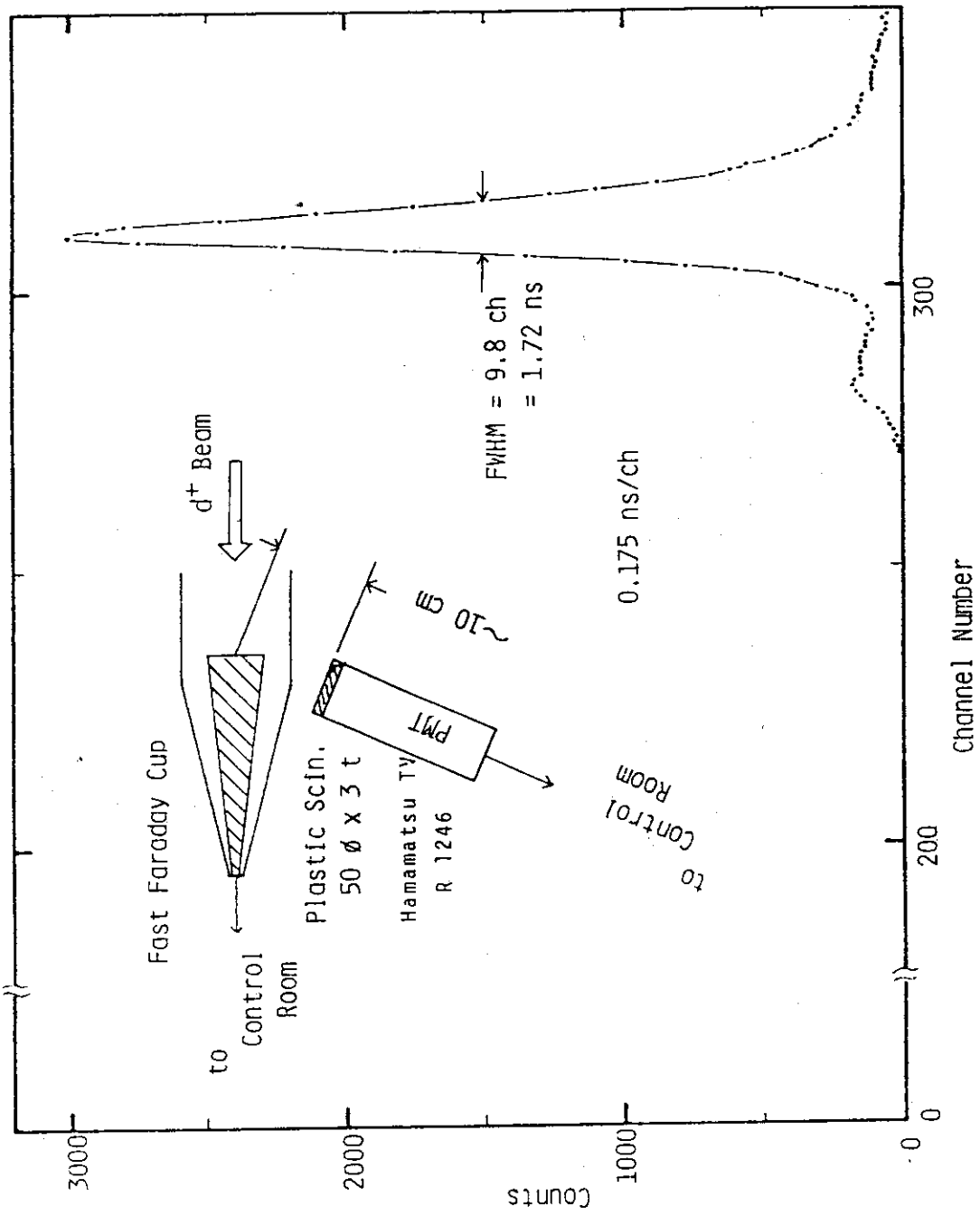


Fig.7.2.3 Typical time distribution of D-D neutrons produced by bunched pulse beam

7.3 Parasitic D-D Neutron Production by Self-Target Reaction in FNS

Y. Oyama, Y. Ikeda, H. Maekawa, S. Tanaka, J. Kusano, C. Kutsukake,
S. Tanaka and T. Nakamura

In the Fusion Neutronics Source (FNS), 14 MeV neutrons are produced by D-T reaction with a 400 KV deuteron accelerator. Parasitic neutrons with 2.5 MeV as mean energy are simultaneously generated at a target disc and beam line components, e.g., an aperture, by D-D reaction with D atoms implanted on them. The character of these parasitic neutrons is important not only on the shielding problem near the beam lines, but also on the background estimation in neutron experiments.

Neutron yields, angular distribution and time dependencies of neutron production rate were measured by a $50.8 \text{ mm}\phi \times 50.8 \text{ mm}$ NE 213 liquid scintillation counter as a neutron detector beforehand the tritium target was used. The neutron yield has been considered to be in proportion to beam current and the number of D atoms in a target metal. In the equilibrium state, the number of D atoms is dependent on target surface temperature¹⁾. In Fig. 7.3.1 and Fig. 7.3.2, the changes of neutron yield with implantation of D atoms in a new copper target and with the release of D atoms from the saturated target due to temperature rise are shown, respectively.

The neutron production rates of copper and titanium plated on copper targets were about 1.1×10^8 neutrons/s.mA and about 4.5×10^9 neutrons/s.mA at the saturated state, respectively. The absorption capacity of D atoms in the titanium layer was about 40 times as much as that in copper. When a Ti-T target is used, the fraction of D-D neutrons to D-T neutrons, whose production rate is expected to be about 2.5×10^{11} neutrons/s.mA, will be about 2% at the saturated state.

References

- 1) Hilton J.L., Kim J. and Hendry G.O.: Proc. of the Workshop on High Intensity Neutron Generators, Las Vegas, Nevada, U.S.A. (1972) pp.194-207.

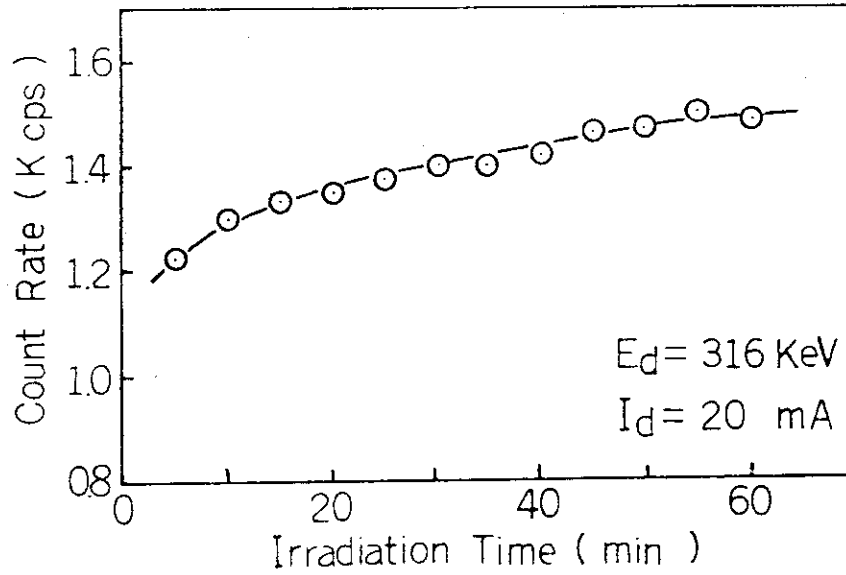


Fig. 7.3.1 Change of neutron yield with implantation of D atoms in Copper target

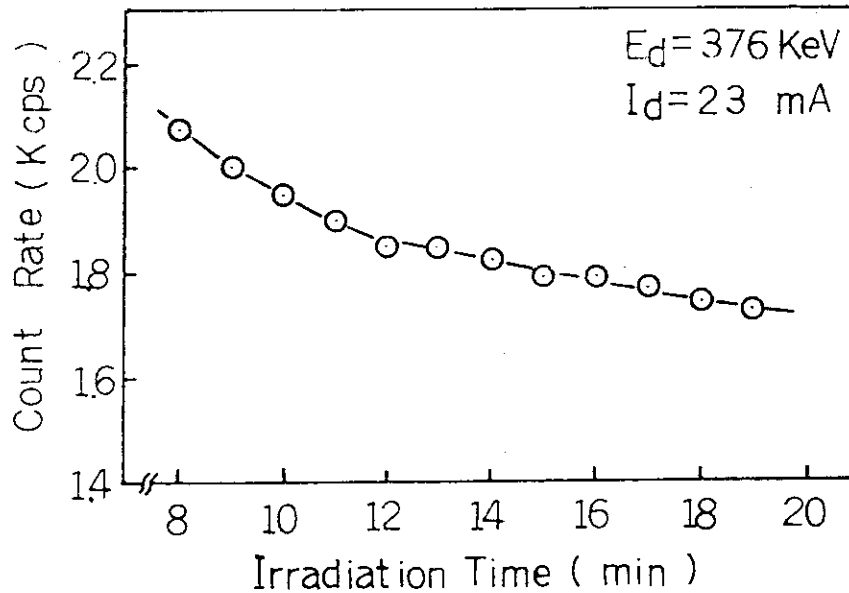


Fig. 7.3.2 Change of neutron yield with release of D atoms from Copper target that was heated up by increasing beam energy

7.4 Surface Temperature and Beam Profile Monitor for Metal Target of FNS

T. Nakamura and H. Maekawa

Tritium metal target releases absorbed gas rapidly when it is heated up to 200°C. Therefore in operating a neutron generator like FNS which delivers high intensity deuteron beam and uses a large quantity of tritium, it is highly desirable to observe continuously the target surface under bombardment and to control beam focus, keeping the temperature below the safety level for the purpose of getting long target lifetime and low tritium concentration at the vacuum exhaust as possible. To meet this requirement a monitor system was developed and equipped in the 80 degree beam line of FNS.

The composition of the device is shown in Fig. 7.4.1. Basically it is a sort of scanning infra-red ray telescope camera. Infra-red radiation originated from the bombarded target surface is taken out by means of a mirror and a sapphire window to the outside of the accelerator vacuum beam duct. The object image is magnified by a set of lenses and is introduced into a infra-red image analyzer. As the beam duct cross sectional size is limited to 35 mm square by experimental requirements, the mirror is so arranged as to cover the whole sectional area except a 25 mm ϕ hole bored at the center of it to let the beam pass through. The optically polished stainless steel mirror is protected by a water cooled aperture lest the spilled beam should hit and heat it up, and the mirror itself is cooled as well.

The thermal image is transformed by the analyzer to a train of electrical signals and transmitted to a digital processor in the control room. After necessary data processing the object thermal image is reconstructed and displayed on the TV monitor screen in 16 colors temperature range scale. A commercial model "Thermal Imager Probe Eye 1400" was chosen as the infra-red image analyzer and processor, and several modifications were applied to satisfy our requirement.

The whole system was tested in the temperature range between 50 to 500°C after installed in the beam line by using a reference source which was calibrated with a standard black-body heat source. In the beam run, it showed good and reliable performance, and has been used in beam adjustment and various target tests. An example of deuteron beam spot on a Ti-D metal target is shown in Fig. 7.4.2.

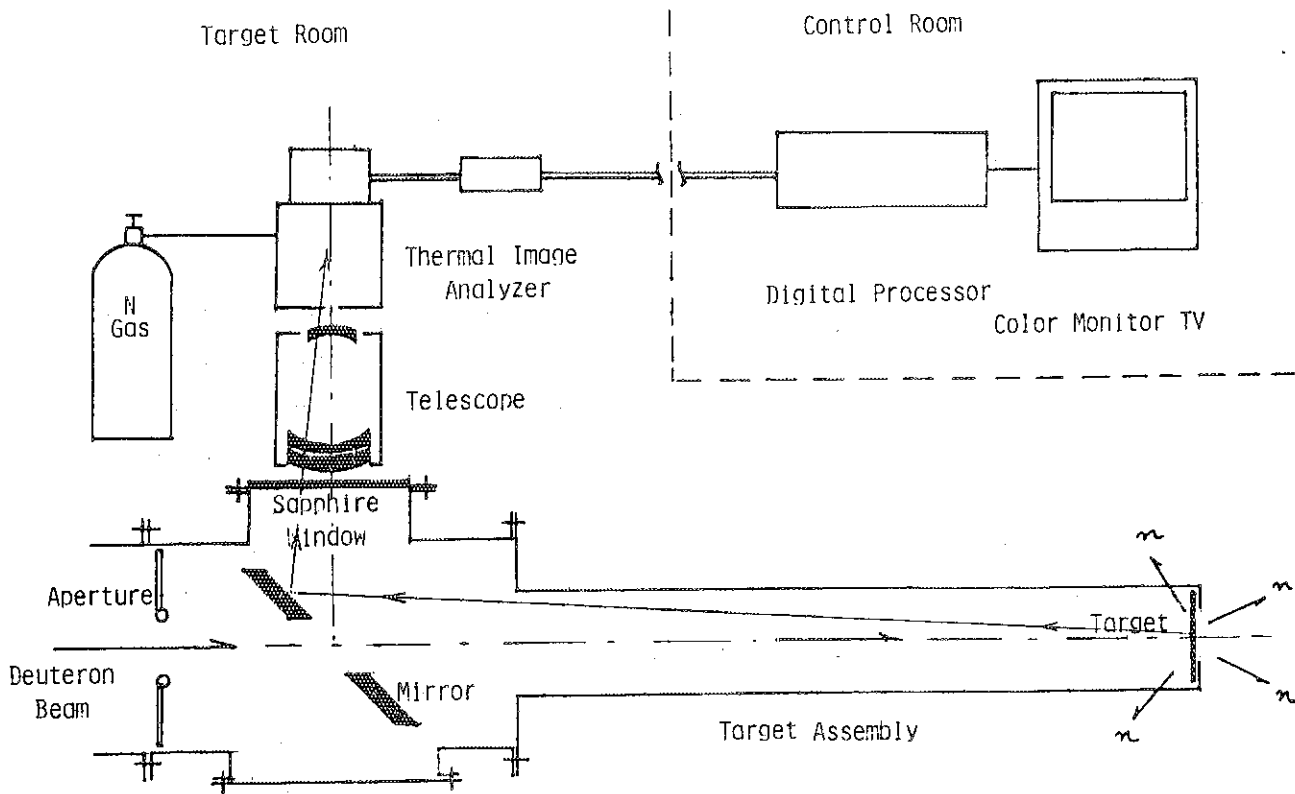


Fig. 7.4.1 Layout of the target surface temperature and beam profile monitor

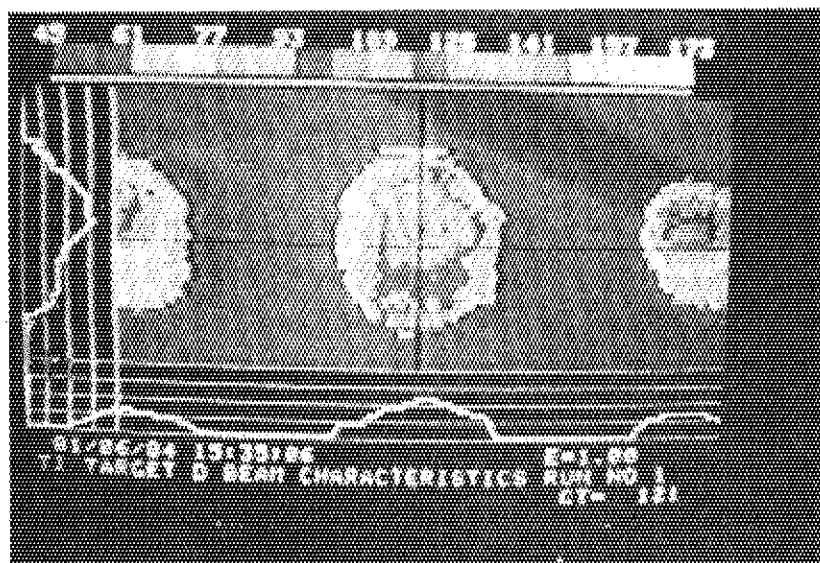


Fig. 7.4.2 Thermal image of the deuteron beam spot on Ti-D metal target

7.5 Modification of Tritium Monitoring System for Tritium Adsorption Plant (TAP)

Y. Ikeda, S. Tanaka, Y. Oyama, H. Maekawa and T. Nakamura

In the Fusion Neutronics Source Facility (FNS), the tritium adsorption plant (TAP) is equipped to collect the exhaust gas from each vacuum lines and to remove the tritium, when the concentration is high, before it is released to the atmosphere. In the original TAP system, the tritium monitoring was performed using an effluent ionization chamber in each line of the monitor and storage tanks.

However it is expected from the preliminary test that once the exhaust gas having a large amount of tritium comes into the ionization chamber, the severe contamination occurs and no more monitoring in the lower range is possible. In order to avoid this situation, a new tritium monitoring system for TAP was designed and reinstalled. The new tritium monitoring lines including two types of effluent ionization chambers, i.e., one is used for high level and the other for low level are shown in Fig. 7.5.1. The high level ionization chamber (HTM) having small volume of about 100 cm^3 covers the range of $10^{-2} \sim 10^2 \text{ } \mu\text{Ci}/\text{cm}^3$ and the low level chamber (LTM) which has the volume of about 1 liter covers the range of $10^{-4} \sim 10^0 \text{ } \mu\text{Ci}/\text{cm}^3$.

In a usual operation mode where the tritium concentration is not so high, the gas passes through the both chambers in series. Once the high concentration tritium gas that exceeds the present level comes into the HTM, the valve NV-1 in Fig. 7.5.1 closes immediately and the valve NV-3 open to purge the possible contamination in the LTM by dry air. When the tritium concentration of the HTM is reduced under the level after the processing, the system returns to the usual operation.

As the result of this modification, a reliable tritium monitoring is now possible in the FNS where total amount of 10,000 Ci per year of tritium metal target is treated.

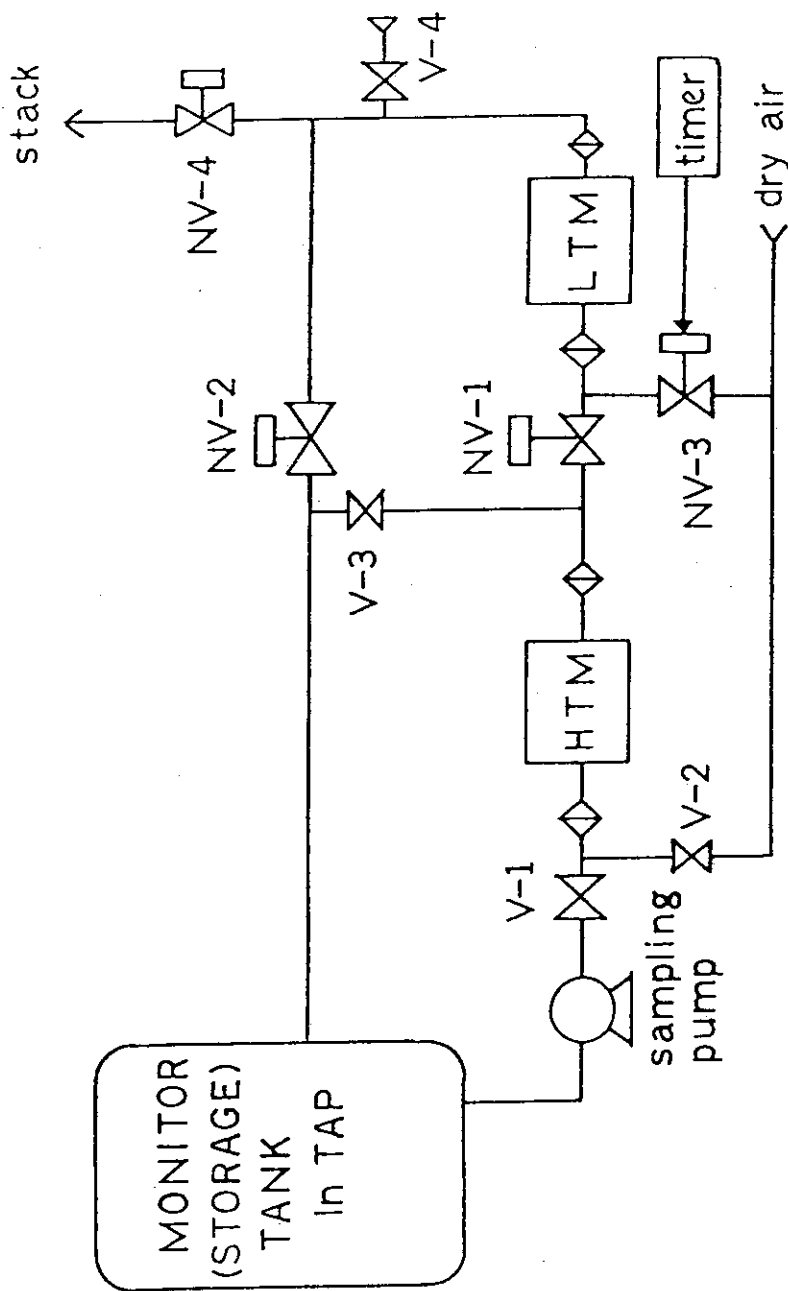


Fig.7.5.1 The new tritium monitoring lines for TAP

7.6 Studies of Tritium Adsorption and Desorption in Ionization Chamber for the Tritium Effluent Monitor

Y. Ikeda, S. Tanaka, Y. Oyama, H. Maekawa and T. Nakamura

It has been considered that as high concentration tritium gas passes temporarily through the ionization chamber, the probability of the adsorption of tritium onto the chamber wall surface increases. The accurate measurement of the tritium concentration is no more possible to continue because the background of monitor rises by the desorbed tritium from the chamber wall. This is one of the most serious problems concerning with the continuous tritium monitoring of gaseous effluent at the facilities where a large amount of tritium is handled. Therefore it is necessary to make clear the relation of the tritium concentration to the amount of the adsorption and desorption, so that we can design a new process monitor to measure the concentration of tritium effectively. On this point of view the adsorption and desorption properties of tritium in two types of ionization chambers, i.e. RIC-510 and SC (sampling chamber) have been studied using standard tritium gases of $6.6 \times 10^{-4} \mu\text{Ci}/\text{cm}^3$, $5 \times 10^{-3} \mu\text{Ci}/\text{cm}^3$ and $4.16 \times 10^{-2} \mu\text{Ci}/\text{cm}^3$. In Fig. 7.6.1, the schematic arrangement of this experiment is shown.

The experiment consisted of two parts of measurements. The first one was performed as follows. The standard tritium gas was sealed in the ionization chamber for certain time. Then the tritium gas in the chamber was purged by dry air of which the flow rate was constant in each run. During these processes, a continuous measurement of tritium concentration was carried out using an electrometer. Observed decay curves of the tritium concentration are shown in Fig. 7.6.2. After background was subtracted from each curve, not only fast decay components which was caused by the ventilation, but also slow decay components clearly exist in these curves. These slow components could be explained by a consideration that as the balance of the adsorption and desorption varied during the air purging, the adsorbed tritium on the chamber wall desorbed into the sensitive volume of the chamber. These curves could be fitted to exponential functions. And an amount of the tritium adsorbed initially on the chamber wall could be deduced. The surface concentration of tritium after sealing the standard tritium gas of $4.16 \times 10^{-2} \mu\text{Ci}/\text{cm}^3$ was estimated about $10^{-4} \mu\text{Ci}/\text{cm}^2$.

The second part of measurements was performed successively following the first measurement. Just after the purging, the ionization chamber was closed. The tritium concentration was continuously measured so far as its concentration had been saturated. The observed curves are shown in Fig. 7.6.3. The curves indicate that the tritium concentration in the chamber is increasing rapidly at the beginning of the measurement and gradually saturates. This phenomenon can be explained by the same consideration as in the first measurement. It is also considered that the increasing rate of the concentration relates to the balance of adsorption and desorption at the surface of chamber wall. Then the surface concentration of the adsorbed tritium after sealing the standard tritium gas for a certain time could be deduced to be about $10^{-4} \mu\text{Ci}/\text{cm}^2$. This value is consistent with the value deduced in the first measurement.

As the conclusion in these measurements, it is said that when the tritium gas of about $10^{-2} \mu\text{Ci}/\text{cm}^3$ is filled in the ionization chamber, the amount of adsorbed tritium on the chamber wall become about $10^{-4} \mu\text{Ci}/\text{cm}^2$.

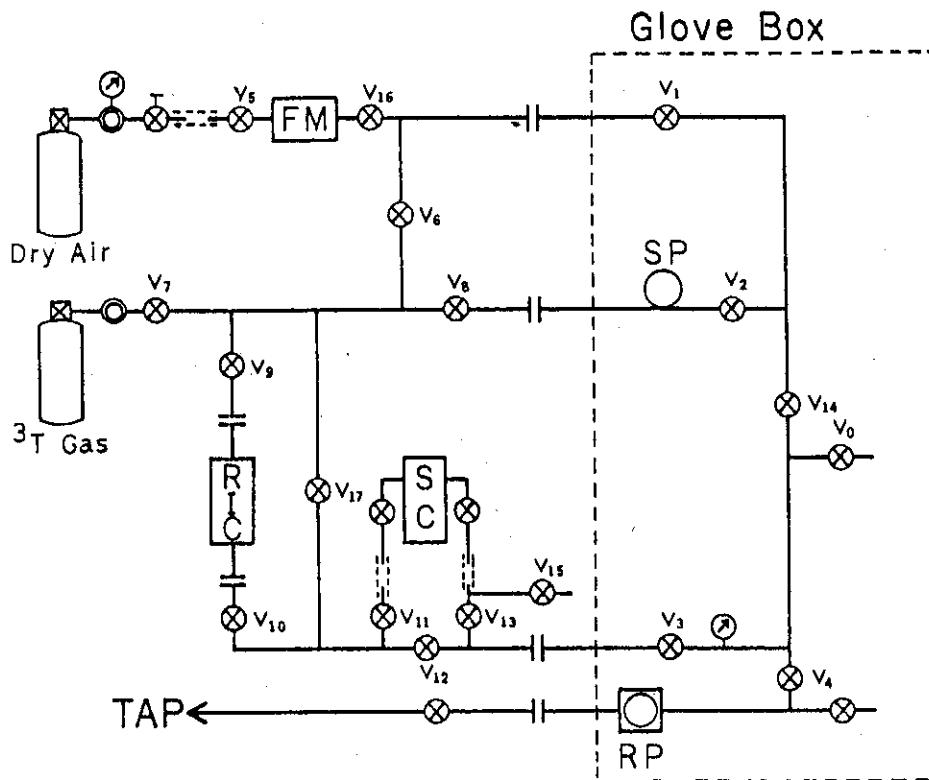


Fig. 7.6.1 Schematic arrangement of this experiment

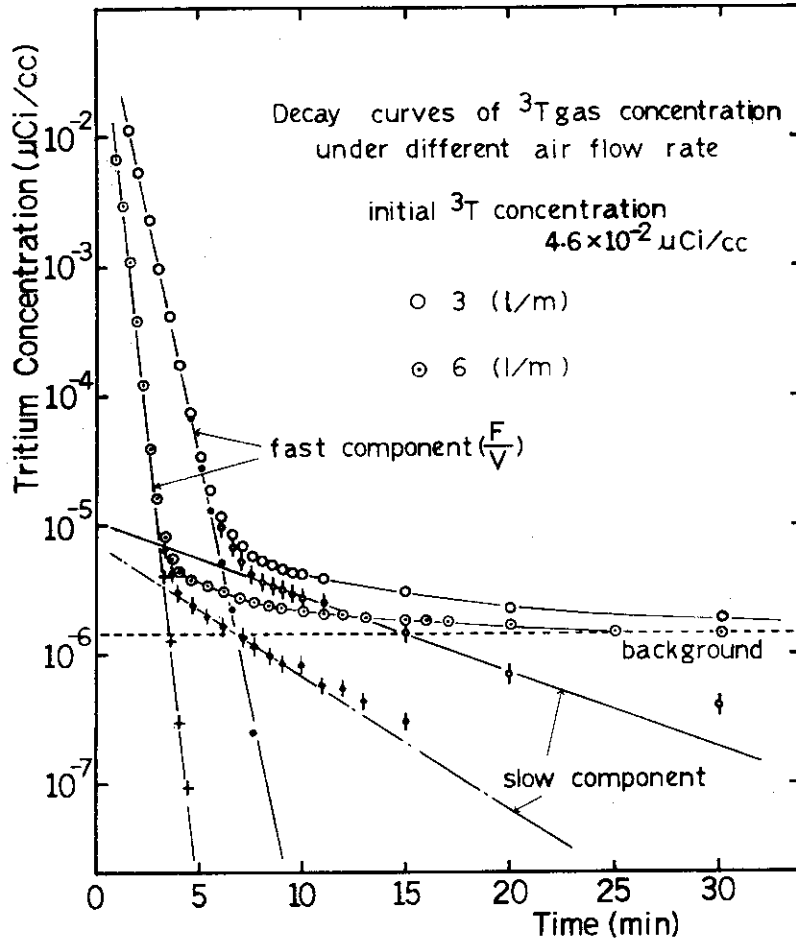


Fig. 7.6.2 Observed decay curves of the tritium concentration under the air flow

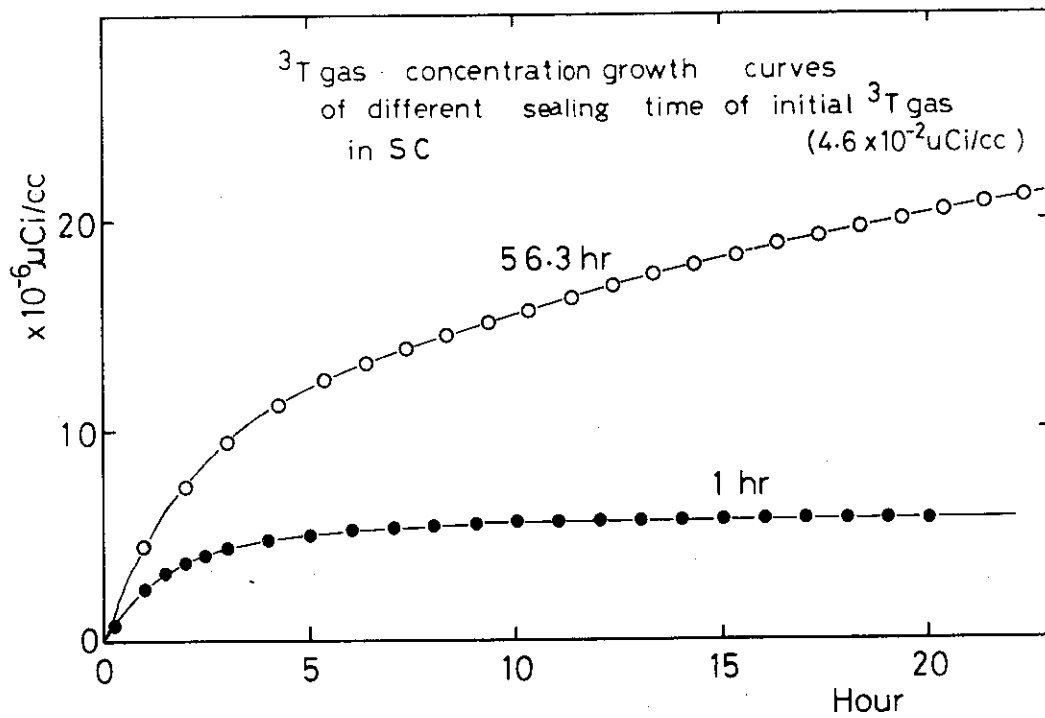


Fig. 7.6.3 Curves of the tritium concentration in the ionization chamber during the chamber was closed

7.7 Neutron Dosimetry by the Spectrum Weighting Function Method with a NE-213 Liquid Scintillator

Y. Oyama and S. Tanaka

We are planning to study the shielding effect and the skyshine phenomenon using the FNS. The spectrum weighting function method with a 50.8 mm ϕ \times 50.8 mm NE 213 liquid scintillator will be adopted to measure a neutron dose equivalent. This method has usually been applied to a low level radiation field¹⁾. A computer code was prepared to obtain a spectrum weighting function from the neutron response matrix of NE 213 liquid scintillator.

The spectrum weighting function, named $G(E_h)$ function, is an operator which converts absorbed energy spectrum $N(E_h)$ into a dose equivalent rate at the detector position. The $G(E_h)$ function is defined as follows:

$$D = \int_{E_{hmin}}^{E_{hmax}} N(E_h) G(E_h) dE_h \quad ,$$

where E_h , $N(E_h)$ and D are absorbed energy of recoil proton in the detector, absorbed energy spectrum and dose equivalent rate at the detector position, respectively. To obtain the $G(E_h)$, the calculation was iterated until the result of operating it to mono-energy neutron responses converged to Flux-Dose Conversion Factors. The $G(E_h)$ function obtained by this calculation and the energy response of this method are shown in Fig. 7.7.1 and Fig. 7.7.2, respectively.

The result of this method was compared with a standard dose equivalent rate obtained by the unfolding method at the same neutron fields of Am-Be and ²⁵²Cf. To obtain the dose equivalent directly in the same principle, a DBM (Discrimination Bias Modulation) circuit¹⁾ that converts electrically detector pulses to it was also used. The results of each method are summarized in Table 7.7.1. The differences between the $G(E_h)$ function method and the unfolding method and between the DBM method and the unfolding method are within 7% and 18%, respectively. These discrepancies will be improved by giving a proper discrimination parameter in the calculation of $G(E_h)$. The sensitivity of the $G(E_h)$ function method for Am-Be neutrons was estimated to be 0.24 mrem/hr/cps using the solid line in Fig. 7.7.1, and it became clear that this method was useful to

apply to low level neutron fields.

Reference

- 1) Moriuchi S.: "A Dosimetric Instrument Based on the Spectrum Weighting Function Method for Environmental Radiation Measurements", JAERI-M 7066 (1977) (in Japanese).

Table 7.7.1 Comparison between the results of each method

Method	Am-Be		Cf-252	
	Result	Ratio	Result	Ratio
Unfolding	2.72×10^{-3}	1	1.27×10^{-2}	1
G-function	2.51×10^{-3}	0.93 (-7%)	1.29×10^{-2}	1.02 (+2%)
DBM	2.34×10^{-3}	0.86 (-14%)	1.04×10^{-2}	0.82 (-18%)

(rem/hr)

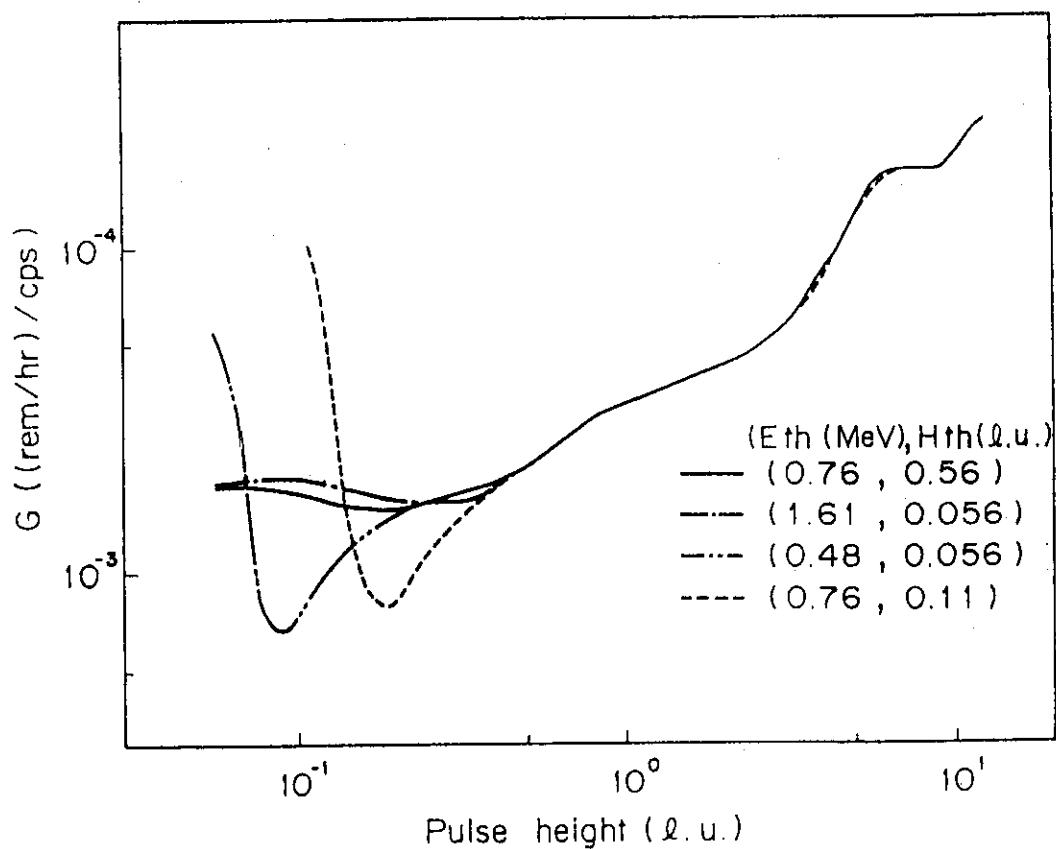


Fig. 7.7.1 $G(E_h)$ function calculated by the present work

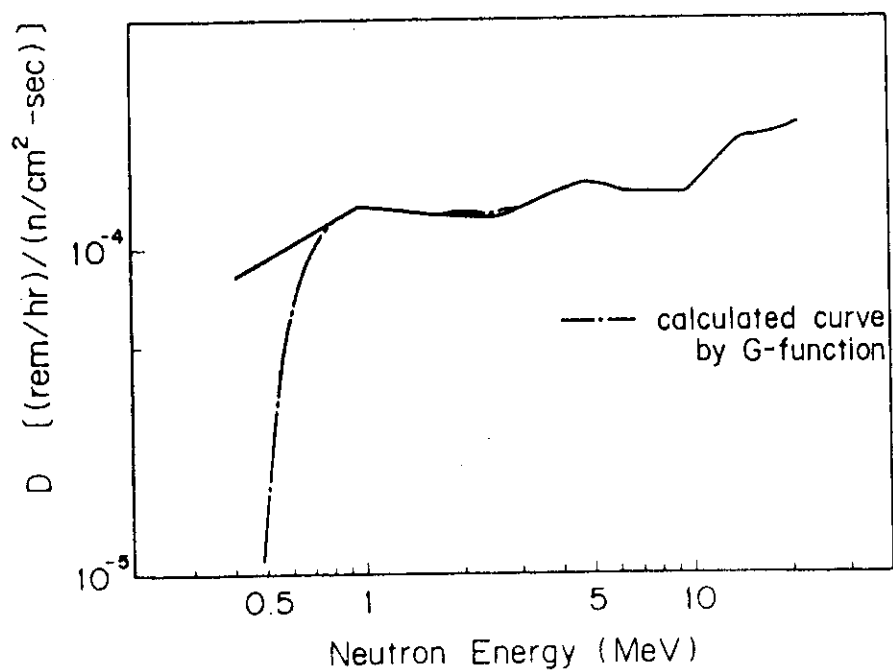


Fig. 7.7.2 Energy response of $G(E_h)$ function method (solid line is Flux-Dose Conversion Factor)

7.8 Depth Distribution of Defects by Ion Bombardment

Y. Taji

Charged atomic projectiles (ions) emerge in the structural materials due to the Knock-on reaction by the fast neutrons emitted by the fission or fusion reactions, or due to the direct entrance of the hot plasma ions. The ions with energies of 10 KeV or 1 MeV penetrate the material from a few hundred Å (for heavier ions) up to a few microns (for lighter ions) and produce the structural defects. It is essential to know accurately the spatial distribution of these defects for the estimation of the growth of the defects.

When the carbon ions with the energy of 1 MeV are injected perpendicularly to the surface of iron (f.c.c. crystal), the distribution of the defects in the depth from the surface has been simulated by making use of the code system CASCMARL¹⁾ (= MARLOWE²⁾ + CLUSTER³⁾ + DAIQUIRI⁴⁾). A primary ion starts from the randomly selected surface point and repeats the binary collisions with the target atoms until the energy of ion becomes smaller than the cutoff energy or the displacement threshold energy. The vacancies and interstitials yielded in the target are stored (MARLOWE). The defects are classified into the various size of cluster and the Frenkel pairs involved in the range of the spontaneous recombination are deleted (CLUSTER). The single interstitials and single vacancies are randomly walked to simulate the thermal annealing (DAIQUIRI). About 80 primary ions are injected and the resulted defects mentioned above have been simply superposed. The simulation scheme of heavy irradiations¹⁾ could not be utilized by the restriction of the memory size. The depth distributions of the vacancy clusters are shown in Fig. 7.8.1 and Fig. 7.8.2, at the stage of the spontaneous recombination and at the stage of the annealation of the single interstitials and vacancies, respectively. As the interatomic potential the Thomas-Fermi screening function has been used in the Moliere approximation. The inelastic energy loss has been taken into account by the Lindhard model¹⁾. The maximum collision impact parameter has been set as 0.45 in the unit of the lattice constant. The efficiency for the incident energy to be expensive for producing the damages has amounted to 7.9%.

Another estimation of the defect distribution $\rho(x)$ has been studied through the spatial distribution of the energy deposited in the target

$S(x)$ as $\rho(x) = (k/2E_d) S(x)$, where E_d is the displacement threshold energy and k is a constant of the order of 0.8. The distribution of the desoposite energy $S(x)$ is obtainable by using the codes of Brice⁵⁾ based on the LSS theory⁶⁾. Because the treatment of the cross sections in the method of binary collision is different from that in the LSS theory, the direct comparison between the results from CASMARL and the LSS theory is rather difficult. However, in the LSS theory, the spatial distribution in the long range becomes flatter than the result of CASCMARL as seen from Fig. 7.8.3, which is a significant difference from the physical point of view. The energy efficiency for the damages has amounted only to 5.9% in this theory.

References

- 1) Asaoka T., et al.: JAERI-M 8178 (1979).
- 2) Robinson M.T. and Torrens I.M.: Phy. Rev. B9 (5008) 1974.
- 3) Besco G.D. and Baumgardt N.R.: GEMP-356 (1965).
- 4) Besco D.G.: GEMP-644 (1967).
- 5) Brice D.K.: SAND 75-0622 (1975).
- 6) Lindhard J., et al.: Kgl. Danske Vid. Sel. m.-f. Med., 33, No.14 (1963).

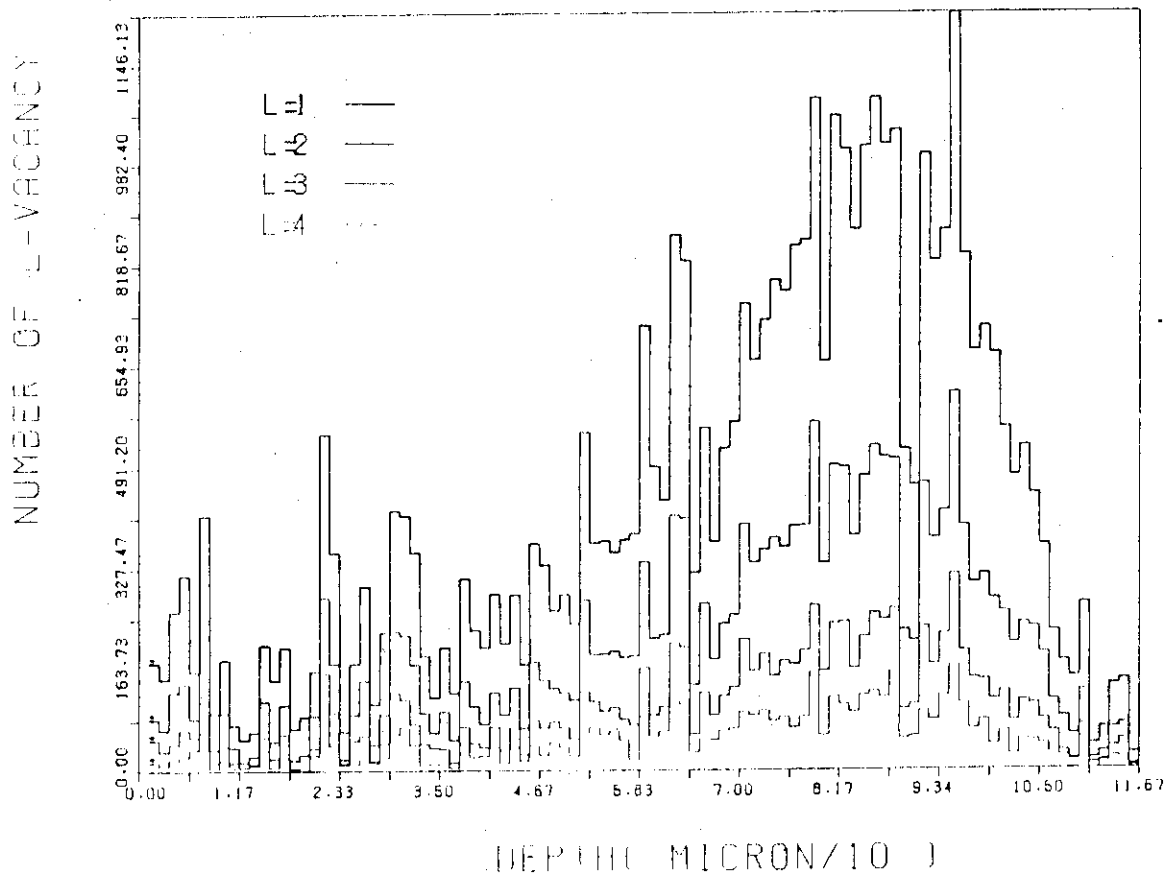


Fig.7.8.1 Depth distribution of vacancy-clusters after the spontaneous recombination

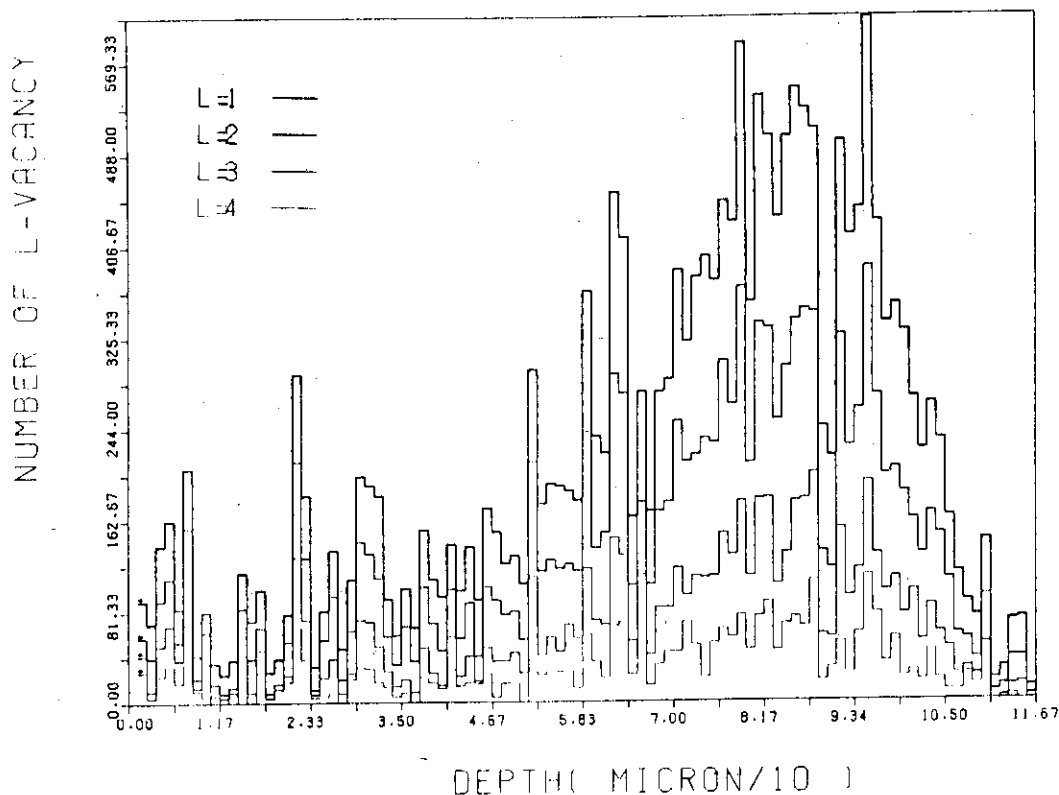


Fig.7.8.2 Depth distribution of vacancy-clusters after annealing the single interstitials and vacancies

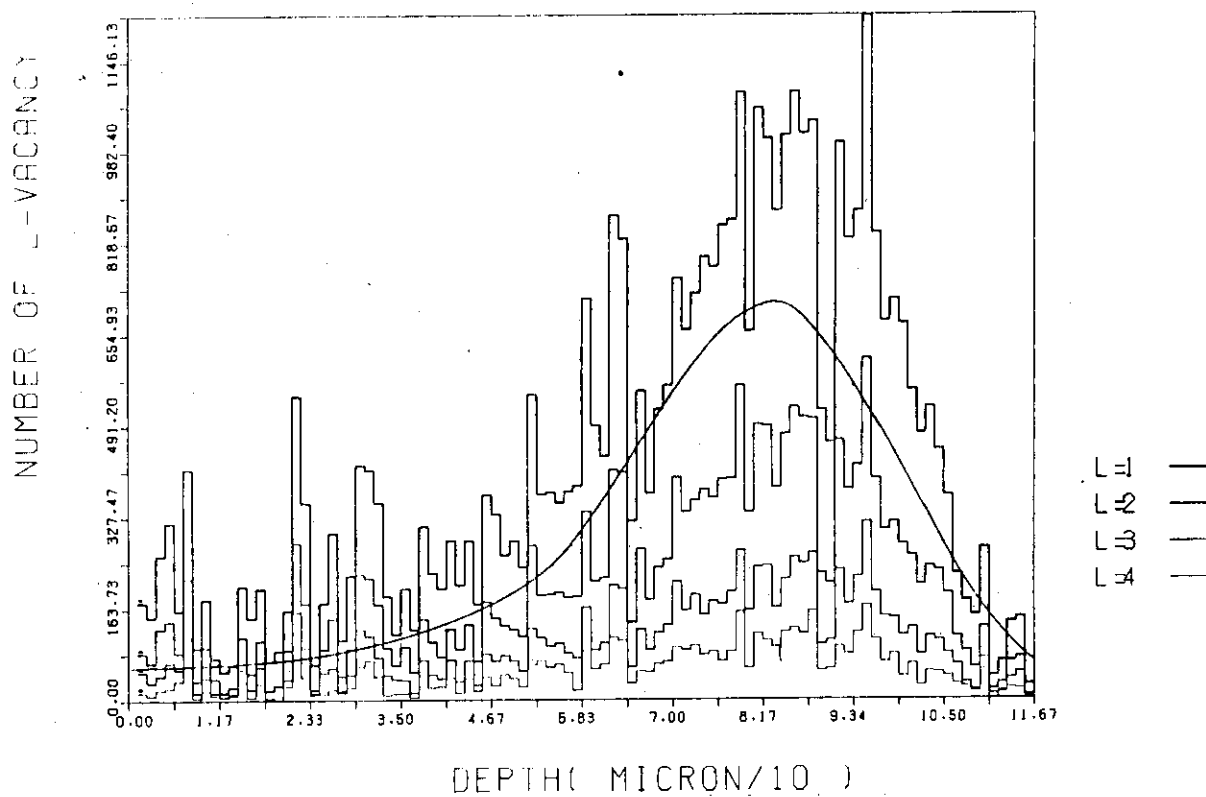


Fig.7.8.3 Comparison of depth distributions calculated by CASCMRL and LSS theory (curved line)

7.9 Development of Thin Film Germanium Bolometer for Plasma Radiation Loss Measurement

M. Katagiri and M. Maeno

In Tokamak, plasma radiation loss measurement is very important to observe and study the instability of the plasma. In this measurement, infrared rays spectrometer or thermister elements have been employed, but they have the slow response time and cannot measure the absolute total absorption of plasma radiation loss. Also, a thin nickel film bolometer was developed to resolve these problems, but this bolometer has a low sensitivity. ¹⁾

Therefore, we developed a new type bolometer with a high sensitivity and a small response time using thin germanium film thermister element. ²⁾ This bolometer is shown in Fig. 7.9.1. The backing metal which absorbs plasma radiation loss was the thin stainless-steel of 28 mm in diameter and of 0.05 mm in thickness. Silicon monooxide was deposited in vacuum onto the stainless-steel plate and thin germanium layer was deposited in high vacuum (10^{-7} Torr) onto the silicon monooxide. Then, aluminium electrodes were deposited so as to form the pattern shown in Fig. 7.9.1. The temperature coefficient was from 2 % to 3.5 % at room temperature.

Figure 7.9.2 shows the typical time behavior of radiation power loss measured with this bolometer in JFT-2, referring to the plasma current. The S/N ratio was about 40 db during discharge and this value was twenty times higher than that of the nickel bolometer. The performances of this bolometer are as follows :

- 1) The response time is short (0.3 msec) :
- 2) The fall time is 2.2 msec :
- 3) The heat capacity is well defined and the absorption coefficient is unity :
- 4) The sensitivity is very high and the detection power density is of the order of 5 mW/cm^2 :

References :

- 1) Kawamura H. et al : J. Nucl. Sci & Technol. 16 (1979) 847.
- 2) Maeno M., Katagiri M. : Jnn. J. Appl. Phys. Vol. 19 (1980) , No.7 , 1433.

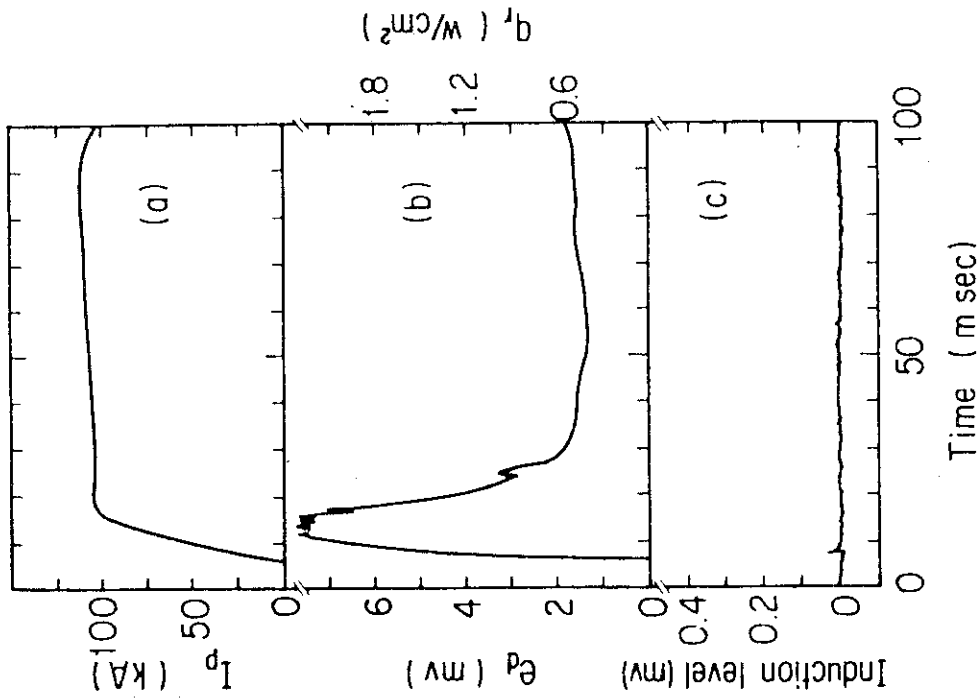


Fig.7.9.2 Typical time behavior of radiation power loss measured with this bolometer in JFT-2

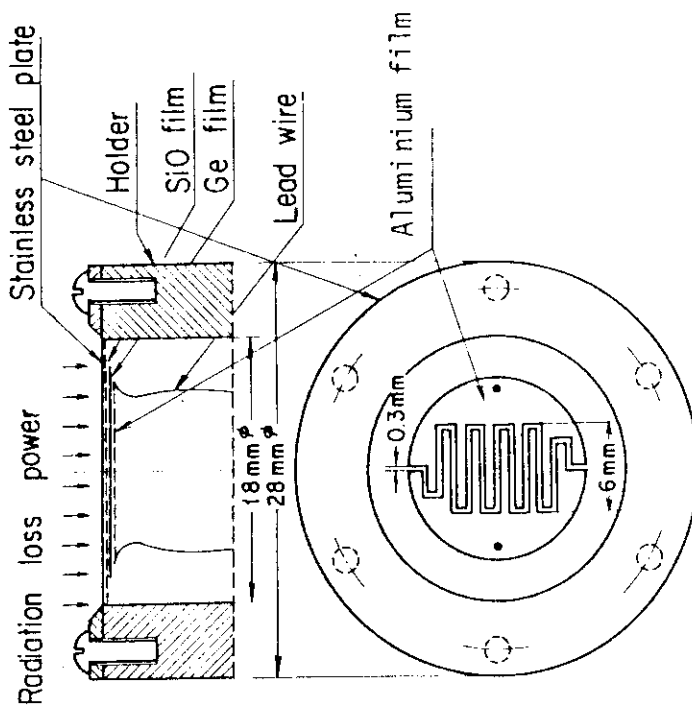


Fig.7.9.1 Structure of the thin film germanium bolometer

8. Activities of the Committees

8.1 Activities Related to the NEA Committee on Reactor Physics

J. Hirota

During this one year period, the Committee on Reactor Physics held the meeting three times, keeping the close relation with the NEA Committee on Reactor Physics (NEACRP). For the 3rd Specialists' Meeting on Reactor Noise (SMORN-III) to be held in Tokyo in 1981, the Preparatory Committee continued work under the Committee until the Japanese Organizing Committee for SMORN-III was set up in December.

The Committee on Reactor Physics held the 36th meeting in April: The plan of the Committee in this fiscal year was discussed with relation to the NEA Data Bank ANL Seminar, 23rd meeting of the NEACRP, Specialists' Meeting on Nuclear Data and Benchmarks for Reactor Shielding, and SMORN-III. A brief summary of the NEACRP Specialist's Meeting on Calculation of 3 - Dimensional Rating Distribution was also reported. Then, problems in analyses and experiments of fusion reactor neutronics were intensively discussed.

The Committee held the 37th meeting in August, mainly for making the preparation to the 23rd meeting of the NEACRP. The research activities in Japan during the period from October 1979 to August 1980 were discussed to prepare the review-paper¹⁾. For contributions from Japan to the topics of the meeting, five papers were presented and discussed, which were as follows; "Fuel Pin and Subassembly Heterogeneity Effect on Neutronics Properties of a Fast Power Reactor", "Utilization of Information from Operating Reactor JOYO", "A study on the Potential Safety Advantage of Heterogeneous LMFBRs (II)", "Validation of KENO-II, ANISN and Hansen-Roach Cross-Section Set on Plutonium Solution Systems" and "Calculational Investigations on Designing Method of Fuel Thickness of Annular Tanks for Plutonium Solutions." Then, an outline of the Benchmark Exercises on Criticality Safety of Spent Fuel Transport Casks proposed by the Committee on Safety of Nuclear Installation (CSNI) was reported. It was recommended that the Committee on Reactor Physics should pay attention to the progress of the Benchmark Exercises.

The Committee held the 38th meeting in February 1981: The plan of the Committee in the next fiscal year, progress of the preparation for SMORN-III and proposal of the 6th International Conference on Reactor Shielding to be held in Tokyo in 1983 were discussed. The summary record of the 23rd meeting

of the NEACRP was distributed and it was stressed that a closer co-operation with the Japanese Nuclear Data Committee would be needed for the Europe-Japan Evaluation Co-ordination Program proposed at the 23rd meeting. Contributions from Japan to the topics of the 24th meeting were also briefly discussed. Then, results of the benchmark calculations carried out in Japan were reported and discussed, which concerned reactivity effect of steam ingress into the core of a gas-cooled fast reactor, criticality safety of spent fuel transport casks and burn-up characteristics of the NEACRP Fast Breeder Benchmark.

Reference

- 1) Hirota J.: "Reactor Physics Activities in Japan - October 1979 to August 1980", NEACRP-L-244 (Japan)

8.2 Activities of the Subcommittees on Reactor Physics

J. Hirota

The Subcommittee on Reactor System, Fusion Reactor and Shielding held the meeting two, three and three times respectively during this one year period, discussing topics of relevance to each field.

The Subcommittee on Reactor System held the 3rd meeting in June: summaries of the Workshop in NEA Data Bank Software held at ANL in May and the NEACRP Specialist's Meeting on Calculation of 3 - Dimensional Rating Distributions in Operating Reactors held at OECD Headquarters in November 1979 were reported. Then, main papers presented at the Specialist's Meeting were reviewed and discussed. The Subcommittee held the 4th meeting in October, mainly to review the papers distributed during the 23rd meeting of the NEACRP held in September: The papers concerned the following topics; structural materials, reactivity effects and activation, pressurized transient studies, problems in the interpretation and analysis of critical experiments, methods of utilization of information from operating reactors, heterogeneous cores and blanket studies.

The Subcommittee on Fusion Reactor held the 3rd meeting in June: After a visit to Fusion Neutronics Source (FNS), present status of accelerators for fusion neutronics research in U.S.A. and neutronics calculations related to the International Tokamak Reactor (INTOR) were reported and discussed. The Subcommittee held the 4th meeting in October: Exchange of the information on fusion neutronics research between Japan and U.S.A. was made by discussions with Mrs. Maskewitz of ORNL. The Subcommittee held the 5th meeting in December: Shielding studies related to fusion reactors in U.S.A. was reported by Dr. Santoro of ORNL. Members of the Subcommittee on Shielding also joined in this meeting.

The Subcommittee on Shielding held the 9th meeting in June: Two papers to be contributed from Japan to the NEACRP Specialist's Meeting on Nuclear Data and Benchmarks for Reactor Shielding were presented and discussed. Activities of the Working Group on Sensitivity and Uncertainty Analysis were reported and the plan of the Working Group on Shielding Analysis Method in this fiscal year was discussed. The Subcommittee held the discussion meeting on shielding research with Mrs. Maskewitz when she visited JAERI Tokai Research Establishment in October. The Subcommittee held the 10th meeting in December: Main papers presented at the 1980 ANS Topical Meeting on Reactor

Physics and Shielding in September were reviewed and discussed, which concerned topics such as present status of shielding research in U.S.A., evaluation of radiation damage and analysis of radiation streaming. In addition, a brief summary of the NEACRP Specialist's Meeting on Nuclear Data and Benchmarks for Reactor Shielding held in October was reported. The subcommittee held the 11th meeting in March 1981: It was discussed how to carry out the Benchmark Exercises proposed at the NEACRP Specialist's Meeting. The activities of the two Working Groups in this fiscal year were reported and the plans in the next fiscal year were discussed. A draft proposal of the 6th International Conference on Reactor Shielding was also discussed.

8.3 Activities of the Japanese Organizing Committee for SMORN-III

J. Hirota and Y. Shinohara

In order to hold the 3rd Specialist's Meeting on Reactor Noise (SMORN-III) in Tokyo in October 1981, the Japanese Organizing Committee has been set up in December 1980. The work of the Preparatory Committee for SMORN-III is continued by the Technical Program Committee organized under the Committee.

The Preparatory Committee held the 6th meeting in April mainly to make the plan in this fiscal year, and the 7th meeting in May to hear the discussions made at the meeting of the International Organizing Committee held in Paris. The Committee held the 8th meeting in June to promote the preparation of the artificial noise data to be used in the Reactor Noise Analysis Benchmark Test and it was decided to carry out the work in August. The Committee held the 9th meeting in September to discuss the test results of the artificial noise data and to prepare the proposal of the Benchmark Test which includes not only the artificial noise data but also the real noise data measured in Borselle reactor. The Committee held the 10th meeting in October to hear the discussions made at the 23rd meeting of the NEACRP and it was decided to add the Phenix data to the Benchmark Test according to the recommendation of the NEACRP.

The Japanese Organizing Committee held the 1st meeting in December: The process and outline of SMORN-III were reported distributing the Information Sheet and Call for Papers (NEACRP-A-404). The outline of the Reactor Noise Analysis Benchmark Test was also reported distributing the document (NEACRP-A-436). Then, several items such as the meeting place, registration fee, participants from Japan and technical visits were discussed.

The Technical Program Committee held the 1st meeting in December mainly to promote the preparation of the Benchmark Test specifications. However, it was obliged to postpone the distribution of the test data tape to the applicants until April 1981, owing to the delay in receiving the Phenix data. The Committee held the 2nd meeting in January 1981 to discuss a draft proposal of the Benchmark Test and it was decided to send this draft to the members of the International Organizing Committee for comments. The Committee held the 3rd meeting in March to select the papers to be presented from Japan. The comments made by the members of the International Organizing Committee on the draft proposal of the Benchmark Test were reported and it was decided to modify the draft taking these comments into account and to present the final

version at the meeting of the International Organizing Committee to be held in April 1981.

Publication Lists

1. Nuclear Data and Group Constants

- (1) Takano H., Ishiguro Y., Matsui Y.* : "TIMS-1: A Processing Code for Production of Group Constants in Heavy Resonant Nuclei", JAERI 1267 (1980).
- (2) Takano H., Kaneko K.* : "Self-Shielding Effect of Inelastic Scattering Cross Sections of Iron on Neutron Spectrum", Nucl. Sci. Eng., 77, 250 (1981).
- (3) Takano H., Matsui Y.* : "Accuracy on Interpolation Methods for Resonance Self-Shielding Factors", J. Nucl. Sci. Technol., 18(2), 152 (1981).
- (4) Takano H., Kaneko K.: "Effective Multiplication Factors and Reaction Rates Calculated with Fission Spectra of U-235, U-238 and Pu-239", J. Nucl. Sci. Technol., 18(3), 236 (1981).
- (5) Kikuchi Y., Narita T., Takano H.: "Preliminary Results of Benchmark Tests on JENDL-2", J. Nucl. Sci. Technol. 17(7), 567 (1980).

2. Theoretical Methods and Code Development

- (1) Nakahara Y.: "Studies on High Energy Spallation and Fission Reactions", Proc. ICANS-IV, Tsukuda, Oct. 20-24, 1980, p.289, KENS Report II (1981).
- (2) Furukawa K., Tsukada K. and Nakahara Y.: "Molten-Salt Target and Blanket Concept", *ibid.* p.349.
- (3) Furukawa K., Nakahara Y. and Tsukada K.: "Single-Fluid-Type Accelerator Molten-Salt Breeder Concept", J. Nucl. Sci. Technol., 18(1), 79 (1981).
- (4) Nishida T.: "Electron Optical Conditions for the formation of Structure Images of Silicon Oriented in (110)", Jap. J. of Appl. Phys., 19(5), 799 (1980).
- (5) Fujimura T., Matsui Y.* : "Effectiveness of an Adaptive Acceleration Method for Inner Iterations in Some Neutron Diffusion Codes", Nucl. Sci. Eng., 77, 360 (1981).
- (6) Fujimura T., Horikami K., Nakahara Y.: "DEPRI, DEPRIM: Programs for Solving Large Linear Optimization Problems by Decomposition Principle", JAERI-M 9315 (1981) (in Japanese).
- (7) Horikami K., Fujimura T., Nakahara Y.: "A Program Package for Solving Linear Optimization Problems: User's Manual", JAERI-M 9048

(1980) (in Japanese).

- (8) Horikami K., Suzuki T., Fujimura T., Nakahara Y.: "A Program Package for Solving Nonlinear Optimization Problems: User's Manual", JAERI-M 9154 (1980) (in Japanese).
- (9) Gotoh Y. "Study of the Stochastic Point Reactor Kinetic Equation", KURRI-TR-203 (1980) (in Japanese).

3. Integral Experiment and Analysis

- (1) Obu M.: "Comparison of Measured and Calculated Neutron Spectra in Fast Critical Assembly," J. Nucl. Sci. Technol., 17(6), 407 (1980).
- (2) Nakano M., Tsunoda H., Hirota J.: "Fission Rate and Sample Worth Measurement in Simulated JMFBF Meltdown Cores," JAERI-M 9090 (1980) (in Japanese).
- (3) Tsunoda H., Nakano M., Hirota J.: "Analysis of Reaction Rate and Sample Worth measured in Simulated LMFBR Meltdown Cores," JAERI-M 9091 (1980) (in Japanese).
- (4) Akino F., Yasuda H. and Kaneko Y.: "Determination of Large Negative Reactivity by Integral Versions of Various Experimental Methods", J. Nucl. Sci. Tech., 17(8) p.593-615 (1980).
- (5) Akino F., Takeuchi M., Kitadate K., Yoshifuji H. and Kaneko Y.: "Measurement of Reactivity Worths of Burnable Poison Rods in Enriched Uranium Graphite-Moderated Core Simulated to High Temperature gas Cooled Reactor", JAERI-M 9223 (1980) (in Japanese).
- (6) Tsuchihashi K. and Gotoh Y.: "CLUPH: A Fortran Program of Collision Probabilities for Hexagonal Lattice and It's Application to VHTR", JAERI-M 9301 (1981).

4. Shielding

- (1) Takeuchi K., Sasamoto N.: "PALLAS-2DCY: A Code for Direct Integration for Transport Equation in Two-Dimensional (R-Z) Geometry", JAERI-M 9014 (1980).
- (2) Takana S.: "EELLOSS: The Program for Calculation of Electron Energy Loss Data", JAERI-M 9151 (1980).

5. Reactor and Nuclear Instrumentation

- (1) Terada H., Sakai E., Katagiri M.: "Environmental Gamma-ray Exposure Rates Measured by In-situ Ge(Li) Spectrometer", J. Nucl. Sci. Technol., 17(4), 281 (1980).

- (2) Sakai E.: "Present Status of Room Temperature Semiconductor Detectors", Proceedings of 1981 INS International Symposium on Nuclear Radiation Detectors, March, 1981, Tokyo.
 - (3) Sekiguchi N., Sakai E., et al.: "Development of Fuel Failure Detection Systems for the Japanese Breeder Reactors", Japan-USSR Seminar, Dec., 1980, Tokyo.
 - (4) Sakai E.: "The Topics around the Latest Gamma-ray Detector", Radiation and Industry, 15, 5 (1980) (in Japanese).
 - (5) Nishino O., Sekiguchi N., Wakayama N., et al.: "Current Status on Reactor Instruments and Instrumentation Systems for Sodium Cooled Fast Breeder Reactors", J. Atom. Ener. Soc. Japan, 22(9), 604 (1980) (in Japanese).
 - (6) Wakayama N., Esaki M., Ara K.: "Current Status of Research and Development on Instrumentation Sensors for High-temperature Gas-cooled Reactors", J. Atom. Ener. Soc. Japan, 22(12), 845 (1980) (in Japanese).
6. Reactor Control and Diagnosis
- (1) Shimazaki J. and Shinohara Y.: "A Method of Estimating Reactivity Components Using an Optimal Estimation Technique", JAERI-M 9177 (1980) (in Japanese).
 - (2) Usui H. and Kudo K.: "Hybrid Computer Simulation of the Dynamics of the Primary System of Experimental Multi-Purpose High-temperature Gas-Cooled Reactor", JAERI-M 8974 (1980) (in Japanese).
 - (3) Shinohara Y.: "Decommissioning of Nuclear Reactors", Journal of SI-CE, 20(2),
 - (4) Shinohara Y.: "Fuzzy Set - Its Concept and Application", Journal of Nucl. Sci. Tech., 23(1) (1981).
 - (5) Shinohara Y., Izume A., Takada Y. and Morioka T.: "Some Recent Activities on Dynamic Simulation of Nuclear Power Plants", Symposium on Simulation Methods for Nuclear Power Systems, (1981).
 - (6) Oguma R.: "Investigation of Resonant Power Oscillation in Halden Boiling Water Reactor Based on Noise Analysis", Journal of Nucl. Sci. Technology, 17(9), 677-686 (1980).
 - (7) Oguma R.: "A Method to Estimate Mechanical State Inside Fuel Rod Based on Noise Analysis", *ibid.*, 17(11), 811-821 (1980).
 - (8) Oguma R. and Matsubara K.: "Dynamic Analysis of a Boiling Water Reactor by Multivariable Autoregressive Modeling Technique", Journal

of the Soci. of Instrument and Control Engineers, 19(7), 626-630 (1980).

- (9) Oguma R., Hayashi K. and Kitajima T.: "Statistical Analysis of Dew-point Data Record at OWL-1 Loop Cubicle and Its Application to Early Detection of Abnormal Water Leakage from the Loop", JAERI-M 9237, (1980).

7. Fusion Reactor Technology

- (1) Oyama Y., Seki Y., Maekawa H. and Nakamura T.: "Cross Section Sensitivity Analysis of ^{235}U and ^{238}U Fission Rates in a Graphite Reflected Lithium Oxide Assembly", JAERI-M 8870 (1980) (in Japanese).
- (2) Maeno M., Katagiri M.: "An application of a Cermanium Film Bolometer for Radiation-loss Measurement in JFT-2 Tokamak", J. Appl. Phys., 19(7), 1433 (1980).

8. Activities of the Committees

- (1) Hirota J.: "Reactor Physics Activities in Japan - October 1979 to August 1980", NEACRP-L-244 Japan.
- (2) Hirota J., Mitani H.: "Summary of NEACRP Views on Actinide Production and Burn-up", Annals of Nuclear Energy, 7(8), 439 (1980).